# TURBULENT NATURAL CONVECTION BOUNDARY LAYERS IN AN ABSORBING AND EMITTING GAS

By

Younes Sh. G. Shabany

B. Sc. (Mechanical Engineering) Sharif University of Technology, Iran

A THESIS SUBMITTED IN PARTIAL FULFILLMENT OF

THE REQUIREMENTS FOR THE DEGREE OF

MASTER OF APPLIED SCIENCE

in

THE FACULTY OF GRADUATE STUDIES

DEPARTMENT OF MECHANICAL ENGINEERING

We accept this thesis as conforming

to the required standard

THE UNIVERSITY OF BRITISH COLUMBIA

May 1994

© Younes Sh. G. Shabany , 1994

In presenting this thesis in partial fulfilment of the requirements for an advanced degree at the University of British Columbia, I agree that the Library shall make it freely available for reference and study. I further agree that permission for extensive copying of this thesis for scholarly purposes may be granted by the head of my department or by his or her representatives. It is understood that copying or publication of this thesis for financial gain shall not be allowed without my written permission.

Department of Mechanical Engineering
The University of British Columbia
2324 Main Mall
Vancouver, Canada
V6T 1Z4

Date: April 8, 1994

## Abstract

Turbulent natural convection boundary layers along a vertical flat plate were numerically simulated for non-absorbing and absorbing gases. By varying the value of absorption coefficient of the gas, the effects of radiative heat transfer on the velocity and temperature profiles of the boundary layer were investigated. A broad range of absorption coefficients, including very high and very low values, were covered.

Three different turbulence models were used to predict the mean characteristics of the turbulent natural convection boundary layer in a non-absorbing gas: the algebraic mixing length model proposed by Cebeci and Khattab; the low-Reynolds-number $k$-$\epsilon$ models of Jones and Launder, and To and Humphrey. It was observed that the Jones and Launder model would predict a later transition if the grids in the flow direction were more refined. However, when the wall functions and extra source terms in the $k$ and $\epsilon$ equations were applied only before the point of maximum velocity, this deficiency was removed. The model in this case was called modified Jones and Launder model. A comparison between the calculated results and the experimental data of Tsuji and Nagana showed that the modified Jones and Launder model was able to predict fairly well the natural convection boundary layer.

Turbulent natural convection boundary layers in an absorbing and emitting gas were then calculated using the modified Jones and Launder turbulence model. The calculations were done for two wall temperatures; $T_w = 60°C$ and $T_w = 200°C$ with $T_\infty = 25°C$ for both cases. It was observed that as the absorption coefficient of the gas increased, velocities and temperatures in the inner region of boundary layer increased, but turbulent viscosities decreased. The convective heat transfer rate also decreased. However, this

trend reversed at some value of absorption coefficient. It was shown that there was a relation between the range of influence of radiation, compared to the boundary layer thickness, and the type of behavior mentioned above. A comparison between the results for different wall temperatures revealed that, for the limiting cases of optically thin and optically thick gas, the normalized velocity profile $u_\tau$, and normalized temperature profile $t_\tau$, were independent of temperature difference between the wall and the medium at a specified Rayleigh number. The convective component of the Nusselt number became a function only of Rayleigh number. For the case of an optically intermediate gas a dependence on wall to gas temperature difference was noted.

## Table of Contents

**Abstract** ii

**Table of Contents** iv

**List of Tables** vii

**List of Figures** viii

**Nomenclature** xiii

**Acknowledgement** xviii

**1 INTRODUCTION** 1

1.1 Preliminary Remarks . . . . . 1

1.2 Description of the Problem . . . . . 2

**2 REVIEW OF THE LITERATURE** 5

2.1 Turbulent Natural Convection . . . . . 5

2.1.1 Experimental Investigations . . . . . 5

2.1.2 Theoretical Works . . . . . 6

2.2 Natural Convection Coupled with Radiation . . . . . 10

2.3 Scope of the Present Investigation . . . . . 12

**3 THEORY** 13

3.1 Physical Model . . . . . 13

3.2 Boundary Layer Equations . . . . . 14
3.3 Turbulence Models . . . . . 17
3.3.1 Algebraic Mixing-Length Model . . . . . 18
3.3.2 Two-Equation Models . . . . . 21
3.4 Radiation Heat Flux . . . . . 27

**4 NUMERICAL METHOD 31**
4.1 Introduction . . . . . 31
4.2 Governing Equations . . . . . 31
4.3 Discretization Method . . . . . 33
4.4 Boundary Conditions . . . . . 37

**5 RESULTS AND DISCUSSIONS-I TURBULENT NATURAL CONVECTION 39**
5.1 Introduction . . . . . 39
5.2 A Modification of the Jones and Launder Model . . . . . 39
5.3 Numerical Results . . . . . 42

**6 RESULTS AND DISCUSSIONS-II NATURAL CONVECTION COUPLED WITH RADIATION 51**
6.1 Introduction . . . . . 51
6.2 Laminar Regime . . . . . 52
6.3 Differential Approximation Method for Laminar Regime . . . . . 58
6.4 Turbulent Regime . . . . . 60
6.4.1 Low Wall Temperature . . . . . 60
6.4.2 High Wall Temperature . . . . . 74
6.4.3 Comparison with Experimental Data . . . . . 77

**7 CONCLUSIONS AND RECOMMENDATIONS** **89**

7.1 Conclusions . . . . . 89

7.2 Recommendations . . . . . 91

**Bibliography** **92**

**Appendices** **97**

**A The Modified Jones and Launder $k$-$\epsilon$ Model** **97**

## List of Tables

3.1 The values of the constants in the $k$-$\epsilon$ model. . . . . 23

3.2 E, D, $\epsilon_w$ and $f$'s functions in the To and Humphrey, and Jones and Launder models. . . . . 26

4.1 The values of general variable $\phi$, diffusion coefficient $\Gamma_\phi$ and source term $S_\phi$ for each transport equation. . . . . 34

## List of Figures


1.1 Natural convection along a hot (left) or a cold (right) plate. . . . . 2

1.2 A typical element of fluid which absorbs, $q_{ri}$, and emits, $q_{ro}$, radiative energy and in general $q_{ri}$ and $q_{ro}$ are not equal. . . . . 3

3.1 Physical model and coordinate system. . . . . 13

3.2 Definition of $\delta$ in the mixing-length model. . . . . 20

4.1 Distribution of grid points and control volumes in the computational domain. . . . . 34

4.2 Control volumes for momentum equation (left) and all the other equations (right). . . . . 35

5.1 Nusselt number calculated by (a) Jones and Launder model and (b) modified Jones and Launder model. . . . . 40

5.2 Comparison between experimental and calculated boundary layer velocity profiles; (a)$Gr_x = 3.62 \times 10^{10}$ (b)$Gr_x = 1.80 \times 10^{11}$. . . . . 43

5.3 Comparison between experimental and calculated near wall velocity profiles; (a)$Gr_x = 3.62 \times 10^{10}$ (b)$Gr_x = 1.80 \times 10^{11}$. . . . . 44

5.4 Comparison between experimental and calculated dimensionless velocity profiles; (a)$Gr_x = 3.62 \times 10^{10}$ (b)$Gr_x = 1.80 \times 10^{11}$. . . . . 45

5.5 Comparison between experimental and calculated temperature profiles; (a)$Gr_x = 3.62 \times 10^{10}$ (b)$Gr_x = 1.80 \times 10^{11}$. . . . . 47

5.6 Comparison between experimental and calculated near wall temperature profiles; (a)$Gr_x = 4.10 \times 10^{10}$ (b)$Gr_x = 3.03 \times 10^{11}$. . . . . 48

5.7 Comparison between experimental and calculated dimensionless temperature profiles; (a)$Gr_x = 3.62 \times 10^{10}$ (b)$Gr_x = 1.80 \times 10^{11}$. . . . . 49

5.8 Comparison between experimental and calculated Nusselt numbers. . . . 50

6.1 Laminar natural convection boundary layer velocity profiles in an absorbing and emitting gas, $Gr_x = 5.81 \times 10^8$. . . . . 53

6.2 Net radiative energy input to fluid in a laminar natural convection boundary layer, $Gr_x = 5.81 \times 10^8$. . . . . 54

6.3 Laminar natural convection boundary layer temperature profiles in an absorbing and emitting gas, $Gr_x = 5.81 \times 10^8$. . . . . 54

6.4 Convective Nusselt number in laminar natural convection boundary layer. 56

6.5 Radiative Nusselt number in laminar natural convection boundary layer. 56

6.6 Velocity and temperature profiles of laminar natural convection boundary layer in terms of similarity variables ($Gr_x = 4.57 \times 10^7, 1.23 \times 10^9$ and $1.16 \times 10^{10}$). . . . . 57

6.7 Comparison between the results obtained by using integral and differential approximation forms of the radiative heat flux, $\kappa_p = 32m^{-1}$. . . . . 58

6.8 Comparison between the results obtained by using integral and differential approximation forms of the radiative heat flux, $\kappa_p = 3.2m^{-1}$. . . . . 59

6.9 Comparison between the results obtained by using integral and differential approximation forms of the radiative heat flux, $\kappa_p = 0.32m^{-1}$. . . . . 59

6.10 Turbulent natural convection velocity and temperature profiles in an absorbing and emitting gas, $T_w = 60°C$ and $Gr_x = 4.24 \times 10^{11}$. . . . . 61

6.11 Net radiative energy input to fluid in the turbulent natural convection of an absorbing and emitting gas, $T_w = 60°C$ and $Gr_x = 4.24 \times 10^{11}$. . . . 63
6.12 Turbulent viscosity in the natural convection boundary layer of an absorbing and emitting gas, $T_w = 60°C$ and $Gr_x = 4.24 \times 10^{11}$. . . . . 64
6.13 Velocity, temperature, net radiative energy to fluid and turbulent viscosity in absorbing and emitting gases with different absorption coefficients, $Gr_x = 5.72 \times 10^9$. . . . . 65
6.14 Velocity, temperature, net radiative energy to fluid and turbulent viscosity in absorbing and emitting gases with different absorption coefficients, $Gr_x = 3.33 \times 10^{10}$. . . . . 66
6.15 Velocity, temperature, net radiative energy to fluid and turbulent viscosity in absorbing and emitting gases with different absorption coefficients, $Gr_x = 2.25 \times 10^{11}$. . . . . 67
6.16 Velocity, temperature, net radiative energy to fluid and turbulent viscosity in absorbing and emitting gases with different absorption coefficients, $Gr_x = 7.15 \times 10^{11}$. . . . . 68
6.17 Velocity, temperature, net radiative energy to fluid and turbulent viscosity in absorbing and emitting gases with different absorption coefficients, $Gr_x = 1.64 \times 10^{12}$. . . . . 69
6.18 Local convective Nusselt number in a turbulent natural convection boundary layer of an absorbing and emitting gas, $T_w = 60°C$. . . . . 70
6.19 Variation of local convective Nusselt number versus absorption coefficient. 72
6.20 The ratio of the convective Nusselt number in an absorbing gas to the convective Nusselt number when gas radiation is neglected. . . . . 72
6.21 Mean convective Nusselt number in a turbulent natural convection boundary layer of an absorbing and emitting gas. . . . . 73

6.22 Local radiative Nusselt number in a turbulent natural convection boundary layer of an absorbing and emitting gas, $T_w = 60°C$. . . . . 74
6.23 Turbulent natural convection velocity and temperature profiles in an absorbing and emitting gas, $T_w = 200°C$ and $Gr_x = 4.24 \times 10^{11}$. . . . . 75
6.24 Net radiative energy to the gas in the turbulent natural convection of an absorbing and emitting gas, $T_w = 200°C$ and $Gr_x = 4.24 \times 10^{11}$. . . . . 76
6.25 Dimensionless velocity profiles in a turbulent natural convection boundary layer of an absorbing and emitting gas. . . . . 78
6.26 Dimensionless temperature profiles in a turbulent natural convection boundary layer of an absorbing and emitting gas. . . . . 79
6.27 Local convective Nusselt number in a turbulent natural convection boundary layer of an absorbing and emitting gas, $T_w = 200°C$. . . . . 80
6.28 Local radiative Nusselt number in a turbulent natural convection boundary layer of an absorbing and emitting gas, $T_w = 200°C$. . . . . 80
6.29 Comparison between the variation of convective Nusselt numbers along the wall in turbulent natural convection of an absorbing and emitting gas with different wall temperatures. . . . . 81
6.30 Comparison between measured [46] and calculated velocity and temperature profiles in nitrogen. . . . . 83
6.31 Comparison between measured [46] and calculated velocity and temperature profiles in a mixture of $10\%CO_2$ and $90\%N_2$. . . . . 85
6.32 Comparison between measured [46] and calculated velocity and temperature profiles in a mixture of $50\%CO_2$ and $50\%N_2$. . . . . 86
6.33 Comparison between measured [46] and calculated velocity and temperature profiles in a mixture of $75\%CO_2$ and $25\%N_2$. . . . . 87

A.1 The variation of turbulent kinetic energy across the boundary layer ($Gr_x = 3.49 \times 10^9 - 6.03 \times 10^{11}$). . . . . 98

A.2 The variation of turbulent dissipation across the boundary layer ($Gr_x = 3.49 \times 10^9 - 6.03 \times 10^{11}$). . . . . 98

A.3 The variation of turbulent viscosity across the boundary layer ($Gr_x = 3.49 \times 10^9 - 6.03 \times 10^{11}$). . . . . 99

A.4 The variation of $D$ across the boundary layer ($Gr_x = 3.49 \times 10^9 - 6.03 \times 10^{11}$). . . . . 100

A.5 The variation of $E$ across the boundary layer ($Gr_x = 3.49 \times 10^9 - 6.03 \times 10^{11}$). . . . . 100

A.6 The sum of the terms of the disspation equation that contain $f_1$ and $f_2$ ($Gr_x = 3.49 \times 10^9 - 6.03 \times 10^{11}$). . . . . 101

## Nomenclature

| | |
|---|---|
| $A^+$ | constant in Eq. 3.18 |
| $B$ | radiosity $[W/m^2]$ |
| $B^+$ | constant defined in Eq. 3.22 |
| $C_g$ | constant in Eq. 3.26 |
| $C'_g$ | constant in Eq. 3.31 |
| $C_{1\epsilon}, C_{2\epsilon}, C_\mu$ | constants in $k$-$\epsilon$ model defined in Table 3.1 |
| $C_p$ | constant pressure specific heat $[kJ/kg^\circ C]$ |
| $D$ | low-Reynolds-number source term in $k$ equation, Table 3.2 |
| $E$ | low-Reynolds-number source term in $\epsilon$ equation, Table 3.2 |
| $E_n(t)$ | exponential-integral function defined by Eq. 3.39, $n = 1, 2, 3, ...$ |
| $e_b$ | black-body emissive power $[W/m^2]$ |
| $f_1, f_2, f_\mu$ | low-Reynolds-number functions, Table 3.2 |
| $G$ | incident radiation $[W/m^2]$ |
| $Gr_L$ | total Grashof number, $(g\beta L^3 \Delta T)/\nu^2$ |
| $Gr_x$ | local Grashof number, $(g\beta x^3 \Delta T)/\nu^2$ |
| $g$ | acceleration of gravity, $9.81 m/s^2$ |
| $h$ | heat transfer coefficient $[W/m^{2\circ}C]$ |
| $I$ | radiative intensity $[W/m^2]$, grid number in $x$ direction |
| $J$ | grid number in $y$ direction |
| $K$ | mean kinetic energy per unit mass $[m^2/s^2]$ |

| | |
|---|---|
| $k$ | turbulent kinetic energy per unit mass $[m^2/s^2]$, thermal conductivity$[W/m^\circ C]$ |
| $L$ | thickness of radiative layer $[m]$, plate length $[m]$ |
| $l$ | turbulent length scale (Eq. 3.14 and Eq. 3.23) $[m]$ |
| $l_m$ | mixing length of turbulent motion (Eq. 3.16) $[m]$ |
| $Nu_L$ | mean Nusselt number, $\overline{h}L/k = 1/k \int_0^L h dx$ |
| $Nu_x$ | local Nusselt number, $hx/k$ |
| $P$ | pressure $[Pa]$ |
| $Pr$ | molecular Prandtl number, $\nu/\alpha$ |
| $q$ | heat flux $[W/m^2]$ |
| $Ra_L$ | total Rayleigh number, $Gr_L Pr$ |
| $Ra_x$ | local Rayleigh number, $Gr_x Pr$ |
| $Re_t$ | turbulent Reynolds number, $k^2/\nu\epsilon$ |
| $S$ | source term in Eq. 3.1 |
| $S_C$ | constant part of $\overline{S_\phi}$ (Eq. 4.16) |
| $S_P$ | coefficient of $\phi^1$ in Eq. 4.16 |
| $S_\phi$ | general source term defined in Table 4.1 |
| $\overline{S_\phi}$ | average value of $S_\phi$ |
| $T$ | mean temperature $[^\circ C]$ |
| $T^+$ | dimensionless temperature, $(T_w - T)/t_\tau$ |
| $t$ | time $[sec]$, dummy variable |
| $t'$ | temperature fluctuation $[^\circ C]$ |
| $t_\tau$ | friction temperature, $q_w/(\rho C_p u_\tau)$ |
| $U$ | mean stream-wise velocity $[m/s]$ |
| $U^+$ | dimensionless velocity, $U/u_\tau$ |

| | |
|---|---|
| $U_b$ | laminar velocity scale, $\sqrt{g\beta\Delta T x}$ |
| $U_{95}$ | velocity defined in Fig. 3.2 |
| $u$ | instantaneous stream-wise velocity $[m/s]$ |
| $u'$ | stream-wise velocity fluctuation $[m/s]$ |
| $u^*$ | characteristic velocity of turbulence (Eq. 3.14) $[m/s]$ |
| $u_\tau$ | friction velocity, $\sqrt{\tau_w/\rho}$ |
| $V$ | mean transverse velocity $[m/s]$ |
| $v$ | instantaneous transverse velocity $[m/s]$ |
| $v'$ | transverse velocity fluctuation $[m/s]$ |
| $x$ | distance from the leading edge of the plate |
| $y$ | distance perpendicular to the plate |
| $y^+$ | dimensionless $y$ coordinate, $yu_\tau/\nu$ |
| $z$ | equal to $k^m l^n$ with specified $m$ and $n$ |

**Greek symbols**

| | |
|---|---|
| $\alpha$ | molecular thermal diffusivity, $k/\rho C_p$ $[m^2/s]$ |
| $\alpha_t$ | turbulent thermal diffusivity, $\nu_t/\sigma_t$ $[m^2/s]$ |
| $\beta$ | coefficient of thermal expansion $[K^{-1}]$ |
| $\Gamma_\phi$ | general diffusion coefficient defined in Table 4.1 |
| $\Delta T$ | temperature differnce between wall and medium, $T_w - T_\infty$ $[^\circ C]$ |
| $\delta$ | boundary layer thickness $[m]$ |
| $\epsilon$ | rate of dissipation of turbulent kinetic energy per unit mass $[m^2/s^3]$, emissivity |
| $\zeta$ | radiation-conduction parameter, $\zeta = (4\kappa_p x^2 \sigma T_f^3)/(kPrGr_x^{1/2})$ |
| $\eta$ | dimensionless coordinate, $y/x(Gr_x/4)^{1/4}$ |

| | |
|---|---|
| $\theta$ | instantaneous temperature $[^{\circ}C]$, |
| | dimensionless mean temperature, $(T - T_\infty)/(T_w - T_\infty)$ |
| $\kappa$ | Von Karman constant (Eq. 3.17) |
| $\kappa_p$ | Planck's mean absorption coefficient defined by Eq. 3.38 |
| $\kappa_\lambda$ | absorption coefficient at wavelength $\lambda$ |
| $\lambda$ | constant in Eq. 3.19, wavelength $[m]$ |
| $\mu$ | a dummy variable in Eq. 3.39 |
| $\nu$ | molecular viscosity $[m^2/s]$ |
| $\nu_t$ | turbulent viscosity $[m^2/s]$ |
| $\xi$ | dimensionless $y$ coordinate, $yNu_x/x$ |
| $\rho$ | density $[kg/m^3]$ |
| $\sigma$ | Stefan-Boltzmann constant, $5.669 \times 10^{-8} W/m^2K^4$ |
| $\sigma_k$ | turbulent Prandtl number for $k$ (Table. 3.1) |
| $\sigma_t$ | turbulent Prandtl number for $T$, $\nu_t/\alpha_t$ |
| $\sigma_\epsilon$ | turbulent Prandtl number for $\epsilon$ (Table. 3.1) |
| $\tau$ | optical coordinate, $\kappa_p y$ |
| $\tau_0$ | optical thickness, $\kappa_p L$ |
| $\tau_w$ | wall shear stress $[N/m^2]$ |
| $\Phi$ | viscous dissipation of thermal energy (Eq. 3.1) |
| $\phi$ | general dependent variable defined in Table 4.1 |

**Superscripts**

| | |
|---|---|
| 0 | the value at the present time step |
| 1 | the value at the next time step |

**subscripts**

| | |
|---|---|
| $c$ | convective |
| $e$ | east face of the control volume |
| $i$ | inner layer, $i$th component, into the element |
| $j$ | $j$th component |
| $max$ | maximum |
| $n$ | north face of the control volume |
| $o$ | outer layer, out of the element |
| $p$ | constant pressure |
| $r$ | radiative |
| $s$ | south face of the control volume |
| $w$ | wall condition, west face of the control volume |
| $x$ | in the $x$ direction |
| $y$ | in the $y$ direction |
| 1 | surface one |
| 2 | surface two |
| $\lambda$ | wavelength |
| $\infty$ | ambient condition |

## Acknowledgement

I wish to express my special thanks to Dr. M. Iqbal and Dr. E. G. Hauptmann for their supervision and encouragement through all stages of this work. The financial support from the Natural Sciences and Engineering Research Council of Canada is gratefully appreciated.

This thesis is dedicated to my father and my mother whose constant concerns and encouragement have been the best support I have in my educational life.

# Chapter 1

# INTRODUCTION

## 1.1 Preliminary Remarks

The problem of the convection-radiation interaction may be divided into two categories: thermal radiation in the presence of a non-absorbing gas, and radiation into an absorbing and emitting gas. In the first case, the radiative heat transfer appears only as a boundary condition at the wall. Radiative and convective heat transfers can be computed separately. On the other hand, when an absorbing and emitting gas is present, the radiative heat transfer through the gas produces a source or sink of thermal energy. The energy equation, and therefore the flow field are coupled with the equation of transfer of the radiative intensity.

Some of very common gases like carbon monoxide, carbon dioxide and water vapor absorb and emit infrared radiative energy as a result of vibrational-rotational bands. It is important to mention that the absorptive characteristics of these gases are very strong even at low temperatures. Because of the presence of these gases in many daily life phenomena and engineering applications, natural convection may be affected by radiation. For example, the flow inside a furnace is a mixed forced and natural convection in an absorbing and emitting medium because water vapor and carbon dioxide are present in the products of combustion. Other examples of this phenomenon are the cooling of electronic devices and heat transfer from solar collectors. Since water vapor and carbon dioxide are usually present in air, it may be said that all natural convection phenomena

in atmospheric air are influenced by gas radiation.

## 1.2 Description of the Problem

Natural convection flows result from the buoyancy forces imposed on the fluid when its density in the proximity of the heat-transfer surface is decreased as a result of heating processes. The buoyancy forces would not be present if the fluid were not acted upon by some external force field such as gravity or centrifugal force. Depending on whether the temperature of the fluid, $T_\infty$, is lower or higher than the surface temperature, $T_w$, the flow direction will be different. These two cases are illustrated in Fig. 1.1. The governing equations for these two cases are basically the same except that the buoyancy term in the momentum equation appears with different signs; positive for a hot wall and negative for a cold wall.

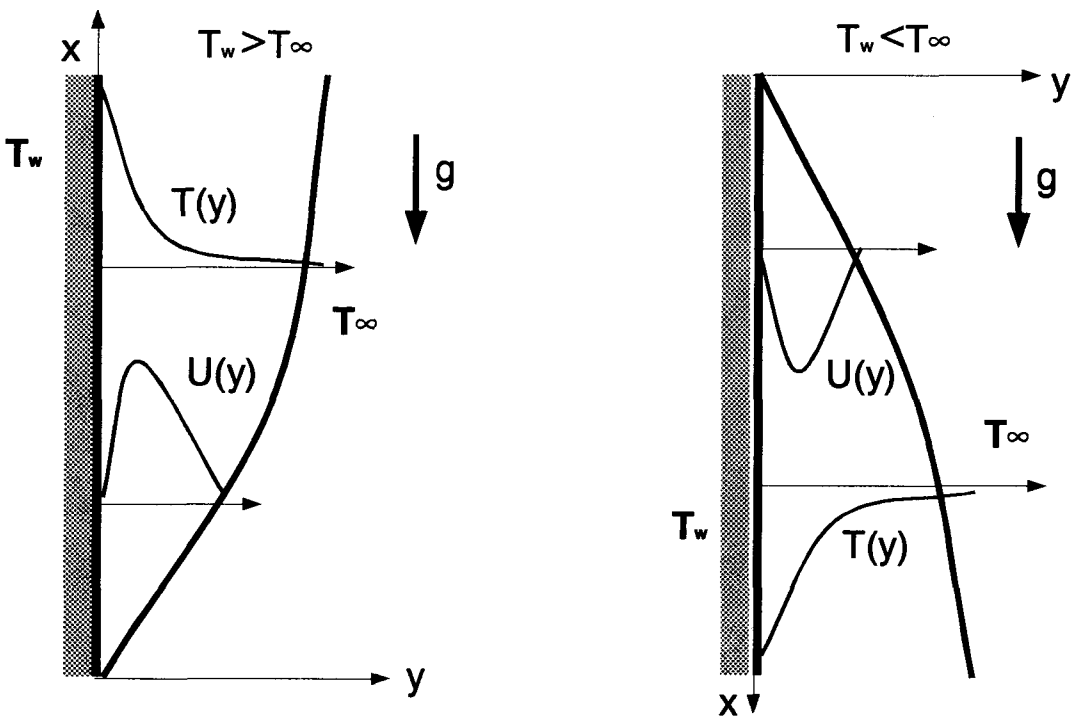


Figure 1.1: Natural convection along a hot (left) or a cold (right) plate.

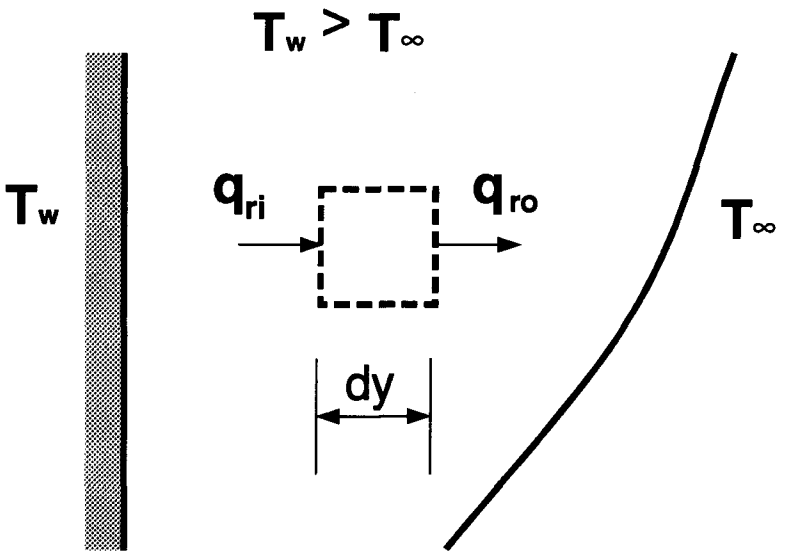


Figure 1.2: A typical element of fluid which absorbs, $q_{ri}$, and emits, $q_{ro}$, radiative energy and in general $q_{ri}$ and $q_{ro}$ are not equal.

There are two different modes of heat transfer between the plate and the medium; convective and radiative. The convective heat transfer rate is calculated by using Fourier's law of conduction at the wall

$$q_c = -k(\frac{\partial T}{\partial y})_w. \tag{1.1}$$

Then, a suitable heat transfer coefficient, $h$, can be defined so that

$$q_c = h(T_w - T_\infty). \tag{1.2}$$

On the other hand, if the gas is non-absorbing, the radiative heat transfer rate from the black wall may be calculated from the relation

$$q_r = \sigma(T_w^4 - T_\infty^4). \tag{1.3}$$

In this case, two different modes of heat transfer are calculated separately. The total heat transfer from the wall is found by simply adding the convection and the radiation heat transfers.

However, if the gas absorbs and emits radiative energy, Fig. 1.2, the radiant energy which reaches an element of fluid may not be equal to the radiation that leaves that element. The temperature profiles, and therefore the flow field, will change due to the radiant energy which is absorbed or emitted by the fluid. Although it is still common to calculate the convection heat transfer by using Eq. 1.2, the value of heat transfer coefficient, $h$, is not the same as it was in the case of a non-absorbing gas. The two modes of heat transfer are not independent of each other. Convection heat transfer is influenced by radiative heat flux, and radiative heat transfer is a function of temperature distribution in the fluid and its radiative properties. Instead of Eq. 1.3, another suitable expression must be used to calculate radiative heat transfer. Therefore, convection and radiation heat transfers must be calculated simultaneously. Then, total heat transfer will be the summation of convective and radiative heat transfers.

# Chapter 2

# REVIEW OF THE LITERATURE

A literature review has been done in order to find the extent of knowledge available in the field of turbulent natural convection, radiative heat transfer in a participating gas, and the interaction of these two modes of heat transfer. This review includes a computer search of papers published during the period 1986-91 and which in some way dealt with natural convection and gas radiation. Using the references mentioned in these papers, it was possible to extend the review to the early 1960s when the first studies on these topics appeared.

## 2.1 Turbulent Natural Convection

### 2.1.1 Experimental Investigations

Cheesewright [1] and Warner and Arpaci [2] presented some of the earliest experimental data of the velocity and temperature profiles of the turbulent natural convection boundary layer. Their results showed that the analytical predictions of Eckert and Jackson [3] did not agree with the measured data.

Lock and Trotter [4] measured the mean velocity and temperature profiles of a turbulent boundary layer formed adjacent to a heated vertical plate immersed in water. They also measured the temperature fluctuations and their frequency distribution. Their results showed that the fluctuations were of the same order as the mean values. They also noticed the existence of two different turbulence scales; one of the order of boundary

layer thickness in the outer region and the other much smaller in the near wall region.

Vliet and Liu [5] measured velocity and temperature profiles as well as local heat transfer rate for laminar, transition and turbulent natural convection of water along a constant heat flux vertical plate. They showed that turbulent heat transfer coefficient slightly decreases with length of the plate.

Kutateladze et al. [6], Papailiou and Lykoudis [7], Cheesewright and Doan [8] and Bill and Gebhart [9] made further measurements of the statistical quantities and space-time correlations of a transient and fully turbulent natural convection boundary layer.

Cheesewright and Ierokiopitis [10] provided the results of measurements of mean and fluctuating velocities that unlike the previous study [1] satisfied an integral energy balance. The measurements were done by laser-doppler anemometry techniques. Miyamoto et al. [11] also used laser-doppler methods as well as thermocouples in order to measure the turbulence quantities along a uniform heat flux vertical plate.

An important contribution to the experimental knowledge of the natural convection boundary layer was given by Tsuji and Nagana [12]. They made a detailed hot-wire measurement of the temperature and velocity fields paying close attention to the near-wall region. Their measurements showed that the wall shear stress increases in the plate height direction whereas the heat transfer rate is almost constant. Thus, there is not the usual analogy between heat and momentum transfer. They also showed that the velocity profile approaches a straight line in the region of much smaller $y^+$ than the corresponding profile in the forced convection flows. Their measured data will be used to verify part of the numerical results obtained in this work.

### 2.1.2 Theoretical Works

Mason and Seban [13] numerically calculated the free convection heat transfer from vertical surfaces by means of a one-equation turbulence model.

Cebeci and Khattab [14] slightly modified the mixing-length model, proposed by Cebeci and Smith [15] for forced convection flows, and used that model for the prediction of turbulent free convection boundary layers. They used an algebraic expression for the calculation of turbulent Prandtl number, though they found that the results obtained by assuming a constant Prandtl number equal to 0.9 were almost the same as those obtained by using a variable Prandtl number.

Plumb and Kennedy [16] applied the low-Reynolds-number $k$-$\epsilon$ model, similar to that proposed by Jones and Launder [17], to the calculation of the turbulent natural convection boundary layer on a vertical, isothermal surface. The wall functions and wall source terms in the $k$ and $\epsilon$ equations were applied only between the wall and the point of maximum velocity. Regarding the buoyancy production of turbulence, which is not present in forced convection flow, they assumed that $\overline{u't'} \propto (kt'^2)^{1/2}$ and solved an equation for $t'^2$ along with the other governing equations. However, they accepted that their proposed constant of proportionality was not a universal one since $\overline{u't'}$ may change sign in a flow.

Lin and Churchill [18] also used the Jones and Launder [17] low-Reynolds-number $k$-$\epsilon$ model to calculate the temperature and velocity fields adjacent to an isothermal, vertical plate. They argued that because of the local isotropy in the turbulent core of the flow, $\overline{u't'}$ should be equal to or at least proportional to $\overline{v't'}$. Therefore, they used $\overline{u't'} \propto \frac{\nu_t}{\sigma_t}\frac{\partial T}{\partial y}$ for the buoyancy production term in the equation of turbulent energy although they had used $\overline{u't'} \propto \frac{\nu_t}{\sigma_t}\frac{\partial T}{\partial x}$ in the thermal energy equation. They also neglected the effect of buoyancy in dissipation equation. However, their final results showed that, at least for air, the inclusion of a buoyancy term in the $k$ equation had a negligible effect. This effect increases as Prandtl number increases.

George and Capp [19] showed that the fully developed natural convection turbulent boundary layer must be treated in two parts with two different length scales; an outer

region consisting of most of the boundary layer in which viscous and conduction terms are negligible and an inner region, called a constant heat flux layer, in which the mean convective terms are negligible. The inner region is further split in a conductive and viscous sublayer, directly touching the wall, and a buoyant sublayer farther away from the wall. By a similarity analysis it was shown that in the buoyant sublayer the velocity and temperature profiles depend on the cube root and the inverse cube root of distance from the wall respectively.

To and Humphrey [20] developed two turbulence models for predicting free convection low Reynolds number turbulent flows. The first, a $k$-$\epsilon$ model differed slightly from Jones and Launder model [17] in that the former did not have any extra terms in the $k$ and $\epsilon$ equation and a non-zero boundary condition was specified at the wall for dissipation rate. The second model, an algebraic stress model in which, by assuming an equilibrium turbulent flow, the turbulent fluxes were calculated from algebraic expressions derived from simplified forms of transport equations for the fluxes. Their test results from the $k$-$\epsilon$ model showed that whether $\overline{u't'} \propto \frac{\partial T}{\partial y}$ or is zero, the effect of buoyant production of turbulence on calculations of heat transfer, mean temperature, and velocity was negligible although the turbulent kinetic energy maximum was decreased by 7% if buoyancy was neglected. Therefore, they neglected this term in the $k$-$\epsilon$ calculations. When the algebraic stress model was used, this term was computed directly without difficulty. Their near wall results supported a $y^{1/3}$ dependence for velocity and a $y^{-1/3}$ dependence for temperature.

Fedotov and Chumakov [21] used a transport equation for turbulent kinetic energy along with an algebraic expression for mixing length to calculate the turbulent viscosity. They modeled the buoyant production of turbulence by using the relation $\overline{u't'} \propto (t'^2 k)^{1/2}$ and solving another transport equation for $t'^2$. The important point of their work was that the proportionality factor they used was not constant across the boundary layer. In fact it could be a negative value very close to the wall to comply with the experimental

data.

The performance of different turbulence models (originally developed for forced convection flows) was tested for the natural convection boundary layer by Henkes and Hoogendoorn [22]. These models include the algebraic mixing-length model, the $k$-$\epsilon$ model with a wall function, and a few different low-Reynolds-number $k$-$\epsilon$ models. They also very roughly compared the predictions of different models with what they called the "best fit" with the experiments. Their results showed that the low-Reynolds-number $k$-$\epsilon$ models of Lam and Bremhorst [23], Chien [24] and Jones and Launder [17] gave the best results in describing the velocity profiles. For Grashof numbers higher than $10^{11}$ the Jones and Launder model was the best.

Henkes and Hoogendoorn [25] also compared numerically predicted wall functions with the previously proposed analytical ones. Their calculations showed that in the conductive/thermo-viscous sublayer the parameters $U_b = \sqrt{g\beta\Delta T x}$ and $xGr_x^{-1/4}$ are suitable scaling parameters for velocity and length. For the dimensionless temperature, $(T - T_\infty)/\Delta T)$, the similarity length was found to be $\xi = yNu_x/x$. For the buoyant sublayer, George and Capp's [19] wall function for temperature was confirmed, but their wall function for velocity was not determined. Instead, the same velocity and length scales as for conductive/thermo-viscous sublayer were also confirmed to be suitable for the buoyant sublayer. George and Capp's [19] defect laws for the velocity and the temperature in the outer layer agreed very well with the numerical predictions. The velocity scale was found to be $U_b Gr_x^{-1/18}$ which was close to the laminar velocity scale, $U_b$. Therefore, they concluded that the laminar velocity scale, $U_b$, was approximately the right velocity scale over the whole thickness of the boundary layer.

## 2.2 Natural Convection Coupled with Radiation

The most basic effects of radiation upon the other modes of heat transfer was illustrated by Cess [26]. He also made the first analytical investigation of the free convection boundary layer of a gray gas along a vertical, black and isothermal plate as a singular perturbation problem [27].

Novotny and Kelleher [28] presented an analysis for the laminar free convection of a gray gas at the stagnation point of a horizontal, black and isothermal cylinder. Novotny [29] also investigated the effect of nongrayness on the same problem. The radiation term of the energy equation was formulated using the exponential wide-band model of Edwards and Menard [30] and the correlation of Tien and Lowder [31] for the total band absorption. There was no conclusion regarding the difference between the results obtained with gray and with nongray gas assumptions.

Arpaci [32] made an analytical study of the laminar heat transfer from a heated vertical plate to a gray and nonscattering radiating gas. The integral formulation of the problem was considered and solved using a perturbation method.

England and Emery [33] performed the first experimental study of the effects of thermal radiation upon the laminar free convection boundary layer of an absorbing and nonscattering gas ($CO_2$) near a vertical, flat and constant heat flux plate. The experimental data were compared with the numerical solution for a gray gas both in an optically thin and constant-property, and in a general, case. Unlike the findings of the other investigators, their analytical and experimental investigations showed that the effect of radiation on the laminar free convection of absorbing gases was negligible. They also concluded that the free convection of gases need only be treated through the use of the optically thin limit.

Audunson and Gebhart [34] investigated experimentally and theoretically the effects

of thermal radiation on the laminar natural convection boundary layer adjacent to a vertical flat surface with uniform heat flux input. In the experiment, air, argon and ammonia were used to observe the radiation effects in non-absorbing and absorbing media. Theoretical results were obtained by a perturbation analysis. Their study showed that for non-absorbing gases the effect of radiation on convection appeared only in the boundary conditions and the convection transport might be formulated as a non-radiative process. However, the absorbing gas, ammonia, caused a strong interaction between radiation and convection. The presence of a radiating gas was seen to increase the convective heat transfer by as much as 40% and to decrease the non-dimensional temperature level by approximately 20%.

Cheng and Ozisik [35] solved the non-similar momentum and energy equations for a constant-temperature vertical plate in an absorbing, emitting, isotropically scattering and gray fluid. Their parametric study showed the effects of scattering albedo, optical thickness and conduction to radiation parameter on temperature and velocity in the boundary layer and heat transfer at the wall.

Bratis and Novotny [36], Lauriat [37, 38], Kurosaki et al. [39], Chang et al. [40], Ratzel and Howell [41], Desrayaud and Lauriat [42], Webb and Viskanta [43], and Fusegi and Farouk [44, 45] investigated the combined radiation and natural convection in enclosures and vertical layers. The last two papers are noteworthy. Nongray gas radiation was analyzed with the P-1 approximation method for the radiative transfer equation and the weighted sum of gray gases model was used. The model postulated that the emissivity of nongray gases could be represented by the sum of gray gas emissivities weighted with a temperature-dependent factor (the gas was carbon dioxide). A $k$-$\epsilon$ model was employed with the standard model constants and turbulent Prandtl number.

Hood [46] studied experimentally and theoretically the turbulent natural convection coupled with thermal radiation in an absorbing gas adjacent to a vertical heated plate.

The momentum and energy equations were solved by an integral technique, with the radiation term modeled by two different methods; the mean beam length method, and the optically thin gray gas method. The experimental work consisted of measuring the temperature and velocity profiles at one location over a range of carbon dioxide and nitrogen gas compositions.

## 2.3 Scope of the Present Investigation

The review of the existing literature shows that there is still a lack of knowledge regarding the fundamental effects of gas absorption and emission on the turbulent natural convection boundary layer. Even for the case of natural convection in a non-absorbing gas, there is not any overall accepted turbulence model to numerically simulate the flow. Therefore, the purposes of this study are:

1. To determine a turbulence model that predicts fairly well the mean characteristics of the turbulent natural convection boundary layer. This will be done by comparing the results obtained by a few different models with the most recent experimental data.

2. To study the effects of gas radiation on the turbulent natural convection boundary layer. The effects of interest are; mean velocity and temperature profiles, heat transfer rate, boundary layer thickness, maximum velocity, mass flow rate, etc. Here it is assumed that a turbulence model that gives a good prediction in the case of a non-absorbing gas is also suitable for an absorbing and emitting gas.

## Chapter 3

## THEORY

### 3.1 Physical Model

The physical model and the coordinate system are shown in Fig. 3.1. The plate temperature, $T_w$, and the surrounding fluid temperature, $T_\infty$, are considered to be constant. The coordinate system is so chosen that the $x$ coordinate will be along the plate and the $y$ coordinate perpendicular and outward to the plate. The boundary layer at the leading

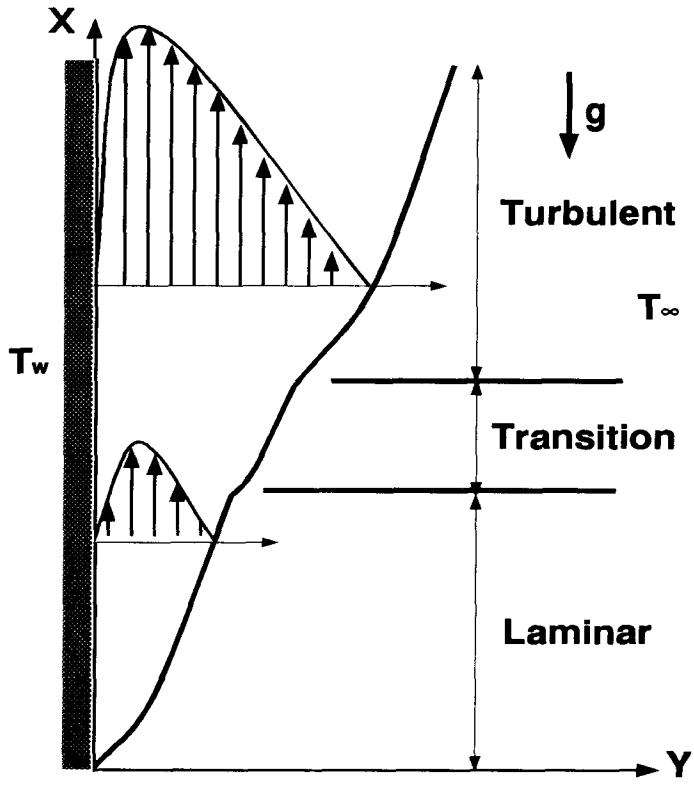


Figure 3.1: Physical model and coordinate system.

edge of the plate is laminar but at some distance from the leading edge, depending on the fluid properties and temperature difference between the plate and medium, transition to a turbulent boundary layer begins. If the plate is long enough, the boundary layer may become fully turbulent. This part of the boundary layer is the subject of interest in this study.

Unlike the more common analyses of natural convection boundary layers, in which the fluid is considered to transmit completely the radiative energy emitted by the plate, here it is assumed that the fluid elements are able to absorb and emit part of the radiation transmitted to them.

## 3.2 Boundary Layer Equations

For a two-dimensional, constant-property, and incompressible flow the continuity, momentum and energy equations can be written as

$$\frac{\partial u}{\partial x} + \frac{\partial v}{\partial y} = 0 \tag{3.1}$$

$$\frac{\partial u}{\partial t} + u\frac{\partial u}{\partial x} + v\frac{\partial u}{\partial y} = -\frac{1}{\rho}\frac{\partial P}{\partial x} - g + \nu(\frac{\partial^2 u}{\partial x^2} + \frac{\partial^2 u}{\partial y^2})$$

$$\frac{\partial v}{\partial t} + u\frac{\partial v}{\partial x} + v\frac{\partial v}{\partial y} = -\frac{1}{\rho}\frac{\partial P}{\partial y} + \nu(\frac{\partial^2 v}{\partial x^2} + \frac{\partial^2 v}{\partial y^2})$$

$$\frac{\partial \theta}{\partial t} + u\frac{\partial \theta}{\partial x} + v\frac{\partial \theta}{\partial y} = \frac{k}{\rho C_p}(\frac{\partial^2 \theta}{\partial x^2} + \frac{\partial^2 \theta}{\partial y^2}) + \frac{\Phi}{\rho C_p} + \frac{S}{\rho C_p},$$

where $\Phi$ and $S$ represent viscous dissipation of energy, and any other source or sink of energy inside the flow respectively [47]. The viscous dissipation term, $\Phi$, is often a negligible effect in natural convection flows where the velocities are very small. Gebhart [48] showed that the ratio of this term to the conductive term becomes important for large $g$ and/or very low temperature, or very large Prandtl number. None of these conditions

are present in the physical phenomena considered in this study; therefore, this term will be simply neglected.

The only source term in the present problem is radiation energy absorbed or emitted by the gas. It can be written as [49]

$$S = -\vec{\nabla}.\vec{q_r} = -(\frac{\partial q_{rx}}{\partial x} + \frac{\partial q_{ry}}{\partial y}). \tag{3.2}$$

Using the usual boundary layer approximations, the simplified form of the governing equations can be expressed as

$$\begin{aligned} \frac{\partial u}{\partial x} + \frac{\partial v}{\partial y} &= 0 \\ \frac{\partial u}{\partial t} + u\frac{\partial u}{\partial x} + v\frac{\partial u}{\partial y} &= -\frac{1}{\rho}\frac{dP}{dx} - g + \nu\frac{\partial^2 u}{\partial y^2} \\ \frac{\partial \theta}{\partial t} + u\frac{\partial \theta}{\partial x} + v\frac{\partial \theta}{\partial y} &= \alpha\frac{\partial^2 \theta}{\partial y^2} - \frac{1}{\rho C_p}(\frac{\partial q_{rx}}{\partial x} + \frac{\partial q_{ry}}{\partial y}). \end{aligned} \tag{3.3}$$

As indicated in the momentum equation above, the pressure is not a function of transverse direction $y$. On the other hand, outside of the boundary layer, the pressure gradient is only due to gravity

$$\frac{dP}{dx} = -\rho_\infty g. \tag{3.4}$$

Substituting Eq. 3.4 into the momentum equation results in

$$\frac{\partial u}{\partial t} + u\frac{\partial u}{\partial x} + v\frac{\partial u}{\partial y} = \frac{1}{\rho}(\rho_\infty - \rho)g + \nu\frac{\partial^2 u}{\partial y^2}. \tag{3.5}$$

The Taylor expansion of $\rho$ about $\rho_\infty$ gives

$$\rho = \rho_\infty + (\frac{\partial \rho}{\partial \theta})_p(\theta - \theta_\infty) + \frac{1}{2}(\frac{\partial^2 \rho}{\partial \theta^2})_p(\theta - \theta_\infty)^2 + ... \approx \rho_\infty - \rho\beta(\theta - \theta_\infty),$$

or

$$\rho_\infty - \rho = \rho\beta(\theta - \theta_\infty), \tag{3.6}$$

where $\beta$ is the coefficient of thermal expansion and is defined as:

$$\beta = -\frac{1}{\rho}(\frac{\partial \rho}{\partial \theta})_p.$$

Sparrow and Cess [49] showed that even for an optically thick gas

$$\frac{1}{\rho C_P}\frac{\partial q_{rx}}{\partial x} \ll u\frac{\partial \theta}{\partial x}. \tag{3.7}$$

Therefore, radiation heat transfer can be considered as a one-dimensional transfer phenomenon.

The final form of the boundary layer equations can be written by combining Eqs. 3.3, 3.5 and 3.6, and using Eq. 3.7 to neglect the radiation flux in $x$ direction. This results in

$$\begin{aligned} \frac{\partial u}{\partial x} + \frac{\partial v}{\partial y} &= 0 \\ \frac{\partial u}{\partial t} + \frac{\partial u^2}{\partial x} + \frac{\partial uv}{\partial y} &= g\beta(\theta - \theta_\infty) + \nu\frac{\partial^2 u}{\partial y^2} \\ \frac{\partial \theta}{\partial t} + \frac{\partial u\theta}{\partial x} + \frac{\partial v\theta}{\partial y} &= \alpha\frac{\partial^2 \theta}{\partial y^2} - \frac{1}{\rho C_p}\frac{dq_r}{dy}. \end{aligned} \tag{3.8}$$

These equations are written in the conservative form which is more suitable for a numerical solution.

In Eqs. 3.8 the velocities and the temperature are instantaneous time-dependent values. If the turbulent flow is statistically steady, the instantaneous values can be considered to be the sum of a mean time-averaged and a fluctuating value

$$\begin{aligned} u &= U + u' \\ v &= V + v' \\ \theta &= T + t'. \end{aligned} \tag{3.9}$$

Introducing the above decompositions into the Eqs. 3.8 and taking the time average results in the following set of time-averaged, two-dimensional, incompressible, natural

convection, turbulent boundary layer equations

$$\frac{\partial U}{\partial x} + \frac{\partial V}{\partial y} = 0$$

$$\frac{\partial U}{\partial t} + \frac{\partial U^2}{\partial x} + \frac{\partial UV}{\partial y} = g\beta(T - T_\infty) + \frac{\partial}{\partial y}(\nu \frac{\partial U}{\partial y} - \overline{u'v'}) \tag{3.10}$$

$$\frac{\partial T}{\partial t} + \frac{\partial UT}{\partial x} + \frac{\partial VT}{\partial y} = \frac{\partial}{\partial y}(\frac{\nu}{Pr}\frac{\partial T}{\partial y} - \overline{v't'}) - \frac{1}{\rho C_p}\frac{dq_r}{dy}.$$

In the derivation of the above equations it was assumed that

$$\frac{\partial \overline{u'^2}}{\partial x} \ll \frac{\partial \overline{u'v'}}{\partial y} \qquad \text{and} \qquad \frac{\partial \overline{u't'}}{\partial x} \ll \frac{\partial \overline{v't'}}{\partial y}.$$

It is seen that the time-averaged equations contain two new unknowns, the turbulent stress and the turbulent heat flux. Since the number of unknowns are more than the number of equations, the above equations do not form a closed set of equations. Solving this closure problem is the subject of turbulence modeling.

## 3.3 Turbulence Models

Turbulence models can be divided into two main categories. First, the models that use Boussinesq's proposition(1877). He suggested that the stress-strain proportionality law for the time-averaged turbulent flows could be represented in the same form as that for a Newtonian fluid in laminar flow. The concept of "turbulent viscosity" was introduced by this assumption in correspondence with the molecular viscosity in laminar flows

$$-\rho\overline{u'v'} = \rho\nu_t\frac{\partial U}{\partial y}. \tag{3.11}$$

Similarly, "turbulent thermal diffusivity" and "turbulent Prandtl number" were introduced to represent turbulent heat flux in terms of mean temperature variation

$$-\overline{v't'} = \alpha_t\frac{\partial T}{\partial y} = \frac{\nu_t}{\sigma_t}\frac{\partial T}{\partial y}. \tag{3.12}$$

Introducing Eqs. 3.11 and 3.12 into Eqs. 3.10 gives the new form of the boundary-layer equations

$$\frac{\partial U}{\partial x} + \frac{\partial V}{\partial y} = 0$$

$$\frac{\partial U}{\partial t} + \frac{\partial U^2}{\partial x} + \frac{\partial UV}{\partial y} = g\beta(T - T_\infty) + \frac{\partial}{\partial y}[(\nu + \nu_t)\frac{\partial U}{\partial y}] \tag{3.13}$$

$$\frac{\partial T}{\partial t} + \frac{\partial UT}{\partial x} + \frac{\partial VT}{\partial y} = \frac{\partial}{\partial y}[(\frac{\nu}{Pr} + \frac{\nu_t}{\sigma_t}\frac{\partial T}{\partial y}] - \frac{1}{\rho C_p}\frac{dq_r}{dy}.$$

Different models have been proposed for calculating turbulent viscosity; including zero equation or otherwise called algebraic models, one-equation and two-equation models.

The second group of models includes those which do not use the Boussinesq's assumption. They provide differential transport equations for the turbulent fluxes themselves. It must be mentioned that the introduction of new transport equations for turbulent fluxes does not solve the closure problem since those equations contain other new unknowns. Therefore, modeling of the new unknowns in terms of the previous ones, or the mean flow parameters, is necessary. These models are very complicated and require considerable computing time.

In this work only the first group of models is investigated. Emphasis is on the two-equation model which now is widely used .

### 3.3.1 Algebraic Mixing-Length Model

In the algebraic models the objective is to relate turbulent viscosity to the local mean parameters of the turbulent flow. Prandtl(1925) was the first to propose such a relation. Influenced by the kinetic theory of gases, he presented his mixing-length hypothesis. According to the kinetic theory of gases, the molecular viscosity is proportional to the product of the mean free path and the root-mean-square velocity of molecules. Analogously, in his mixing-length theory, Prandtl assumed the turbulent viscosity to be proportional

to the product of a mixing length and a characteristic velocity of turbulent fluctuations

$$\nu_t = lu^*, \tag{3.14}$$

where $l$ is a length scale characteristic of the size of momentum transferring eddies and $u^*$ is a characteristic velocity of turbulence. Prandtl assumed that the magnitude of the velocity fluctuations in lateral and longitudinal directions are proportional to each other; and those are proportional to the turbulent characteristic length scale times the mean-velocity gradient

$$u^* \propto l|\frac{\partial U}{\partial y}|. \tag{3.15}$$

Taking the proportionality constant as one, the Prandtl mixing-length formula for turbulent viscosity could be written as

$$\nu_t = l_m^2|\frac{\partial U}{\partial y}|. \tag{3.16}$$

In above, $l_m$ is called the mixing length of turbulent motion. There is still the question of how $l_m$ is to be determined? Based on the argument that the mixing length must vanish at the wall and that the eddy sizes are controlled by the distance from the wall, Prandtl introduced the following linear relation

$$l_m = \kappa y, \qquad \text{with} \qquad \kappa = 0.4. \tag{3.17}$$

Actually, close to the wall the mixing length is smaller than that indicated by the above equation. Van Driest(1956) incorporated this effect by introducing an exponentially damping factor into the equation

$$l_m = \kappa y[1 - exp(-y^+/A^+)], \tag{3.18}$$

$$y^+ = \frac{yu_\tau}{\nu} \qquad , \qquad A^+ = 26.$$

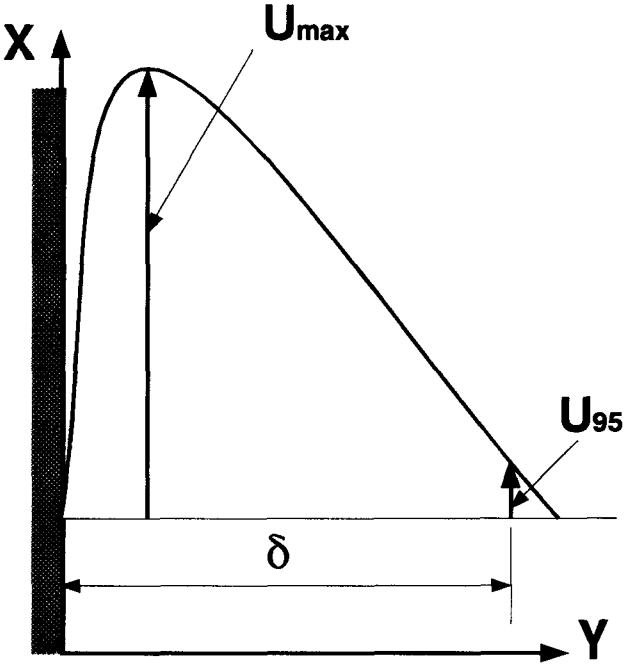


Figure 3.2: Definition of $\delta$ in the mixing-length model.

In the outer region of boundary layer, $l_m$ does not continue to increase, but remains approximately constant

$$l_m = \lambda.\delta, \qquad \text{with} \qquad \lambda = 0.075 - 0.09. \tag{3.19}$$

Cebeci and Smith [15] used this model to describe the turbulence in a forced convection boundary layer. The model was modified by Cebeci and Khattab [14] for a natural convection boundary layer. In this model

$$\nu_t = \begin{cases} \nu_i = [\kappa y(1 - exp(-y^+/A^+))]^2 |\frac{\partial U}{\partial y}| & \nu_i \leq \nu_o \\ \nu_o = (0.075\delta)^2 |\frac{\partial U}{\partial y}| & \nu_o \leq \nu_i \end{cases} \tag{3.20}$$

and $\delta$ is the y-position of $U_{95}$; $|U_{95} - U_\infty| = 0.05U_{max}$ (see Fig. 3.2).

Cebeci and Smith also gave the following expression for the turbulent Prandtl number

$$\sigma_t = \frac{0.4[1 - exp(-y^+/A^+)]}{0.44[1 - exp(-y^+/B^+)]}, \tag{3.21}$$

where

$$B^+ = \frac{1}{\sqrt{Pr}} \sum_{i=1}^{5} c_i (log(Pr))^{i-1}, \tag{3.22}$$

and $c_1 = 34.96$ , $c_2 = 28.79$ , $c_3 = 33.95$ , $c_4 = 6.33$ , $c_5 = -1.186$.

### 3.3.2 Two-Equation Models

In a review of turbulence models, the two-equation models might be considered after one-equation models. However, one-equation models are not described here because of their limited popularity and small advantages they offer compared to the mixing-length model. It may be mentioned that in these types of models it is assumed that turbulent viscosity is proportional to a characteristic length scale times the square root of the turbulent energy;

$$\nu_t = l.k^{1/2}. \tag{3.23}$$

A differential equation for $k$ is then derived and some of the terms of that equation are modeled to keep the number of unknowns unchanged. On the other hand, $l$ must be prescribed before the set of equations can be solved.

The two-equation models also employ Eq. 3.23 for turbulent viscosity. Here, both the turbulent energy and the length scale are determined by suitable transport equations. It is not necessary to choose the length scale as the dependent variable of the differential equation. Any variable $z = k^m l^n$ with specified $m$ and $n$ might be used. Different variables have been adopted by different investigators. Kolmogorov(1942) chose a quantity proportional to the mean frequency of the most energetic motions, $k^{1/2}/l$. Other workers have used the product of turbulent energy and length scale, $kl$, as their second dependent variable. The rate of turbulent energy dissipation, $\epsilon = k^{3/2}/l$, has been favored by more workers than any other variables. The reason for this lies partly in the relative ease with which an equation for $\epsilon$ can be derived and partly in the fact that $\epsilon$ appears directly as an unknown in the equation for $k$.

### High-Reynolds-Number $k$-$\epsilon$ Model

The equation for mean kinetic energy, $K = U^2/2$, is derived by multiplying the momentum equation by $U$ [50]

$$\frac{\partial K}{\partial t} + U\frac{\partial K}{\partial x} + V\frac{\partial K}{\partial y} = g\beta U(T - T_\infty) + \frac{\partial}{\partial y}(\nu\frac{\partial K}{\partial y} - U\overline{u'v'}) + \overline{u'v'}\frac{\partial U}{\partial y} - \nu(\frac{\partial U}{\partial y})^2. \quad (3.24)$$

The equation for turbulent kinetic energy can be derived by multiplying the instantaneous momentum equation in the $i$ direction by $u_i(t)$, taking the time average of the resultant equation and subtracting the mean energy equation ,Eq. 3.24, from it [50]

$$\frac{\partial k}{\partial t} + U\frac{\partial k}{\partial x} + V\frac{\partial k}{\partial y} = g\beta\overline{u't'} + \frac{\partial}{\partial y}(\nu\frac{\partial k}{\partial y} - \overline{v'k}) - \overline{u'v'}\frac{\partial U}{\partial y} - \nu\overline{(\frac{\partial u_i'}{\partial x_j})^2}. \quad (3.25)$$

The left hand side of the above equation represents the rate of change and convection of turbulent kinetic energy. The terms on the right hand side represent buoyant production or dissipation of turbulent energy, molecular and turbulent diffusion, production of turbulent kinetic energy through interaction with mean flow, and viscous dissipation of turbulent energy. This equation contains several turbulent correlations which have to be approximated in terms of quantities which we know or can determine. These approximations include [50]

$$\overline{u't'} = -C_g\frac{\nu_t}{\sigma_t}\frac{\partial T}{\partial x}, \quad (3.26)$$

$$\overline{v'k} = -\frac{\nu_t}{\sigma_k}\frac{\partial k}{\partial y}, \quad (3.27)$$

$$\overline{u'v'} = -\nu_t\frac{\partial U}{\partial y}, \quad (3.28)$$

$$\text{and} \quad \nu\overline{(\frac{\partial u_i'}{\partial x_j})^2} = \epsilon. \quad (3.29)$$

When the approximated forms of the terms are introduced into the original equation, the final form of the equation becomes

$$\frac{\partial k}{\partial t} + U\frac{\partial k}{\partial x} + V\frac{\partial k}{\partial y} = \frac{\partial}{\partial y}[(\nu + \frac{\nu_t}{\sigma_k})\frac{\partial k}{\partial y}] + \nu_t(\frac{\partial U}{\partial y})^2 - \epsilon - C_g g\beta\frac{\nu_t}{\sigma_t}\frac{\partial T}{\partial x} \quad (3.30)$$

The transport equation for isotropic dissipation $\epsilon = \nu\overline{(\partial u_i'/\partial x_j)^2}$ can be obtained by the cartesian tensor operation $\nu\overline{(\partial u_i'/\partial x_j)\partial/\partial x_j}$ on the $i$th component of the momentum equation, time averaging, and some modeling approximations [50]. The final form of the equation is

$$\frac{\partial \epsilon}{\partial t} + U\frac{\partial \epsilon}{\partial x} + V\frac{\partial \epsilon}{\partial y} = \frac{\partial}{\partial y}[(\nu + \frac{\nu_t}{\sigma_\epsilon})\frac{\partial \epsilon}{\partial y}] + [C_{1\epsilon}\nu_t(\frac{\partial U}{\partial y})^2 - C_{2\epsilon}\epsilon - C_g' g\beta\frac{\nu_t}{\sigma_t}\frac{\partial T}{\partial x}]\frac{\epsilon}{k}. \quad (3.31)$$

The relation between the turbulent viscosity, the turbulent kinetic energy, and the rate of turbulent energy dissipation can be found as;

$$\nu_t \propto k^{1/2}l, \qquad \text{and} \qquad l \propto \frac{k^{3/2}}{\epsilon}, \qquad \text{therefore} \qquad \nu_t \propto \frac{k^2}{\epsilon},$$

or

$$\nu_t = C_\mu\frac{k^2}{\epsilon}. \quad (3.32)$$

The turbulent Prandtl number for temperature, kinetic energy and dissipation, and also all the C's must be determined experimentally. Table 3.1 shows the values recommended by Launder and Spalding [51] for forced convection flows and are widely used for free convection flows also.

Table 3.1: The values of the constants in the $k$-$\epsilon$ model.

| $C_\mu$ | $C_{1\epsilon}$ | $C_{2\epsilon}$ | $\sigma_t$ | $\sigma_k$ | $\sigma_\epsilon$ |
|---|---|---|---|---|---|
| 0.09 | 1.44 | 1.92 | 0.9 | 1.0 | 1.3 |

Regarding the values of $C_g$ and $C_g'$ there are no accepted values. To and Humphrey [20] and Henkes and Hoogendoorn [22] argued that because of boundary layer approximations the buoyancy production has a small effect on the results and therefore dropped that term. Lin and Churchill [18] reasoned that $\overline{u't'}$ must be equal or at least proportional to $\overline{v't'}$ and therefore substituted $\partial T/\partial x$ by $\partial T/\partial y$. Plumb and Kennedy [16] assumed that

$\overline{u't'} \propto (kt'^2)^{1/2}$ and solved an equation for $\overline{t'^2}$ along with the other governing equations. However, they accepted that their proposed constant of proportionality is not a universal one for all free convection-type flows since $\overline{u't'}$ may change sign. Experimental works [12] clearly showed that $\overline{u't'}$ is zero or has a very small negative value near the wall. It increases rapidly in the positive direction near the location of the maximum temperature fluctuation and reaches a maximum at a location almost equivalent to the maximum velocity location. Numerical prediction of temperature fields showed that, in a fully turbulent flow near the wall, $\partial T/\partial x$ is a small negative value and then becomes positive. Therefore, proportionality between $\overline{u't'}$ and $\partial T/\partial x$ seems to be more realistic than that between $\overline{u't'}$ and $\partial T/\partial y$ or $(kt'^2)^{1/2}$, which do not change sign across the boundary layer. It is noted that there is not yet any acceptable method to model the effect of buoyancy on the turbulent production or dissipation. On the other hand, as far as gases are concerned, the previous works [18, 20] showed that the effect of buoyancy on the final results were very small and possibly negligible. Therefore, in this work this effect is neglected; this means that $C_g = C'_g = 0$.

The above $k$ and $\epsilon$ equations along with the continuity, momentum and energy equations form a closed set of differential equations for turbulent flows. Since the $\epsilon$ equation is an equation for rate of isotropic dissipation of turbulent energy, and the dissipation very close to wall is not an isotropic phenomena, the presented $k$-$\epsilon$ model is called a high-Reynolds-number $k$-$\epsilon$ model. Here, turbulent Reynolds number is defined as $k^2/\nu\epsilon$, and is proportional to the ratio of turbulent to molecular viscosity. If one wants to use the high-Reynolds-number $k$-$\epsilon$ model, the first computational node near the wall must be out of the viscous sublayer which is the low-Reynolds-number region of the flow. In a forced convection flow with negligible pressure gradient, it is known that close to a fixed wall the velocity and temperature profiles can be approximated by logarithmic wall functions. These wall functions are used along with the high-Reynolds-number $k$-$\epsilon$ model

to compute turbulent flow fields. On the other hand, as yet there is no generally accepted wall function for turbulent natural convection flows. Experimental investigations by Tsuji and Nagana [12] showed that there is not such a logarithmic velocity profile in the turbulent free convection boundary layer although their mean temperature profiles showed a logarithmic region in the range $30 \leq y^+ \leq 200$. They also concluded that the linear velocity profile, $u^+ = y^+$, which holds for a forced convection boundary layer in the range $y^+ \leq 5$ does not hold even at $y^+ \simeq 1$ for the free convection flow. Therefore, a $k$-$\epsilon$ model which covers both high and low Reynolds number regions is required.

### Low-Reynolds-Number $k$-$\epsilon$ Model

Like all other turbulent models, the low-Reynolds-number $k$-$\epsilon$ model was developed based on research results for the forced convection flows. Jones and Launder [17] suggested that in order to provide predictions of the flow within the viscous sublayer adjacent to the wall, the terms containing $C$'s must become dependent upon the Reynolds number of turbulence, $k^2/\nu\epsilon$, and further terms must be added to account for the fact that the dissipation processes are not isotropic. The complete form of their proposed model is

$$\frac{\partial k}{\partial t} + U\frac{\partial k}{\partial x} + V\frac{\partial k}{\partial y} = \frac{\partial}{\partial y}[(\nu + \frac{\nu_t}{\sigma_k})\frac{\partial k}{\partial y}] + \nu_t(\frac{\partial U}{\partial y})^2 - \epsilon + D, \tag{3.33}$$

$$\frac{\partial \epsilon}{\partial t} + U\frac{\partial \epsilon}{\partial x} + V\frac{\partial \epsilon}{\partial y} = \frac{\partial}{\partial y}[(\nu + \frac{\nu_t}{\sigma_\epsilon})\frac{\partial \epsilon}{\partial y}] + [C_{1\epsilon}f_1\nu_t(\frac{\partial U}{\partial y})^2 - C_{2\epsilon}f_2\epsilon]\frac{\epsilon}{k} + E, \tag{3.34}$$

$$\nu_t = C_\mu f_\mu \frac{k^2}{\epsilon}. \tag{3.35}$$

In the above equations, the $C$'s and the $\sigma$'s retain the values assigned before (Table 3.1). The influence of turbulent Reynolds number is introduced by the way of the $f$'s functions.

Different versions of the low-Reynolds-number $k$-$\epsilon$ model were introduced by other workers. They can be divided into two main categories:

1. First, those which use non-zero wall boundary condition for $\epsilon$ and do not have any extra terms in $k$ and $\epsilon$ equations, D and E.

2. The second group of models specify zero wall boundary condition for $\epsilon$ and have extra terms in the $k$ and $\epsilon$ equations.

The recently developed To and Humphrey model [20], which is the only model claimed to be developed for free convection flows, is from the first group of models described above. Table 3.2 illustrates the distinctions between the Jones and Launder model and the To and Humphrey model.

Table 3.2: E, D, $\epsilon_w$ and $f$'s functions in the To and Humphrey, and Jones and Launder models.

| | Jones and Launder | To and Humphrey |
|---|---|---|
| $D$ | $-2\nu(\frac{\partial\sqrt{k}}{\partial y})^2$ | 0 |
| $E$ | $2\nu\nu_t(\frac{\partial^2 U}{\partial y^2})^2$ | 0 |
| $\epsilon_w$ | 0 | $2\nu(\frac{\partial\sqrt{k}}{\partial y})^2$ |
| $f_1$ | 1.0 | 1.0 |
| $f_2$ | $1-0.3exp(-Re_t^2)$ | $(1-0.3exp(-Re_t^2))f_3$ <br> $f_3=\{^{1}_{1-exp(-Re_t^2)}\ \ ^{y^+\geq 5}_{y^+\leq 5}$ |
| $f_\mu$ | $exp(\frac{-2.5}{1+Re_t/50})$ | $exp(\frac{-2.5}{1+Re_t/50})$ |

According to Jones and Launder, the need for the term $-2\nu(\frac{\partial\sqrt{k}}{\partial y})^{1/2}$ in the turbulent energy equation arises from the fact that there are decisive computational advantages from letting $\epsilon$ go to zero at the wall; $\epsilon$ may therefore be interpreted as the isotropic part

of the energy dissipation. This new term in the energy equation indeed reduces to the value of energy dissipation at the wall.

The last term on the right side of the dissipation equation is also one which does not appear in the high-Reynolds-number form of the model. Here there is no physical argument for its adoption. Its inclusion was simply in order to match the calculated turbulent energy profile with the experimental one.

## 3.4 Radiation Heat Flux

For a gray and nonscattering medium bounded between two parallel, infinite, gray and diffuse plates, the radiation flux is given by [49]

$$q_r(\tau) = 2B_1E_3(\tau) - 2B_2E_3(\tau_0 - \tau) + 2\int_0^{\tau} \sigma T^4(t)E_2(\tau - t)dt - 2\int_{\tau}^{\tau_0} \sigma T^4(t)E_2(t - \tau)dt, \tag{3.36}$$

and correspondingly

$$-\frac{dq_r(\tau)}{d\tau} = 2B_1E_2(\tau) + 2B_2E_2(\tau_0 - \tau) + 2\int_0^{\tau_0} \sigma T^4(t)E_1(|\tau - t|)dt - 4\sigma T^4(\tau). \tag{3.37}$$

In above, $\tau$ and $\tau_0$ represent the optical coordinate and the optical thickness of the medium respectively; for a gray gas they are defined as:

$$\tau = \kappa_p y \qquad \text{and} \qquad \tau_0 = \kappa_p L,$$

where $\kappa_p$ is the Planck's mean absorption coefficient given by:

$$\kappa_p = \frac{\int_0^{\infty} \kappa_\lambda e_{b\lambda} d\lambda}{\int_0^{\infty} e_{b\lambda} d\lambda}, \tag{3.38}$$

and $E_n(t)$ is the exponential-integral function which is defined as:

$$E_n(t) = \int_0^1 \mu^{n-2} e^{-t/\mu} d\mu. \tag{3.39}$$

For a boundary-layer problem there is only one bounding plate and the other side is infinity (considered to be a black body). Therefore, the radiosities $B_1$ and $B_2$ are

$$\begin{gathered} B_1 = \epsilon_w \sigma T_w^4 + 2(1-\epsilon_w)[\sigma T_\infty^4 E_3(\tau_\infty) + \textstyle\int_0^{\tau_\infty} \sigma T^4(t) E_2(t) dt], \\ B_2 = \sigma T_\infty^4. \end{gathered} \tag{3.40}$$

Substituting Eqs. 3.40 into Eqs. 3.36 and 3.37 and noting that for large values of $t$, $E_n(t) \to 0$, the radiative flux equations for a boundary layer of nonscattering and gray medium along a diffuse and gray plate are obtained as

$$\begin{aligned} q_r(\tau) &= 2\epsilon_w \sigma T_w^4 E_3(\tau) + 4(1-\epsilon_w) E_3(\tau) \int_0^\infty \sigma T^4(t) E_2(t) dt + 2\int_0^\tau \sigma T^4(t) E_2(\tau - t) dt \\ &\quad - 2\int_\tau^\infty \sigma T^4(t) E_2(t-\tau) dt, \end{aligned} \tag{3.41}$$

and

$$\begin{aligned} -\frac{dq_r(\tau)}{d\tau} &= 2\epsilon_w \sigma T_w^4 E_2(\tau) + 4(1-\epsilon_w) E_2(\tau) \int_0^\infty \sigma T^4(t) E_2(t) dt \\ &\quad + 2\int_0^\infty \sigma T^4(t) E_1(|\tau - t|) dt - 4\sigma T^4(\tau). \end{aligned} \tag{3.42}$$

In this study it is assumed that the plate is a black surface, $\epsilon_w = 1$. Therefore, the second terms in Eqs. 3.41 and 3.42 disappear.

It is seen that the equations for the radiative heat flux are in an integral form. Therefore, the enrgy equation which contains the net rate of radiative heat flux as a source term will become an integro-differential equation. In general, the solution of an integro-differential equation is much more difficult and time consuming than the solution of a differential equation.

Different approximations were proposed to make the radiation problem a tractable one. One of these methods, which is called the spherical harmonics or $P_N$-approximation, transforms the integral equation into a set of simultaneous partial differential equations. For detailed description of the development of the general $P_N$-method the reader is referred to Modest [52], and only the basic ideas are described as follows.

The radiative intensity, $I$, is expressed in terms of a two-dimensional generalized Fourier series by using the spherical harmonics, which are the solutions of Laplace's equation in spherical coordinates, and then $I$ is substituted into the general equation of radiative transfer. Exploiting the orthogonality properties of spherical harmonics leads to an infinite number of coupled partial differential equations in the unknown position-dependent functions. Up to this point the representation is an exact method for the determination of the intensity field. To simplify the problem, an approximation is now made by truncating the Fourier series after very few terms. The methods most often employed are the $P_1$ or the differential approximation, which is used in this work, and the $P_3$-approximation.

It can be shown that for a gray and nonscattering medium the $P_1$ method leads to the following differential equation for the incident radiation $G$ [52]

$$\nabla_\tau^2 G = 3(G - 4e_b). \tag{3.43}$$

Once the incident radiation has been determined, the radiative heat flux and its divergence can be determined from

$$\vec{q_r} = -\frac{1}{3}\vec{\nabla}_\tau G, \tag{3.44}$$

$$\vec{\nabla}_\tau . \vec{q_r} = 4e_b - G. \tag{3.45}$$

For a one-dimensional radiation, assumed in this study, the above equations take the following simple forms

$$\frac{d^2G}{d\tau^2} = 3(G - 4e_b), \tag{3.46}$$

$$q_r = -\frac{1}{3}\frac{dG}{d\tau}, \tag{3.47}$$

$$\text{and} \quad \frac{dq_r}{d\tau} = 4e_b - G. \tag{3.48}$$

If Eq. 3.48 is differentiated once and Eq. 3.47 is used to substitute for the first derivative of $G$, the following differential equation in terms of radiative heat flux is

obtained

$$\frac{d^2 q_r}{d\tau^2} - 3q_r = 4\frac{de_b}{d\tau}. \tag{3.49}$$

Eq. 3.49 is a second order differential equation and therefore needs two boundary conditions. For a black wall the boundary condition for the incident radiation was shown to be [52]

$$\tau = 0 \qquad , \qquad -\frac{2}{3}(\frac{dG}{d\tau})_w + G_w = 4e_{bw}, \tag{3.50}$$

and by substituting $G_w$ and $(\frac{dG}{d\tau})_w$ from Eqs. 3.47 and 3.48 into Eq. 3.50, the boundary condition for radiative heat flux at the wall is obtained as

$$\tau = 0 \qquad , \qquad 2q_{rw} - (\frac{dq_r}{d\tau})_w = 0. \tag{3.51}$$

On the other hand, at infinity both the radiative heat flux and its derivative are zero. Therefore, the second boundary condition may be written as

$$\tau = \infty \qquad , \qquad \frac{dq_r}{d\tau} = 0. \tag{3.52}$$

# Chapter 4

# NUMERICAL METHOD

## 4.1 Introduction

The boundary-layer equations were solved for a semi-infinite isothermal vertical plate in an isothermal environment by a finite difference method. The computational domain was covered with uniform grids in $x$ direction and non-uniform geometrically propagated grids in $y$ direction. A very dense distribution of grids was used near the wall to cover the steep gradients of velocity and temperature there. The first point near the wall was so chosen that the value of $y^+$ at that point would be less than one. It was observed that the near wall grid size could be increased, at least by a factor of two, without any important effect on the temperature profile. However, the velocity profile near the wall changed appreciably with that amount of change in the grid size.

Although the steady state solution of the equations was required, the transient equations were used because of the inherent and useful underrelaxation effect they offer with small time steps.

## 4.2 Governing Equations

The governing equations which had to be solved for this problem are:

- Continuity equation

$$\frac{\partial U}{\partial x} + \frac{\partial V}{\partial y} = 0, \tag{4.1}$$

- $x$-component of momentum equation

$$\frac{\partial U}{\partial t} + \frac{\partial U^2}{\partial x} + \frac{\partial UV}{\partial y} = g\beta(T - T_\infty) + \frac{\partial}{\partial y}[(\nu + \nu_t)\frac{\partial U}{\partial y}], \tag{4.2}$$

- Energy equation

$$\frac{\partial T}{\partial t} + \frac{\partial UT}{\partial x} + \frac{\partial VT}{\partial y} = \frac{\partial}{\partial y}[(\frac{\nu}{Pr} + \frac{\nu_t}{\sigma_t})\frac{\partial T}{\partial y}] - \frac{1}{\rho C_p}\frac{dq_r}{dy}, \tag{4.3}$$

- Turbulence-modeling equations

  1. Algebraic-mixing-length model

$$\nu_t = \begin{cases} \nu_i = [\kappa y(1 - exp(-y^+/A^+))]^2|\frac{\partial U}{\partial y}| & \nu_i \leq \nu_o \\ \nu_o = (0.075\delta)^2|\frac{\partial U}{\partial y}| & \nu_o \leq \nu_i, \end{cases} \tag{4.4}$$

  2. Low-Reynolds-number $k$-$\epsilon$ model

$$\frac{\partial k}{\partial t} + \frac{\partial Uk}{\partial x} + \frac{\partial Vk}{\partial y} = \frac{\partial}{\partial y}[(\nu + \frac{\nu_t}{\sigma_k})\frac{\partial k}{\partial y}] + \nu_t(\frac{\partial U}{\partial y})^2 - \epsilon + D, \tag{4.5}$$

$$\frac{\partial \epsilon}{\partial t} + \frac{\partial U\epsilon}{\partial x} + \frac{\partial V\epsilon}{\partial y} = \frac{\partial}{\partial y}[(\nu + \frac{\nu_t}{\sigma_\epsilon})\frac{\partial \epsilon}{\partial y}] + [C_{1\epsilon}f_1\nu_t(\frac{\partial U}{\partial y})^2 - C_{2\epsilon}f_2\epsilon]\frac{\epsilon}{k} + E, \tag{4.6}$$

$$\nu_t = C_\mu f_\mu \frac{k^2}{\epsilon}. \tag{4.7}$$

  The values of D, E, $C$'s and $\sigma$'s as well as $f$'s functions were as given in Section 3.3.2.

- The radiative term in energy equation might be calculated directly by the following integral

$$-\frac{dq_r}{dy} = \kappa_p[2\sigma T_w^4 E_2(\tau) + 2\int_0^\infty \sigma T^4(t)E_1(|\tau - t|)dt - 4\sigma T^4(\tau)], \tag{4.8}$$

  or by solving a differential equation for radiative heat flux if the differential approximation was going to be used

$$\frac{d^2 q_r}{dy^2} - 3\kappa_p^2 q_r = 4\kappa_p \frac{de_b}{dy}. \tag{4.9}$$

## 4.3 Discretization Method

The control-volume finite difference scheme of Patankar [53] was used to discretize the differential equations. In this method, the calculation domain is divided into a number of non-overlapping control volumes such that there is one control volume surrounding each grid point. Then, the differential equations are integrated over each control volume. Piecewise profiles expressing the variation of the parameter of interest between the grid points are used to evaluate the required integrals. The result is the discretized equations containing the values of the parameter for a group of grid points. The discretized equation obtained in this manner expresses the conservation principle for the parameter for the finite control volumes, just as the differential equation expresses it for an infinitesimal control volume.

Fig. 4.1 shows a sample of a computational domain with the control volumes surrounding the grid points. The velocities are calculated at the boundaries of each control volume, whereas all the scalar quantities and all properties are calculated at the grid points at the center of control volumes. The staggered grids is used for $x$-component of velocity, $U$. Therefore, the control volumes used for integrating the momentum equation are different from those used for other equations.

The general form of the governing equations, except Eq. 4.9, may be written as

$$\frac{\partial \phi}{\partial t} + \frac{\partial U\phi}{\partial x} + \frac{\partial V\phi}{\partial y} = \frac{\partial}{\partial y}(\Gamma_\phi \frac{\partial \phi}{\partial y}) + S_\phi, \tag{4.10}$$

where the general dependent variable $\phi$, the diffusion coefficient $\Gamma_\phi$, and the source term $S_\phi$, are defined in Table 4.1 for each of the transport equations.

Eq. 4.10 has to be integrated over a control volume with dimensions $\Delta x$ and $\Delta y$ and over the time interval $\Delta t$

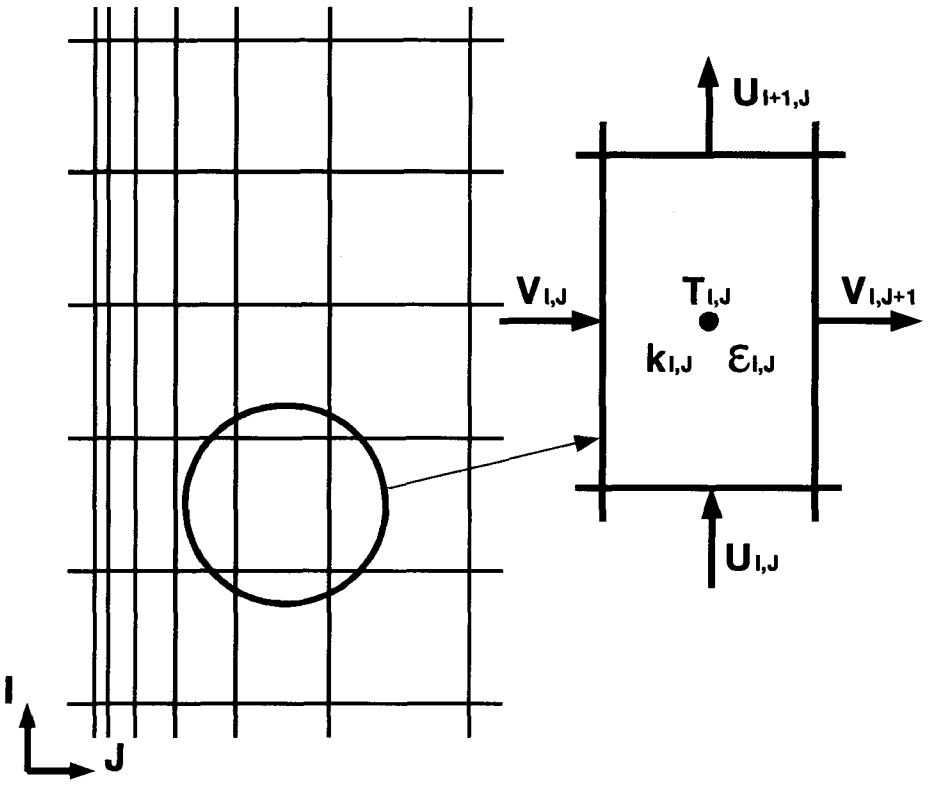


Figure 4.1: Distribution of grid points and control volumes in the computational domain.

Table 4.1: The values of general variable $\phi$, diffusion coefficient $\Gamma_\phi$ and source term $S_\phi$ for each transport equation.

| Transport Equation | $\phi$ | $\Gamma_\phi$ | $S_\phi$ |
|---|---|---|---|
| Continuity | 1 | 0 | 0 |
| Momentum | $U$ | $\nu + \nu_t$ | $g\beta(T - T_\infty)$ |
| Energy | $T$ | $\frac{\nu}{Pr} + \frac{\nu_t}{\sigma_t}$ | $-\frac{1}{\rho C_p}\frac{dq_r}{dy}$ |
| Turbulent Kinetic Energy | $k$ | $\nu + \frac{\nu_t}{\sigma_k}$ | $\nu_t(\frac{\partial U}{\partial y})^2 - \epsilon + D$ |
| Rate of Dissipation of Turbulent Kinetic Energy | $\epsilon$ | $\nu + \frac{\nu_t}{\sigma_\epsilon}$ | $[C_{1\epsilon} f_1 \nu_t(\frac{\partial U}{\partial y})^2 - C_{2\epsilon} f_2 \epsilon]\frac{\epsilon}{k} + E$ |

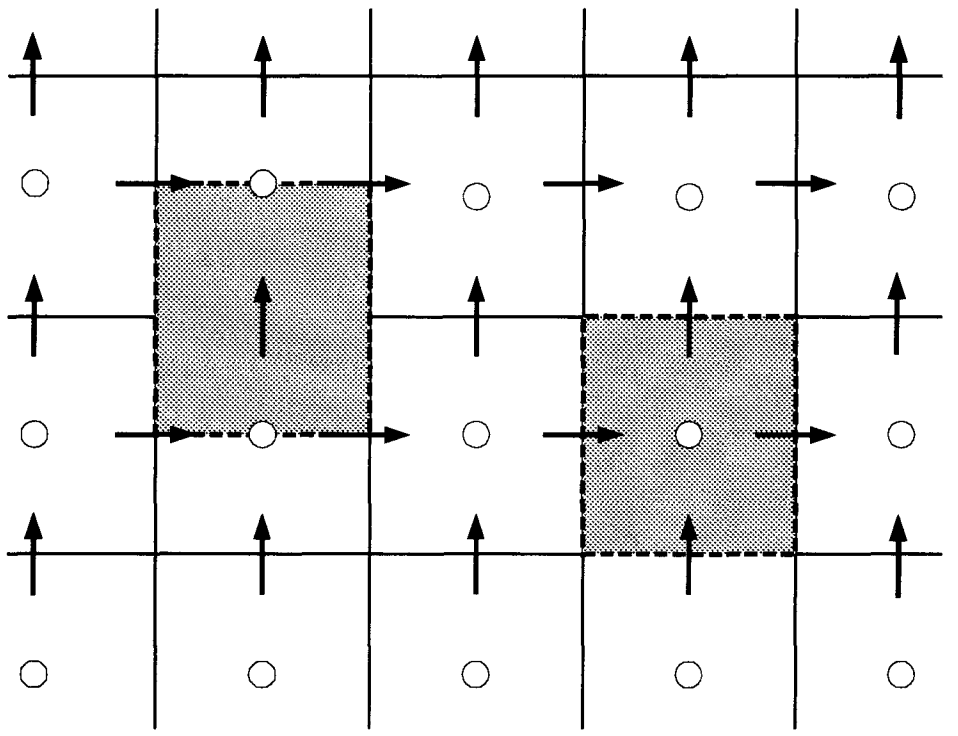

Figure 4.2: Control volumes for momentum equation (left) and all the other equations (right).

$$\int_x^{x+\Delta x}\int_y^{y+\Delta y}\int_t^{t+\Delta t}[\frac{\partial\phi}{\partial t}+\frac{\partial U\phi}{\partial x}+\frac{\partial V\phi}{\partial y}]dxdydt =$$

$$\int_x^{x+\Delta x}\int_y^{y+\Delta y}\int_t^{t+\Delta t}[\frac{\partial}{\partial y}(\Gamma_\phi\frac{\partial\phi}{\partial y})+S_\phi]dxdydt. \tag{4.11}$$

Fig. 4.2 shows two different control volumes used for this problem; one for the momentum equation, and the other for all the remaining equations. Some assumptions are necessary in order to do this integration. These assumptions are:

1. The transient term, $\frac{\partial\phi}{\partial t}$, is considered to be constant over the control volume. Therefore

$$\int_x^{x+\Delta x}\int_y^{y+\Delta y}\int_t^{t+\Delta t}\frac{\partial\phi}{\partial t}dxdydt = (\phi^1-\phi^0)\Delta x\Delta y, \tag{4.12}$$

where $\phi^0$ and $\phi^1$ represent the values of $\phi$ at times $t$ and $t + \Delta t$ respectively.

2. The first and second convective terms are constant along the $y$ and $x$ directions of the control volume respectively, and during the time interval $\Delta t$. A fully implicit method is used here. Therefore, all values are to be regarded as the values at time $t + \Delta t$

$$\int_x^{x+\Delta x}\int_y^{y+\Delta y}\int_t^{t+\Delta t}(\frac{\partial U\phi}{\partial x}+\frac{\partial V\phi}{\partial y})dxdydt = [(U\phi)_n^1-(U\phi)_s^1]\Delta y\Delta t + [(V\phi)_e^1-(V\phi)_w^1]\Delta x\Delta t. \quad (4.13)$$

The indices $n$,$s$,$e$ and $w$ indicate that the variables must be calculated at the north, south, east or west face of the control volume. An upwind scheme is used to calculate the values of $\phi$ at the interfaces of the control volume; the value of $\phi$ at an interface is equal to the value of $\phi$ at the grid point on the upwind side of the face.

3. The diffusion term is considered to be constant along the $x$-direction of the control volume and during the time period $\Delta t$. Again a fully implicit scheme is used

$$\int_x^{x+\Delta x}\int_y^{y+\Delta y}\int_t^{t+\Delta t}\frac{\partial}{\partial y}(\Gamma_\phi\frac{\partial\phi}{\partial y})dxdydt = [(\Gamma_\phi\frac{\partial\phi}{\partial y})_e^1-(\Gamma_\phi\frac{\partial\phi}{\partial y})_w^1]\Delta x\Delta t. \quad (4.14)$$

A piecewise-linear profile is assumed for the variation of $\phi$ between the adjacent grids; the value of $\frac{\partial\phi}{\partial y}$ at each face will be equal to the slope of this line. The value of diffusion coefficient, $\Gamma_\phi$, is a suitable average of the values of $\Gamma_\phi$ at neighboring points.

4. The source term is simply integrated by assuming an average value, $\overline{S_\phi}$, over the control volume and during the time period

$$\int_x^{x+\Delta x}\int_y^{y+\Delta y}\int_t^{t+\Delta t}S_\phi dxdydt = \overline{S_\phi}\Delta x\Delta y\Delta t. \quad (4.15)$$

Often the source term is a function of the dependent variable $\phi$ itself. Whether this relation is linear or not, it is always possible to linearize the relation. It is sufficient to express the average value $\overline{S_\phi}$ as

$$\overline{S_\phi} = S_C + S_P \phi^1, \tag{4.16}$$

where $S_C$ stands for the constant part of $\overline{S_\phi}$, while $S_P$ is the coefficient of $\phi^1$. The appearance of $\phi^1$ in Eq. 4.16 reveals that it is assumed that the value of $\phi^1$ prevails over the control volume and during the time period.

Substituting Eqs. 4.12-4.16 into Eq. 4.11 results in the required discretized equation.

## 4.4 Boundary Conditions

Since the fully turbulent natural convection heat transfer characteristics were the main concern of this work, the turbulent model was applied from the very leading edge of the plate.

The boundary conditions for velocities and temperature were as given below:

$$x = 0 \quad , \quad U = 0, \quad \text{and} \quad T = T_\infty,$$

$$y = 0 \quad , \quad U = V = 0, \quad \text{and} \quad T = T_w,$$

$$y = \infty \quad , \quad U = 0, \quad \text{and} \quad T = T_\infty.$$

The infinity in the numerical simulation was considered to be that distance from the plate the increase of which would not produce any important change in the final results.

Regarding the turbulent quantities, the following boundary conditions were applied wherever a $k$-$\epsilon$ model was used

$$x = 0 \quad , \quad k = \epsilon = 0,$$

$$y = 0 \quad , \quad k = 0,$$

$$y = \infty \quad , \quad \frac{\partial k}{\partial y} = \frac{\partial \epsilon}{\partial y} = 0.$$

The value of $\epsilon$ at the wall was dependent on the turbulent model which was used here. In the Jones and Launder model, $\epsilon_w = 0$; whereas in the To and Humphrey model, $\epsilon_w = 2\nu(\frac{\partial\sqrt{k}}{\partial y})^2_w$.

Difficulties were observed in reaching a turbulent solution with the low Reynolds number $k$-$\epsilon$ model. If this model were used with homogeneous boundary conditions for $k$ and $\epsilon$ at the wall and at the outer edge of the boundary layer, the solution would remain laminar. Usually a small amount of turbulent kinetic energy is introduced, along with some turbulent dissipation (balanced with shearing production of turbulence) at the specified transition point. The solution far downstream from the transition point would be independent of the amount of artificially introduced turbulent energy and even the location of the point of transition. However, in this work another method was used. Since the simple mixing-length model gives the solution in a small computational time, this model was first used to find an initial guess for $k$-$\epsilon$ model, especially an initial distribution of turbulent viscosity, $\nu_t$. In this way there was no need to specify any artificial turbulent kinetic energy and the final solution showed turbulent flow characteristics.

# Chapter 5

# RESULTS AND DISCUSSIONS-I
# TURBULENT NATURAL CONVECTION

## 5.1 Introduction

As mentioned in Section 2.3 one of the objectives of this work was to find a turbulence model that predicts fairly well the mean characteristics of the turbulent natural convection boundary layer. This chapter includes the results obtained in this investigation. Three different models were tried in this work: the algebraic mixing-length model of Cebeci and Khattab [14]; the Jones and Launder [17], and the To and Humphrey [20] low-Reynolds-number $k$-$\epsilon$ models.

Since the Jones and Launder model is supported by a large amount of experimental data from forced convection flows, most of the efforts of the present study were spent investigating how this model would predict the natural convection turbulent boundary layer.

The experimental data provided by Tsuji and Nagano [12] were used to compare the extent of accuracy of the numerical results obtained by using different models.

## 5.2 A Modification of the Jones and Launder Model

One difficulty in applying the original form of the Jones and Launder model for natural convection was observed when studying the effect of $x$-direction grid refinement on the final results. Fig. 5.1-a shows the variation of Nusselt number versus Rayleigh number

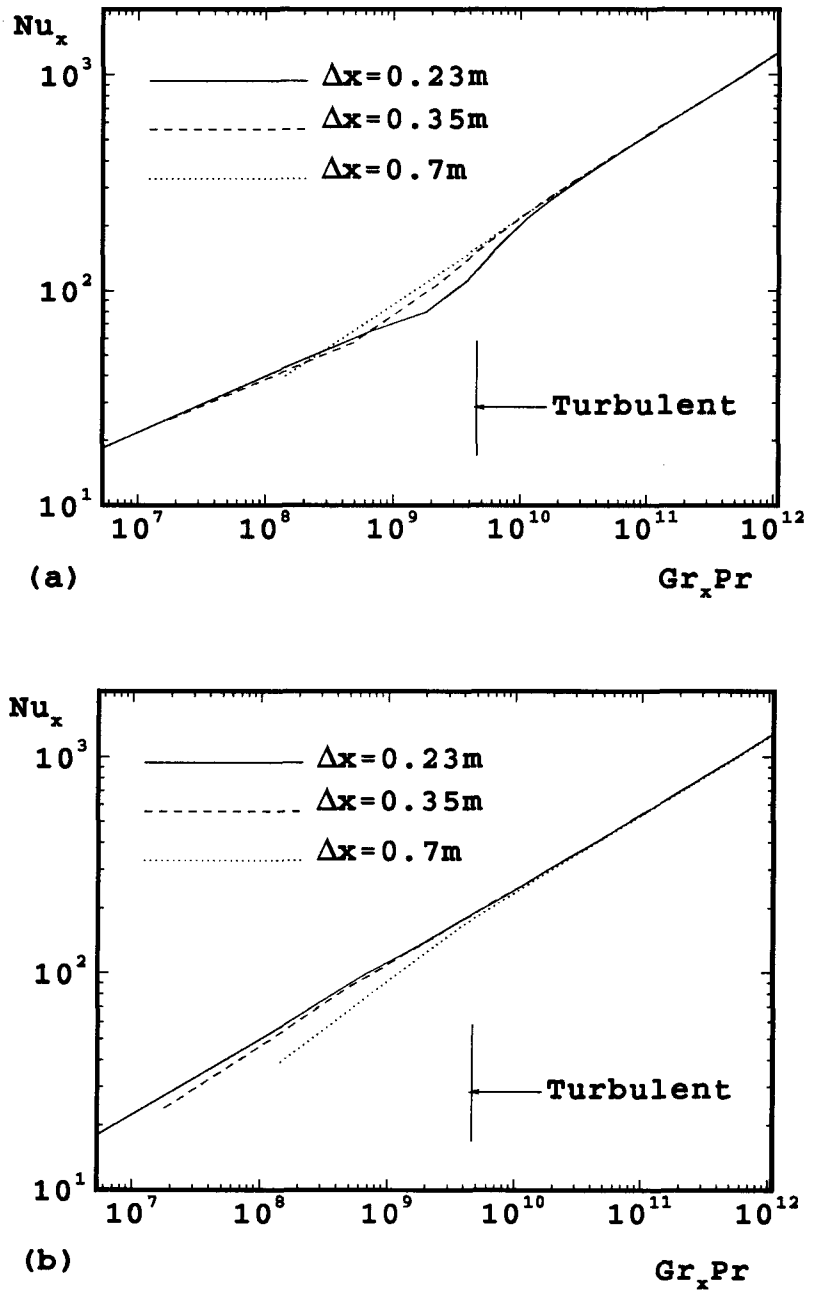


Figure 5.1: Nusselt number calculated by (a) Jones and Launder model and (b) modified Jones and Launder model.

obtained by three different sizes of grids in the $x$ direction. It is seen that as grids are refined, the transition point moves toward the end of the plate. In fact the solution would be completely laminar if the grids in $x$ direction were refined more and more. Therefore, there is no grid independent behavior in this sense.

One of the modifications that can be applied to the Jones and Launder model was first introduced by Plumb and Kennedy [16]. The wall terms, $D$ and $E$, and the $f$'s functions, in the equations of turbulent kinetic energy and rate of dissipation of turbulent energy act to damp the turbulent kinetic energy in the viscous sublayer where the molecular viscosity dominates. Plumb and Kennedy argued that in forced flows, the importance of these terms decreases as one moves toward the free stream. However, in buoyant flows, the maximum velocity occurs within the boundary layer, very close to the wall, and these terms will also influence the damping at the outer edge of the boundary layer. Therefore, they proposed applying these terms only in the region before the location of maximum velocity. Applied in this way, the model is called the modified Jones and Launder model. One concern may raise regarding the variation of turbulent quantities in the vicinity of maximum-velocity point. However, it was noted that the profiles of turbulent quantities, predicted by the modified Jones and Launder model, are smooth around the points corresponding to the maximum velocities. For a more detailed discussion and illustrative graphs the reader is referred to Appendix A.

The most important difference between the original and the modified model is that the modified model produced a $x$-direction grid independent solution. Fig. 5.1-b shows this very clearly. This is in fact the main justification for using the modified model.

It must be mentioned that the results obtained by these two forms of Jones and Launder model, for the near wall region, are almost the same at high Grashof numbers, and the original model can produce a fully turbulent solution.

## 5.3 Numerical Results

Numerical results were obtained at the same conditions reported for the experimental data [12]. Wall and free stream temperature values of $T_w = 60°C$ and $T_\infty = 16°C$ were used, and properties were calculated at the film temperature, $(T_w + T_\infty)/2$, except that $\beta$ was defined as $\frac{1}{T_\infty}$. This was consistent with the experimental data. It must be mentioned that all computations with the Jones and Launder model were so done that the results would be a fully turbulent flow. In some cases the suitable grids in the $x$ direction had to be twice as coarse as the grids used with the other models.

Fig. 5.2 shows the velocity profiles for two different Grashof numbers. The near wall region of the profiles are shown in Fig. 5.3. It is seen that the mixing-length model predicts the highest and the sharpest maximum velocity and the smallest boundary layer thickness. The location and value of the maximum velocity were predicted reasonably well by the Jones and Launder model at low Grashof number, while at high Grashof number the modified form of the Jones and Launder model was preferable. None of the models predicted well the outer part of the profile and the thickness of the boundary layer; although the prediction of the Jones and Launder model is fairly acceptable. The relatively high velocities that the modified Jones and Launder model predicts in the outer region of boundary layer can be due to an overprediction of the values of the turbulent viscosity there.

Regarding the near wall region, the best agreement with the experimental data was obtained by both forms of the Jones and Launder model. All models predicted steeper profiles at the wall than the experiments showed.

Mean velocity profiles, normalized by the friction velocity $u_\tau$, are shown in Fig. 5.4. In the turbulent forced convection boundary layer, it is well known that the relation $U^+ = y^+$ holds in the viscous sublayer, $y^+ \leq 5$. But, as can be seen in Fig. 5.4, in

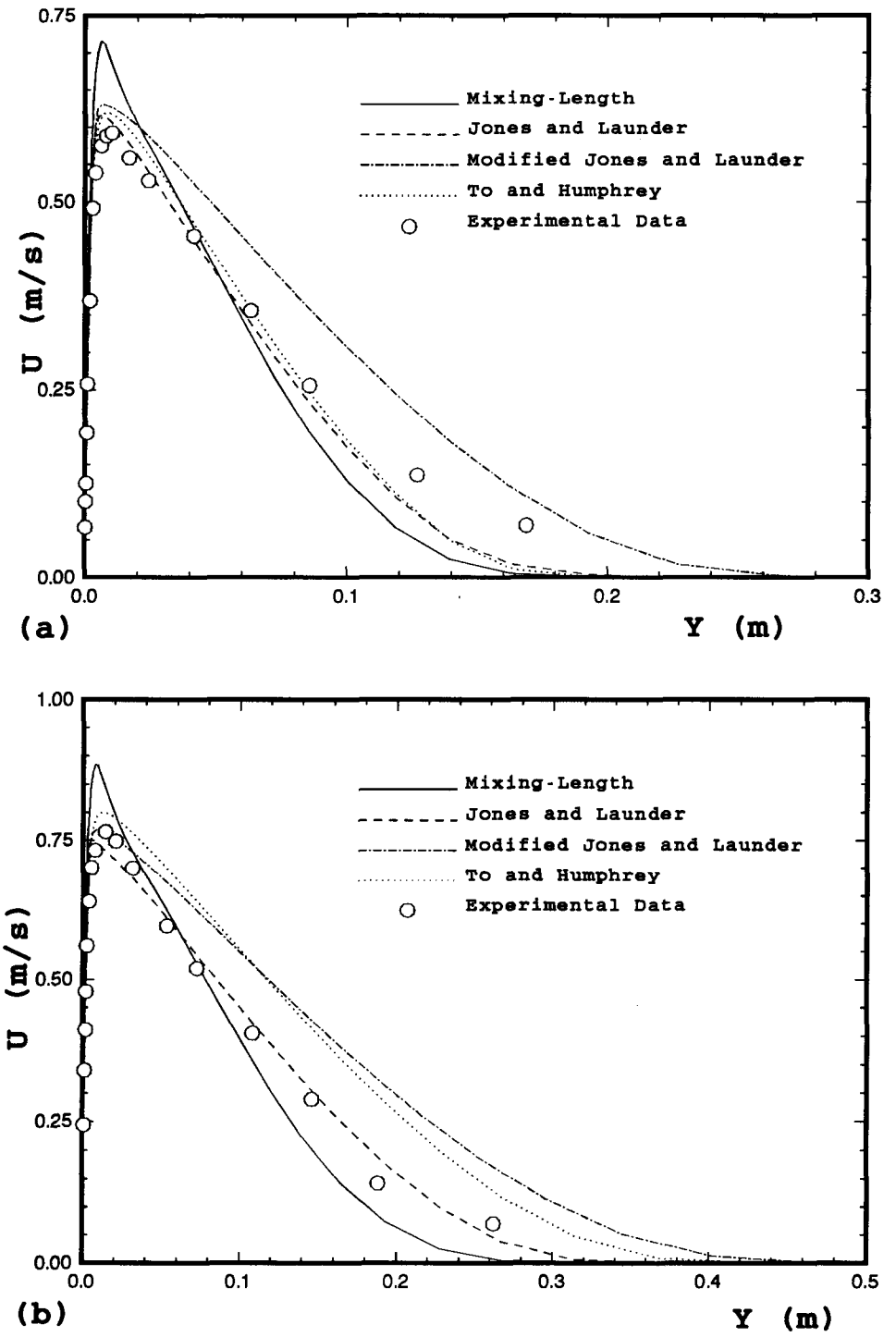


Figure 5.2: Comparison between experimental and calculated boundary layer velocity profiles; (a)$Gr_x = 3.62 \times 10^{10}$ (b)$Gr_x = 1.80 \times 10^{11}$.

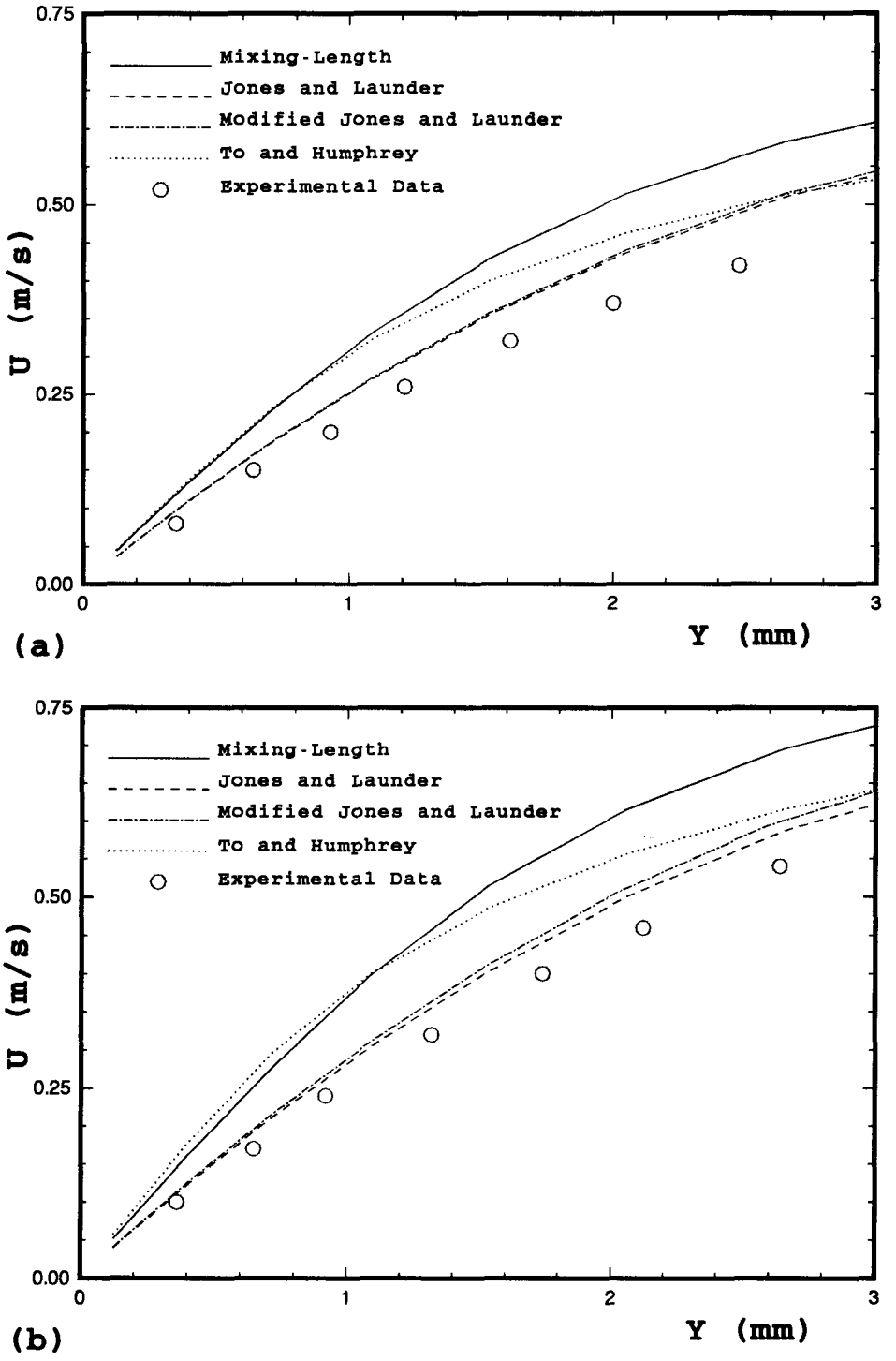


Figure 5.3: Comparison between experimental and calculated near wall velocity profiles; (a)$Gr_x = 3.62 \times 10^{10}$ (b)$Gr_x = 1.80 \times 10^{11}$.

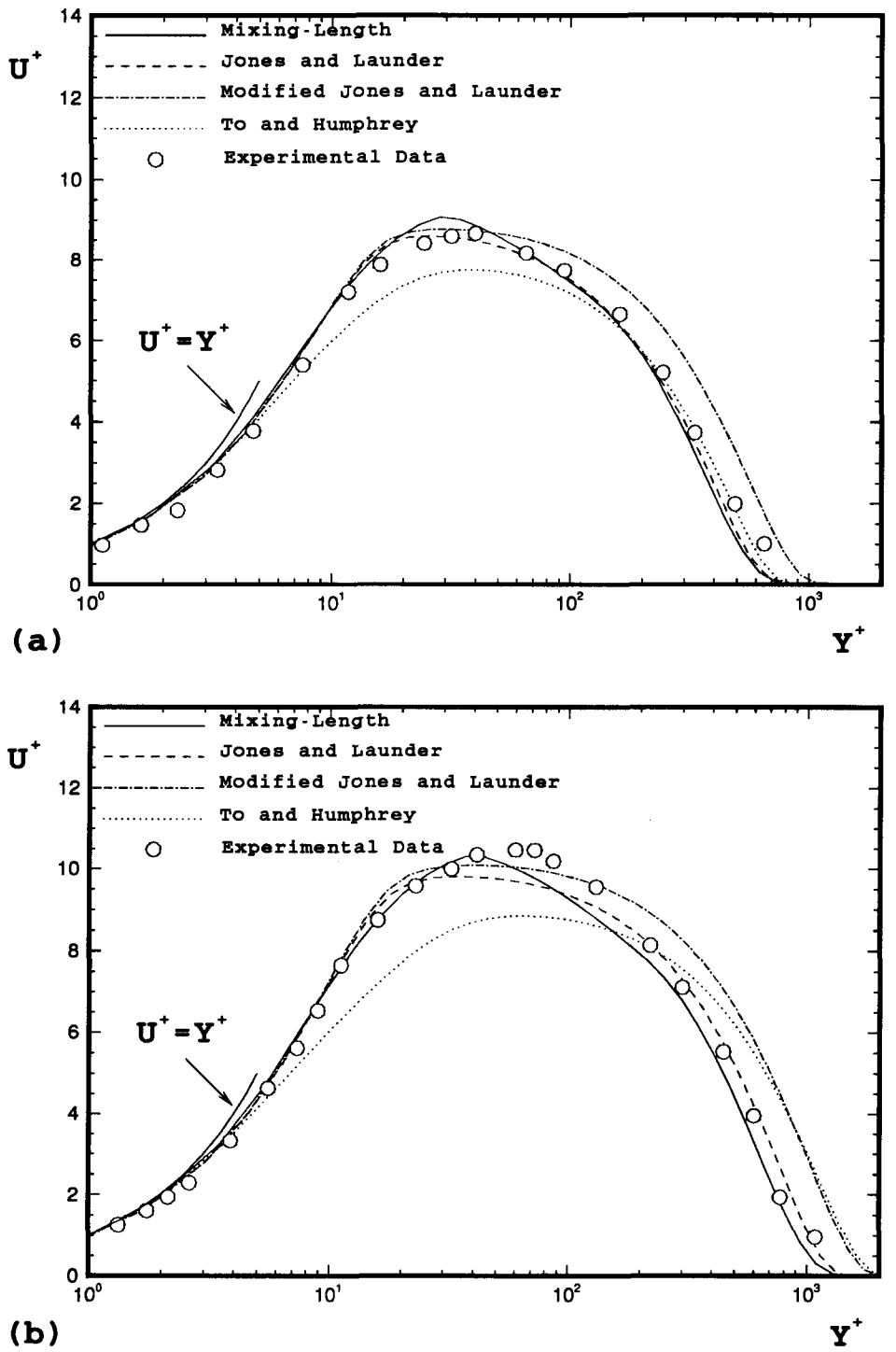


Figure 5.4: Comparison between experimental and calculated dimensionless velocity profiles; (a)$Gr_x = 3.62 \times 10^{10}$ (b)$Gr_x = 1.80 \times 10^{11}$.

the turbulent natural convection boundary layer, because of the effect of buoyancy, this relation is not valid.

Temperature profiles, $\theta = (T - T_\infty)/(T_w - T_\infty)$, for two different Grashof numbers are shown in Fig. 5.5. The near wall region of temperature profiles for two other Grashof numbers are shown in Fig. 5.6. The agreement between predicted and experimental values near the wall is excellent in the case of both forms of Jones and Launder model. The mixing-length model predicted a more gradual change in the near wall region and a steeper change in the outer layer. On the other hand, the To and Humphrey model predicted a much steeper gradient for the near wall part of the temperature profile. Regarding the shape of the outer layer, there is a fair agreement between the experimental data and the modified Jones and Launder, and To and Humphrey models.

Fig. 5.7 shows the variation of dimensionless temperature, $T^+ = (T_w - T)/t_\tau$, versus $y^+$ for two different Grashof numbers. A good agreement is seen between the experimental data and the predictions of modified Jones and Launder model. At higher Grashof number, this model and the original Jones and Launder model gave the same results. It can be shown by an analytical approach that in the viscous sublayer, which is a constant heat flux layer, the linear relation $T^+ = Pr.y^+$ describes the temperature profile. Both experimental data and computational results show this very well.

Fig. 5.8 illustrates the variation of Nusselt number versus Rayleigh number. There are different empirical relations for turbulent natural convection Nusselt number. Here, the following relation which is in very good agreement with experimental data of Tsuji and Nagano is used

$$Nu_x = 0.120(Gr_x Pr)^{1/3} \quad , \quad Gr_x Pr > 3.5 \times 10^9. \tag{5.1}$$

It is seen that the mixing-length and the To and Humphrey models give a too low and a too high Nusselt numbers respectively. The best agreement with experimental

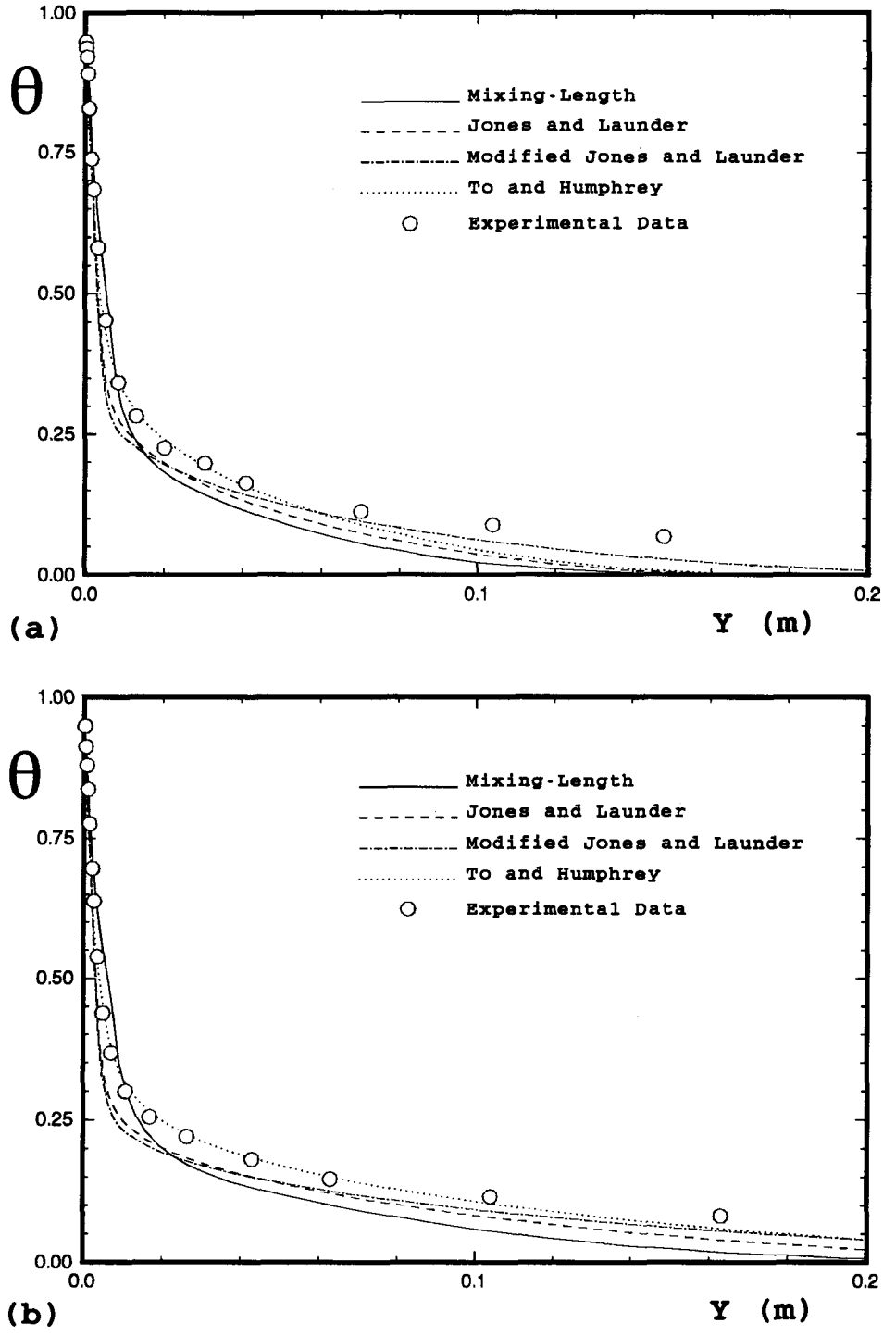


Figure 5.5: Comparison between experimental and calculated temperature profiles; (a)$Gr_x = 3.62 \times 10^{10}$ (b)$Gr_x = 1.80 \times 10^{11}$.

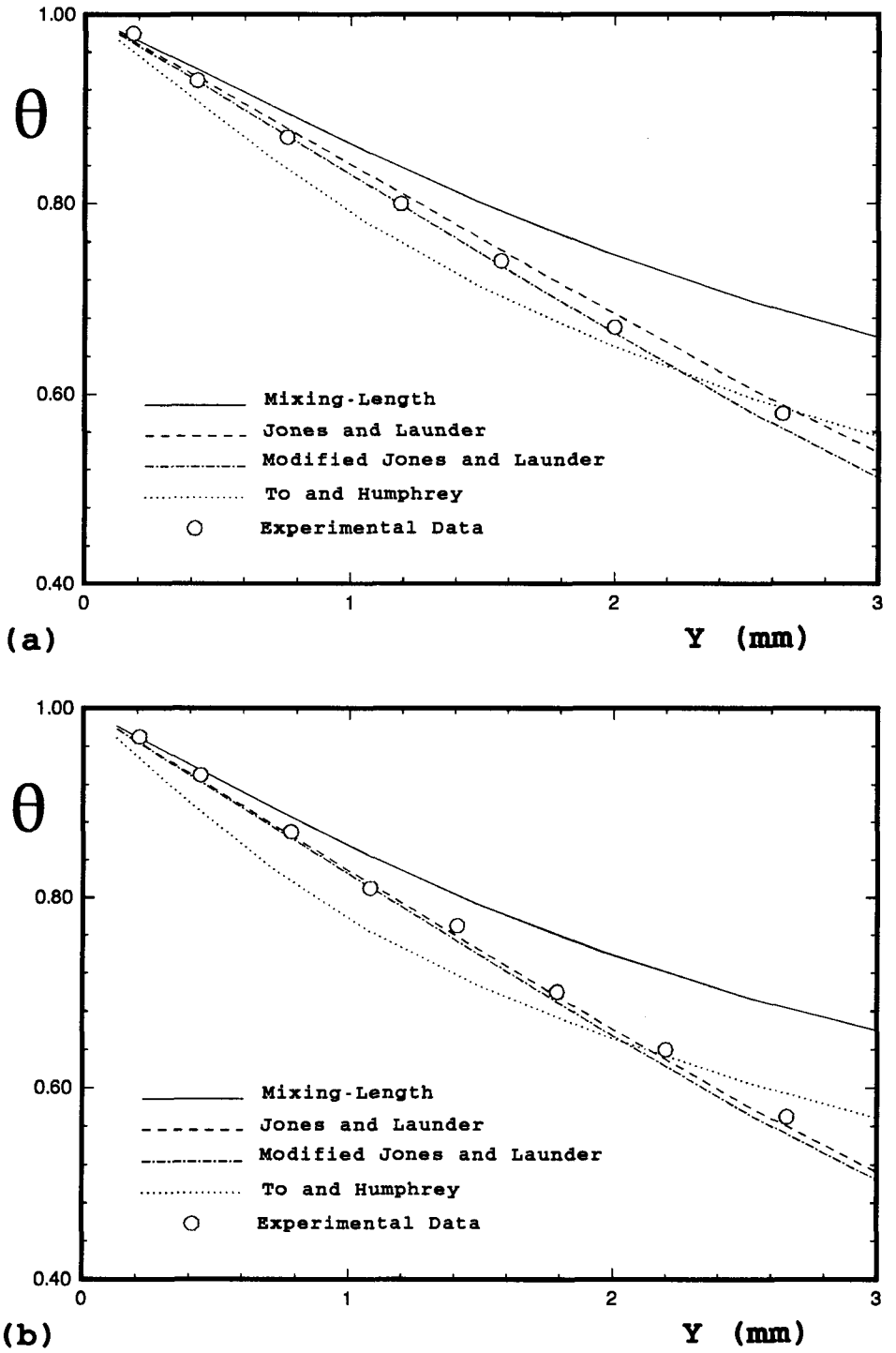


Figure 5.6: Comparison between experimental and calculated near wall temperature profiles; (a)$Gr_x = 4.10 \times 10^{10}$ (b)$Gr_x = 3.03 \times 10^{11}$.

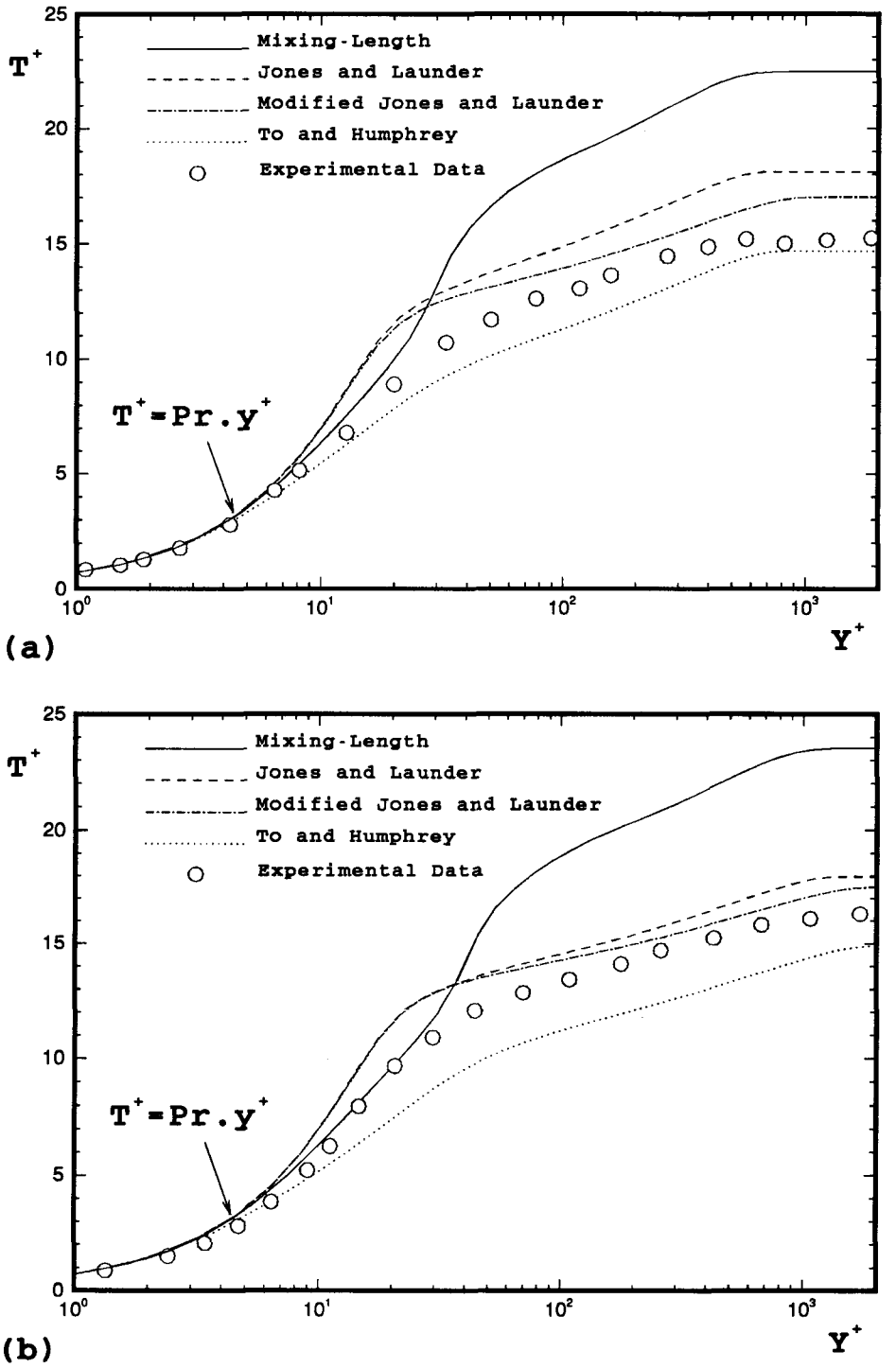


Figure 5.7: Comparison between experimental and calculated dimensionless temperature profiles; (a)$Gr_x = 3.62 \times 10^{10}$ (b)$Gr_x = 1.80 \times 10^{11}$.

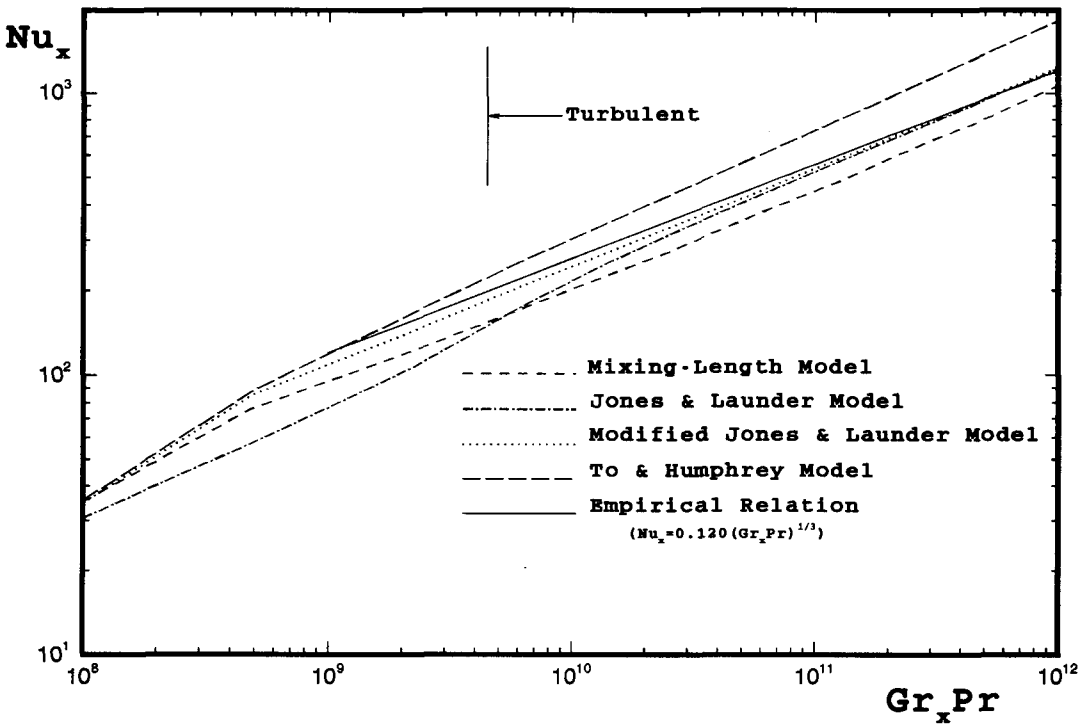


Figure 5.8: Comparison between experimental and calculated Nusselt numbers.

data was obtained by modified Jones and Launder model. The Jones and Launder model showed a late transition, whereas the modified form of this model gave a fully turbulent result for the whole range of interest. The results of these two models are the same at high Rayleigh numbers.

# Chapter 6

# RESULTS AND DISCUSSIONS-II
# NATURAL CONVECTION COUPLED WITH RADIATION

## 6.1 Introduction

In the preceding chapter it was shown that the modified Jones and Launder model is able to predict fairly well the mean characteristics of turbulent natural convection boundary layers. This model was then used to investigate the behavior of turbulent natural convection boundary layers in an absorbing and emitting gas.

The original form of Jones and Launder model was also tried in this investigation. However, the tendency of the model to give laminar solutions was even more pronounced than in the case of non-absorbing gases. Therefore, the modified model was preferred for this work.

Since the effects of gas absorptivity were the primary concern of this investigation, all other properties were assumed to be constant when the absorption coefficient was changed. While this assumption may seem unrealistic, this ensures that all the changes between the two different conditions were as a result of the change in the absorption coefficient of the gas. Since the absorption coefficient of a gas mixture is proportional to the partial pressure of the absorptive gases, it may be possible in some cases to find different mixtures with the same molecular properties but different absorption coefficients.

Carbon dioxide was chosen as the absorbing gas because it is the strongest among the gases whose Planck mean absorption coefficients are known. By keeping all properties

constant and changing the absorption coefficient of the gas the effects of gas absorptivity were investigated. It should be noted that the absorption coefficient of a gas indicates two important characteristics of radiative heat transfer: strength, and thickness of the radiative layer. A higher absorption coefficient signifies a stronger radiative heat flux and a thinner radiative layer.

## 6.2 Laminar Regime

The numerical calculation of laminar flows is much easier and faster than that of turbulent flows. On the other hand, the effects of thermal radiation upon the laminar natural convection boundary layer of an absorbing and emitting gas are easier to understand and to elaborate. Therefore, if the calculated results for the laminar regime are physically correct, the same conclusion might be drawn for the turbulent regime. This assumption is supported by two facts. First, the turbulence model was able to predict the flow fairly well without radiation. Second, the radiation only appears as a source term in the thermal energy equation and it has no direct effect on the equations of turbulence modeling.

The calculations of laminar flow were only done for the low wall temperature; $T_w = 60°C$ and $T_\infty = 25°C$. It should be mentioned that carbon dioxide is very absorptive at this temperature. The Planck mean absorption coefficient of $CO_2$ at this temperature and atmospheric pressure is about $32m^{-1}$. The integral form of the radiant energy flux, Eq. 4.8, was used.

Fig. 6.1 shows the velocity profiles of a laminar natural convection boundary layer for different values of absorption coefficients. It is seen that as the absorption coefficient increases, the maximum velocity and the level of velocities close to the wall increase

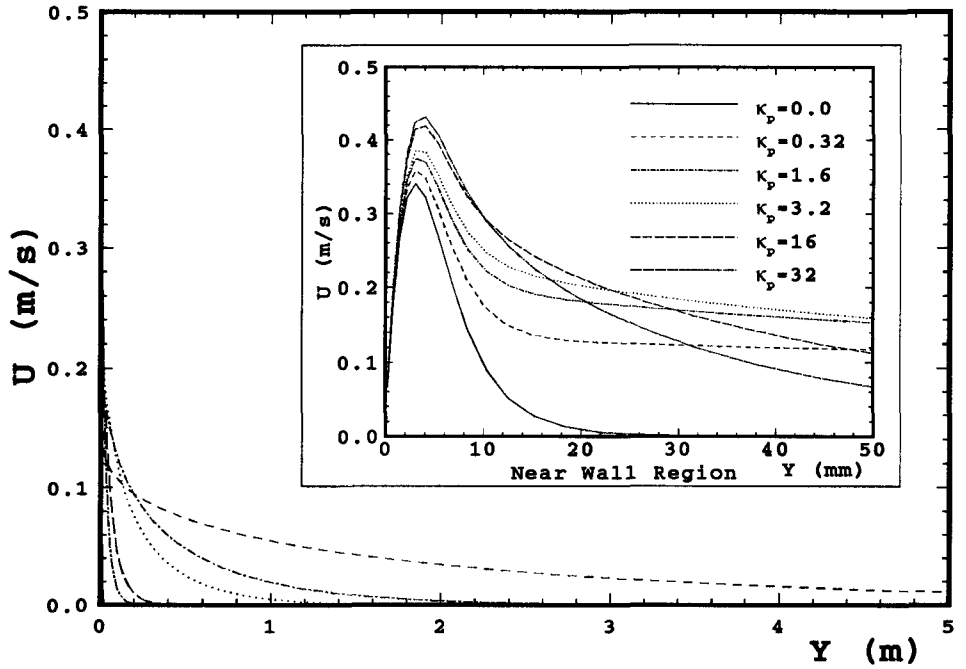


Figure 6.1: Laminar natural convection boundary layer velocity profiles in an absorbing and emitting gas, $Gr_x = 5.81 \times 10^8$.

monotonically. On the other hand, in the outer part of boundary layer the lower absorptivities correspond to the higher velocities. In fact, the thickness of this part of boundary layer, which may be called the radiative layer, increases as the absorptivity decreases. This is simply explained by referring to Fig. 6.2, which shows the net radiant energy input to the gas. If the gas is very absorptive, the largest part of radiant energy is absorbed by the gas near the wall; and farther from the wall there will be no trace of radiant energy emitted by the wall. However, with small absorptivity, the effects of radiation will be small but the range of these effects will go much farther.

Fig. 6.3 shows the temperature profiles corresponding to the velocity profiles shown in Fig. 6.1. It is again seen that the temperatures near the wall increase as the absorption coefficient increases. However, these changes are very small in the region very close to the wall while farther away there are appreciable increases in temperature levels,

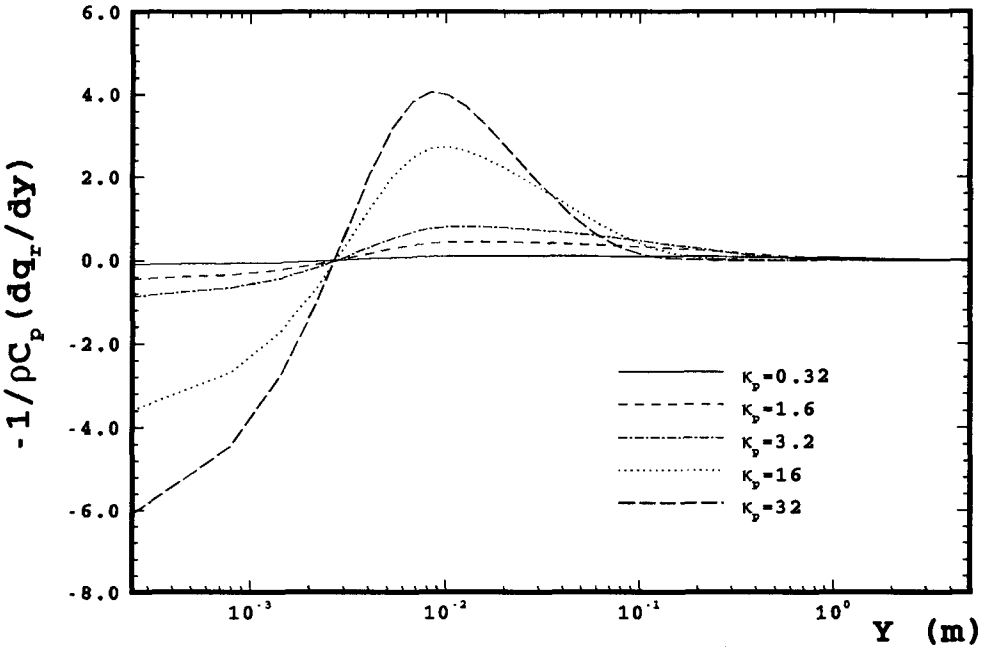


Figure 6.2: Net radiative energy input to fluid in a laminar natural convection boundary layer, $Gr_x = 5.81 \times 10^8$.

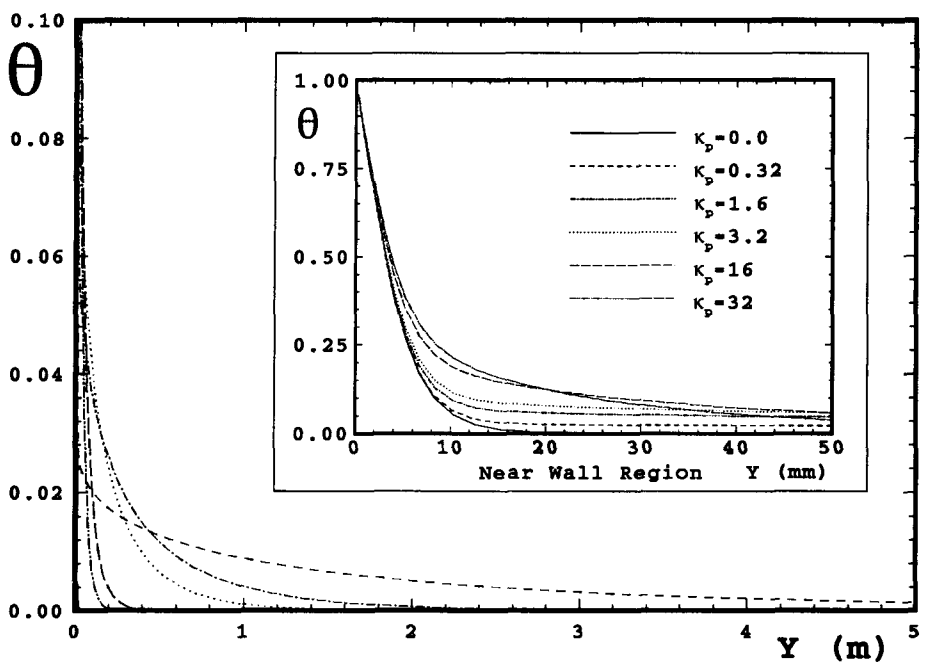


Figure 6.3: Laminar natural convection boundary layer temperature profiles in an absorbing and emitting gas, $Gr_x = 5.81 \times 10^8$.

especially for higher absorption coefficients. In the outer part of boundary layer, the lower absorptivities correspond to the higher temperatures.

An interesting point in Fig. 6.2 is that very close to the wall the radiative source term of energy equation is negative and therefore, the radiative heat flux is positive. This means that the gas in this region is more emissive than absorptive. This is because the temperature difference between the wall and the gas, in this region, is smaller than the difference between the gas and the medium temperature.

The point mentioned above may seem to be in contradiction with the increase of temperatures close to the wall; a negative source term in the energy equation is supposed to decrease the temperatures whereas we see that the temperatures slightly increase as absorption coefficient increases, see Fig. 6.3. However, a close look at Fig. 6.2 reveals that the region in which the energy source term is negative is much smaller than that in which it is positive. It seems that the higher temperatures produced as a result of positive source terms are able to diffuse toward the wall and compensate the effect of negative source term very close to the wall.

The variation of convective Nusselt number versus Rayleigh number is shown in Fig. 6.4. It is seen that, except for very small values of absorption coefficient, the convection heat transfer slightly decreases as the absorption coefficient increases. The increase of Nusselt numbers in the case of $\kappa_p = 0.32m^{-1}$ are very small. It can be just a computational error or a result of negative source term close to the wall. Fig. 6.5 shows that the radiation heat transfer decreases as the absorptivity increases. This is a well known fact that an absorbent gas operates like a shield against radiation heat transfer.

A well known behavior of laminar natural convection boundary layers is their self-similar nature. The velocity or temperature profiles for different Grashof numbers can be represented by a single curve if they are scaled suitably. This behavior was investigated for the present problem. Fig. 6.6 shows the dimensionless velocity and temperature profiles

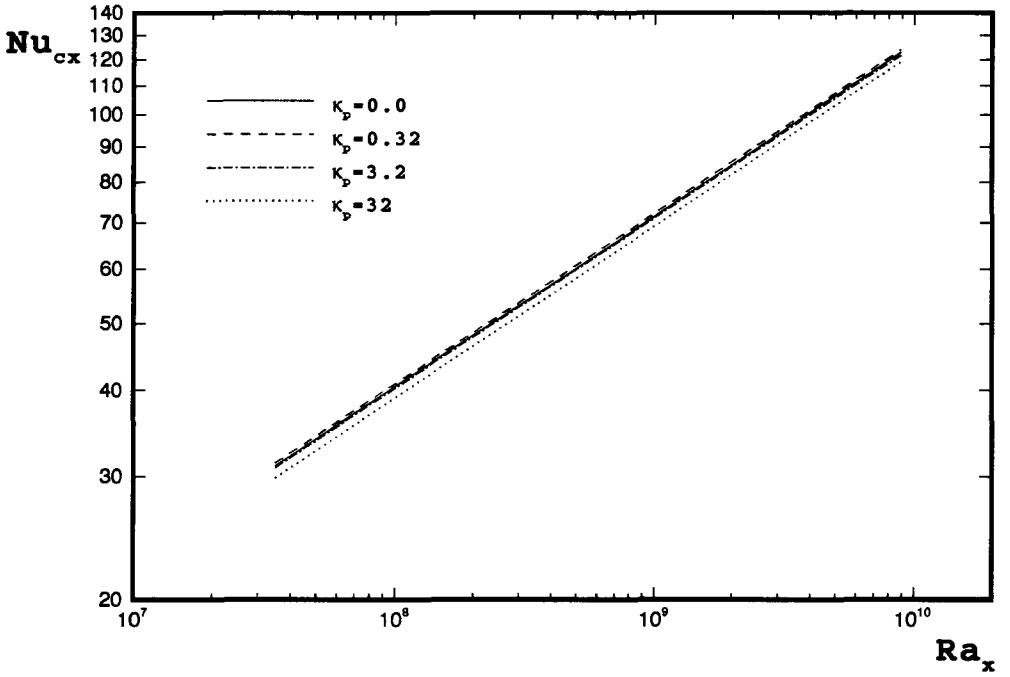


Figure 6.4: Convective Nusselt number in laminar natural convection boundary layer.

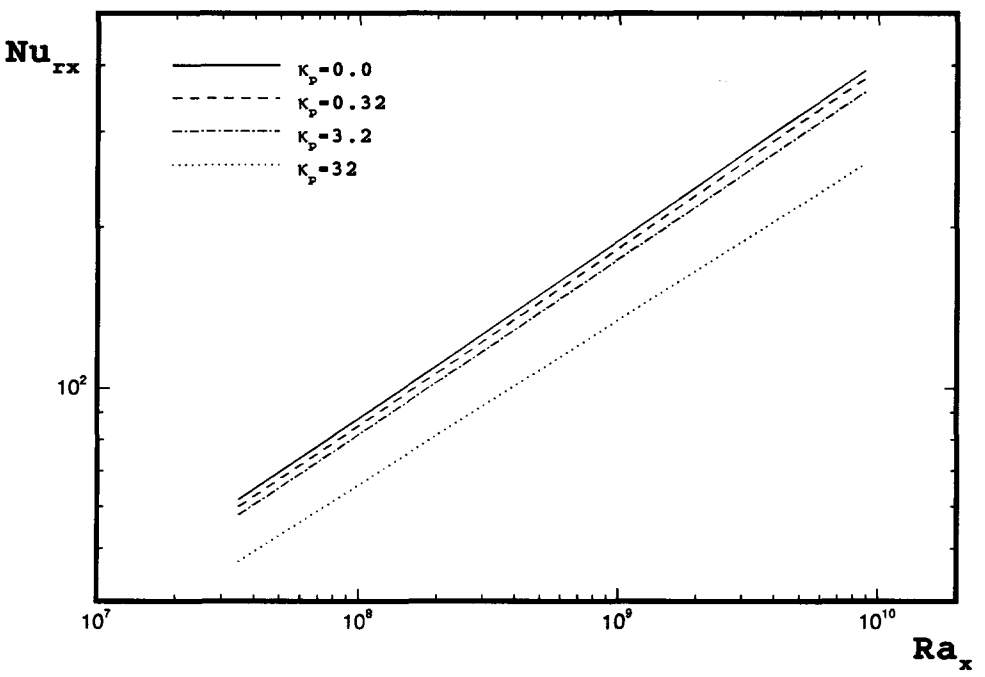


Figure 6.5: Radiative Nusselt number in laminar natural convection boundary layer.

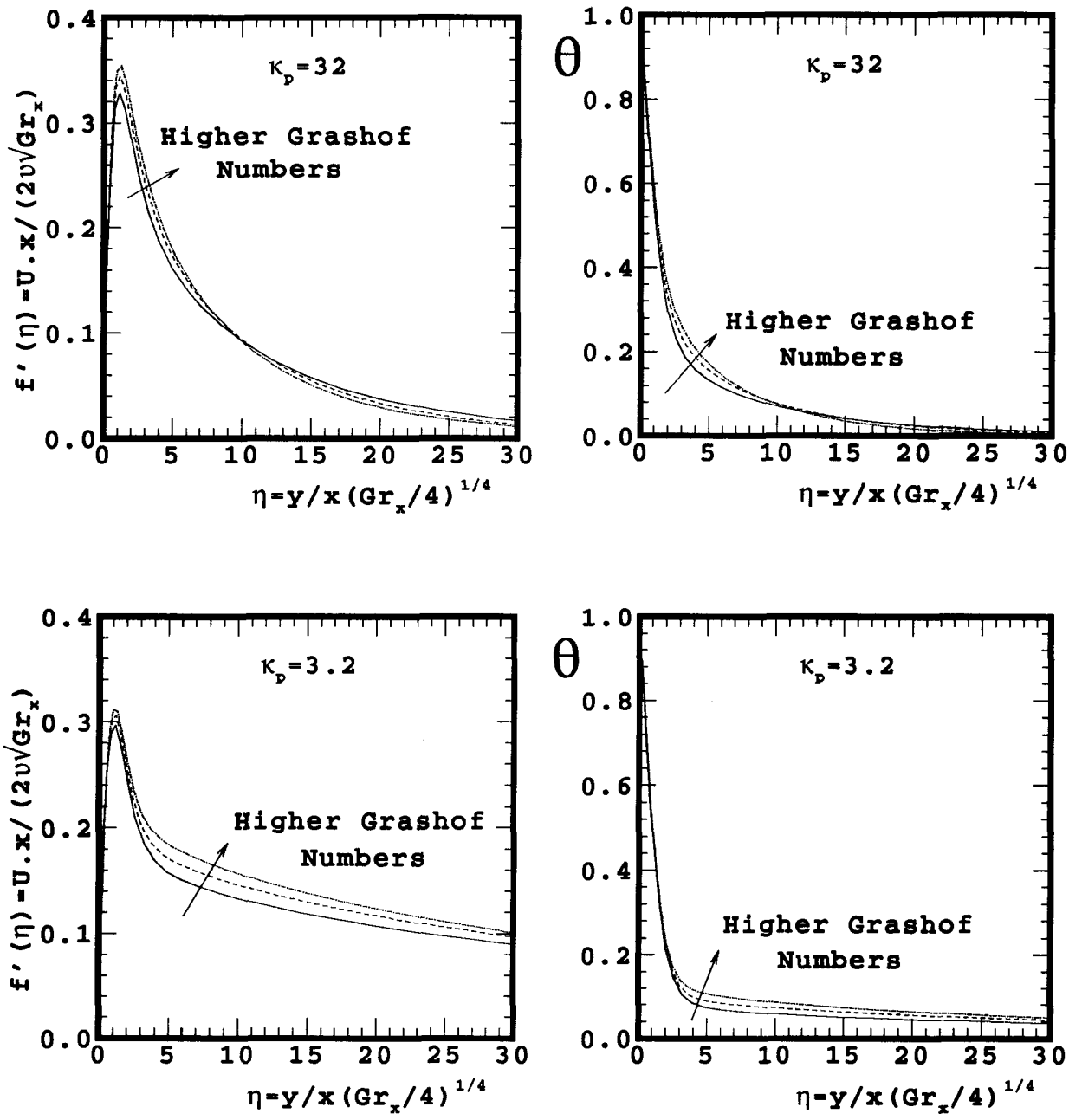


Figure 6.6: Velocity and temperature profiles of laminar natural convection boundary layer in terms of similarity variables ($Gr_x = 4.57 \times 10^7, 1.23 \times 10^9$ and $1.16 \times 10^{10}$).

for two different values of absorption coefficients. It is seen that there is a deviation from the classical similarity solution.

## 6.3 Differential Approximation Method for Laminar Regime

Using the integral formulation of the radiative heat flux made the computational time very long, even for the laminar regime. It could be expected that the turbulent calculation would need much more time. On the other hand, the differential approximation method is now widely used in problems involving radiation heat transfer. Therefore, an attempt to solve the present problem was made using the differential approximation method, and to compare the results with those already obtained by using the integral formulation of the radiative heat flux.

Figs. 6.7-6.9 compare the calculated velocity profiles as well as the variation of radiative heat flux for a typical laminar Grashof number, $Gr_x = 1.23 \times 10^9$. A range of

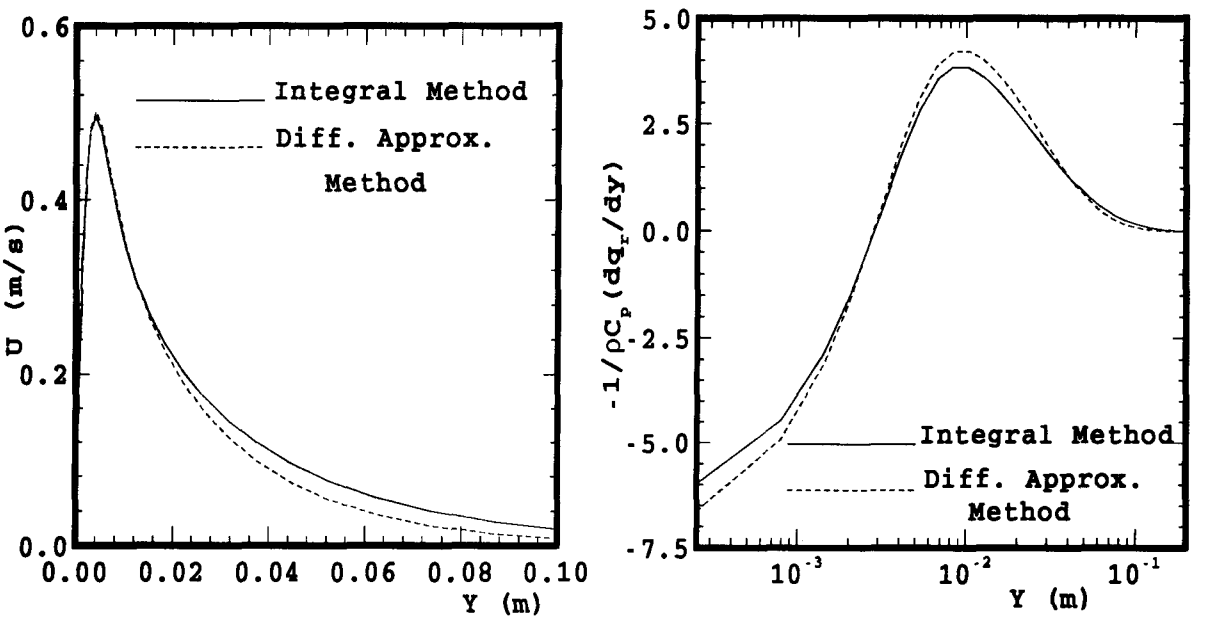


Figure 6.7: Comparison between the results obtained by using integral and differential approximation forms of the radiative heat flux, $\kappa_p = 32m^{-1}$.

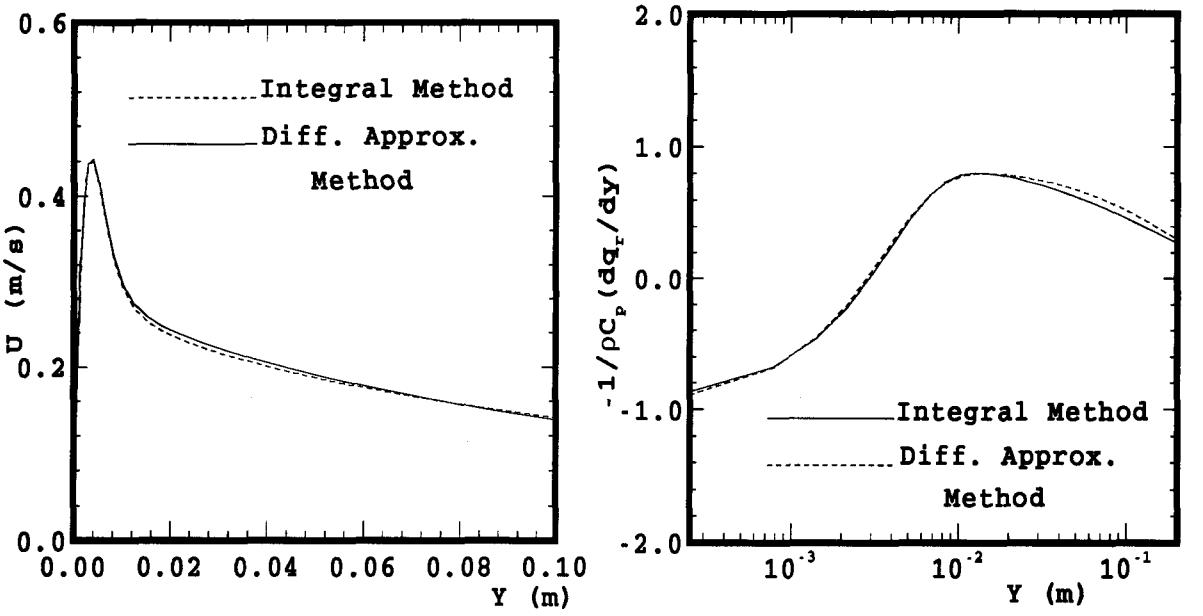


Figure 6.8: Comparison between the results obtained by using integral and differential approximation forms of the radiative heat flux, $\kappa_p = 3.2m^{-1}$.

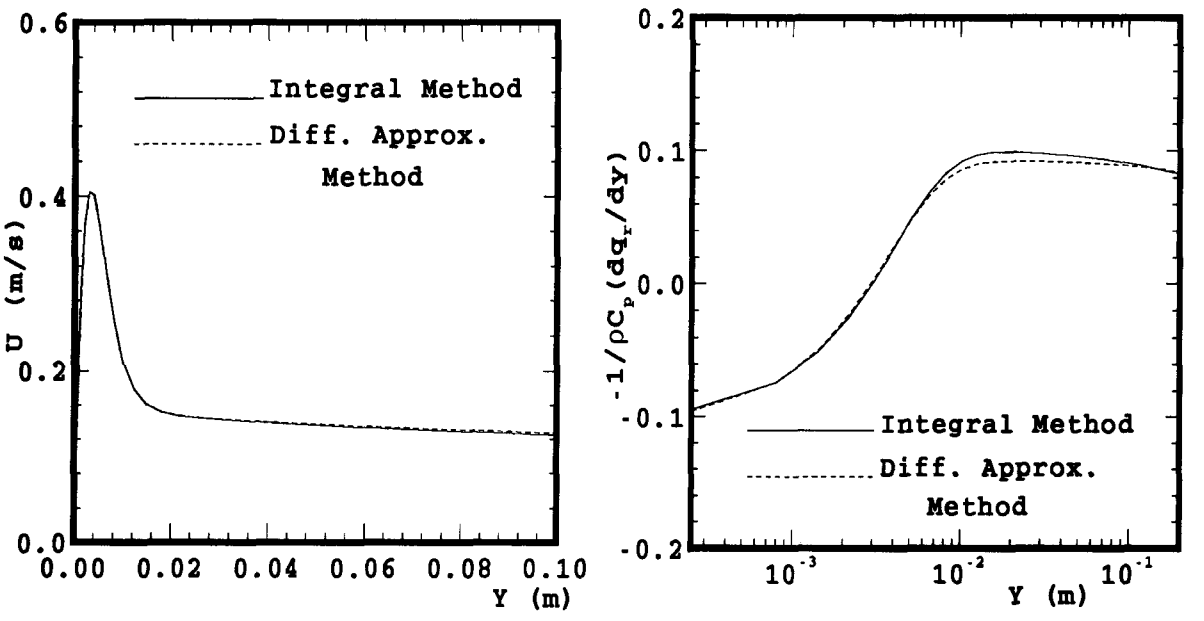


Figure 6.9: Comparison between the results obtained by using integral and differential approximation forms of the radiative heat flux, $\kappa_p = 0.32m^{-1}$.

absorption coefficients from high to low values are covered by these Figures. As far as the near wall region is concerned, good agreements between the velocity profiles obtained by the two different methods are seen. Regarding the outer layer, the agreement is very good in the case of moderate and low absorption coefficients. This agreement is fairly acceptable when absorption coefficient is high, Fig. 6.7. Therefore, it is concluded that the results obtained by using the differential approximation of radiative heat flux are nearly equivalent to those obtained by using the integral form of radiative heat flux.

## 6.4 Turbulent Regime

Turbulent natural convection boundary layer flow in an absorbing and emitting gas was calculated using the modified Jones and Launder turbulence model. The calculations were done for two different wall temperatures, low and high, to investigate the effects of temperature on the final results. The differential approximation method was used for the calculation of radiative heat flux.

### 6.4.1 Low Wall Temperature

This section includes the results obtained for wall temperature of $T_w = 60°C$ and medium temperature of $T_\infty = 25°C$. As mentioned before, gases like $CO_2$ and water vapor can strongly absorb and emit radiative energy even at these low temperatures.

Fig. 6.10 illustrates the velocity and temperature profiles for a typical turbulent Grashof number, $Gr_x = 4.24 \times 10^{11}$. The region very far from the wall is not shown here because that region is only a radiative layer and very similar to that in the laminar flow, see Figs. 6.1 and 6.3. It is seen that, as the absorption coefficient increases the velocities in the boundary layer increase at least up to some values of absorption coefficient. This is very similar to the behavior observed in the laminar regime. But, with higher absorption

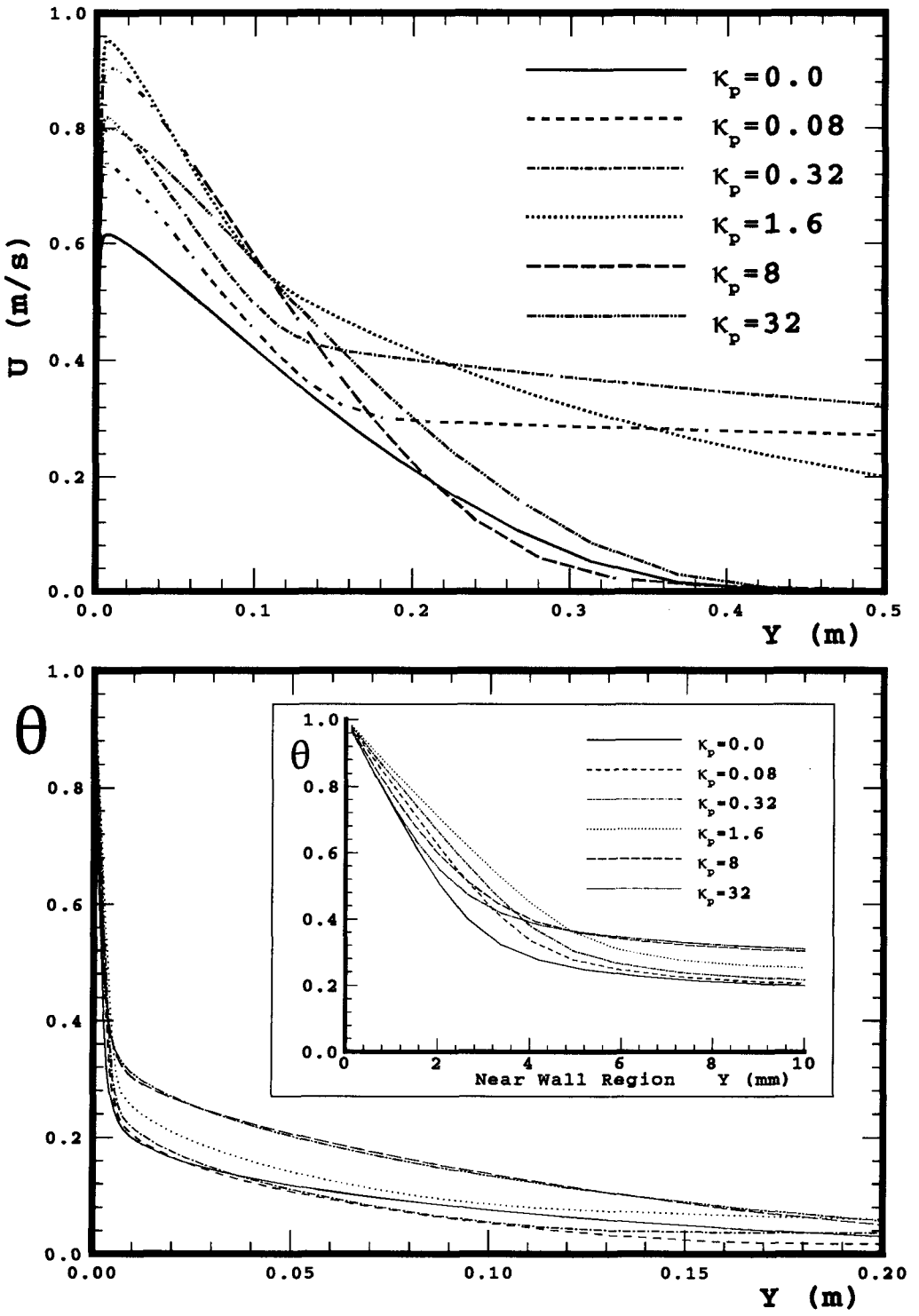


Figure 6.10: Turbulent natural convection velocity and temperature profiles in an absorbing and emitting gas, $T_w = 60°C$ and $Gr_x = 4.24 \times 10^{11}$.

coefficients the velocities start becoming smaller and smaller. In Fig. 6.10 velocities increase as the absorption coefficient increases from $\kappa_p = 0.0m^{-1}$ to $\kappa_p = 1.6m^{-1}$ and they decrease as the absorption coefficient goes from $\kappa_p = 8m^{-1}$ to $\kappa_p = 32m^{-1}$. The value of the absorption coefficient which produces the highest maximum velocity must be between $\kappa_p = 1.6m^{-1}$ and $\kappa_p = 8m^{-1}$. It seems that the velocity profile for a non-absorbing gas is the limit of velocity profiles in an absorbing and emitting gas both for very high and very low absorption coefficients. When the absorption coefficient is very low, the effect of gas radiation is very small and therefore the boundary layer will be similar to a non-absorbing one (the optically thin limit). On the other hand, if the absorption coefficient is very high, the effect of radiation will be limited to a very small region close to the wall (the optically thick limit). Thus, most of the boundary layer does not sense any radiative heat transfer and behaves as a non-absorbing gas. Fig. 6.11 shows that for high values of absorption coefficients the radiative heat flux vanishes at a small distance from the wall, inside the boundary layer.

If we look at Figs. 6.1 and 6.2 again, it can be seen that even in the case of high absorption coefficients, the radiative heat flux has a non-zero value in the whole range of boundary layer and even beyond that. This means that the laminar boundary layer operates similar, but not exactly, to an optically thin layer. Clearly, this is not the case for a turbulent boundary layer. A turbulent boundary layer may be an optically thin, thick or intermediate layer based on the physical thickness of the layer and the value of the absorption coefficient of the gas.

The near wall region of the temperature profiles, shown in Fig. 6.10, shows that as the absorption coefficient increases, temperature gradients at the wall decrease up to $\kappa_p = 1.6m^{-1}$. This behavior is similar to that observed with laminar flow. With higher absorptivities, the temperature gradient at the wall starts increasing again. This can be related to the strong negative source term in the energy equation in this region. In fact,

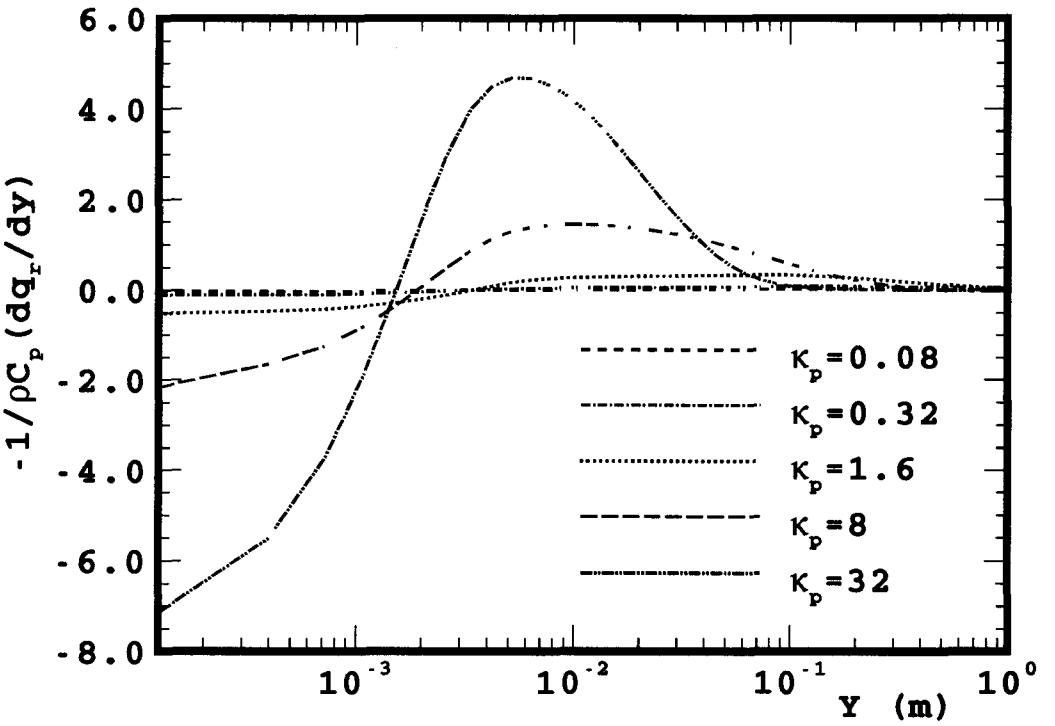


Figure 6.11: Net radiative energy input to fluid in the turbulent natural convection of an absorbing and emitting gas, $T_w = 60°C$ and $Gr_x = 4.24 \times 10^{11}$.

for very high absorptivities, this temperature gradient could be higher than that in a non-absorbing gas.

Fig. 6.12 shows the variation of turbulent viscosity in the boundary layer. It is seen that for some values of absorption coefficients, turbulent viscosities are much smaller than those in a non-absorbing gas. If we look at Fig. 6.10, it will be noted that those values of absorption coefficients that correspond to small turbulent viscosities are those which produce a more flattened velocity profiles in the outer part of the boundary layer. Since turbulence production is a function of the amount of shear in the flow, the almost uniform flows produced in this region contribute less in turbulence production. Therefore, turbulent viscosities will be lower compared to those in a non-absorbing gas. On the othe hand, if the absorption coefficient is high enough so that radiation effects remain inside the boundary layer, turbulent viscosities may increase because of higher maximum

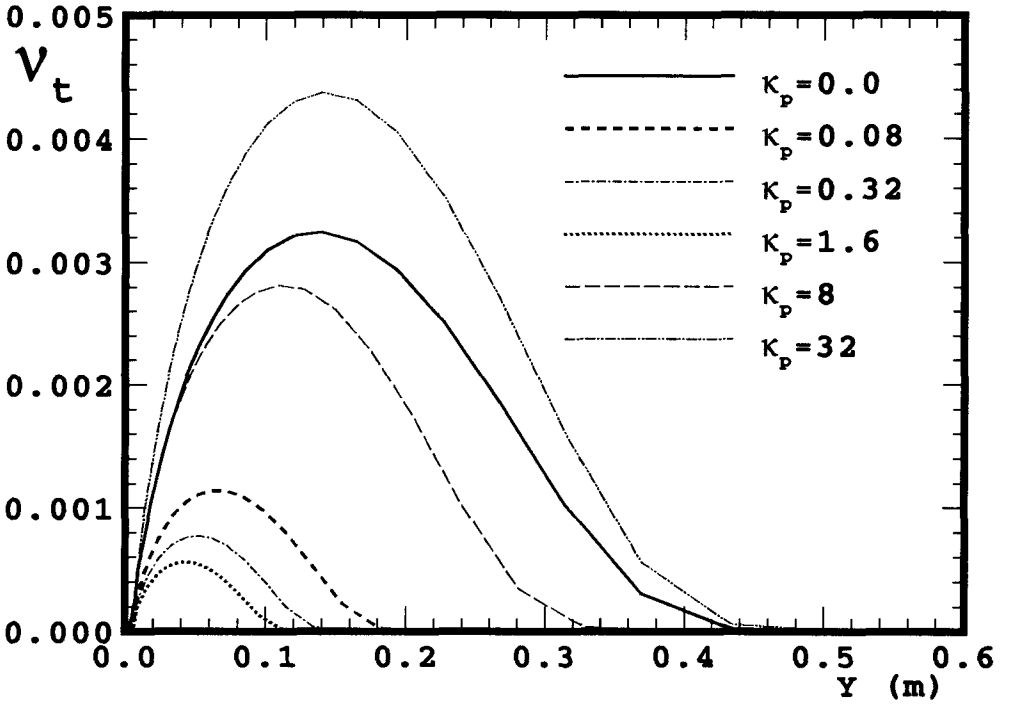


Figure 6.12: Turbulent viscosity in the natural convection boundary layer of an absorbing and emitting gas, $T_w = 60°C$ and $Gr_x = 4.24 \times 10^{11}$.

velocities and higher shear production of turbulence.

There is another important difference between the effects of radiation on turbulent and laminar boundary layers. The changes in velocities and temperatures for turbulent flows are greater than those observed in laminar flow. This can be explained by considering the effect of turbulent viscosity and turbulent thermal diffusivity, which are much higher than the corresponding values in the laminar regime.

The behavior of a turbulent natural convection boundary layer in an absorbing and emitting gas is very much dependent on the value of Grashof number. The thickness of the boundary layer in a non-absorbing gas is proportional to the value of Grashof number. Therefore, as the Grashof number increases, the boundary layer becomes an optically thick layer even for smaller values of absorption coefficients. Figs. 6.13-6.17 show the velocity, temperature, turbulent viscosity and radiative heat flux for five different Grashof

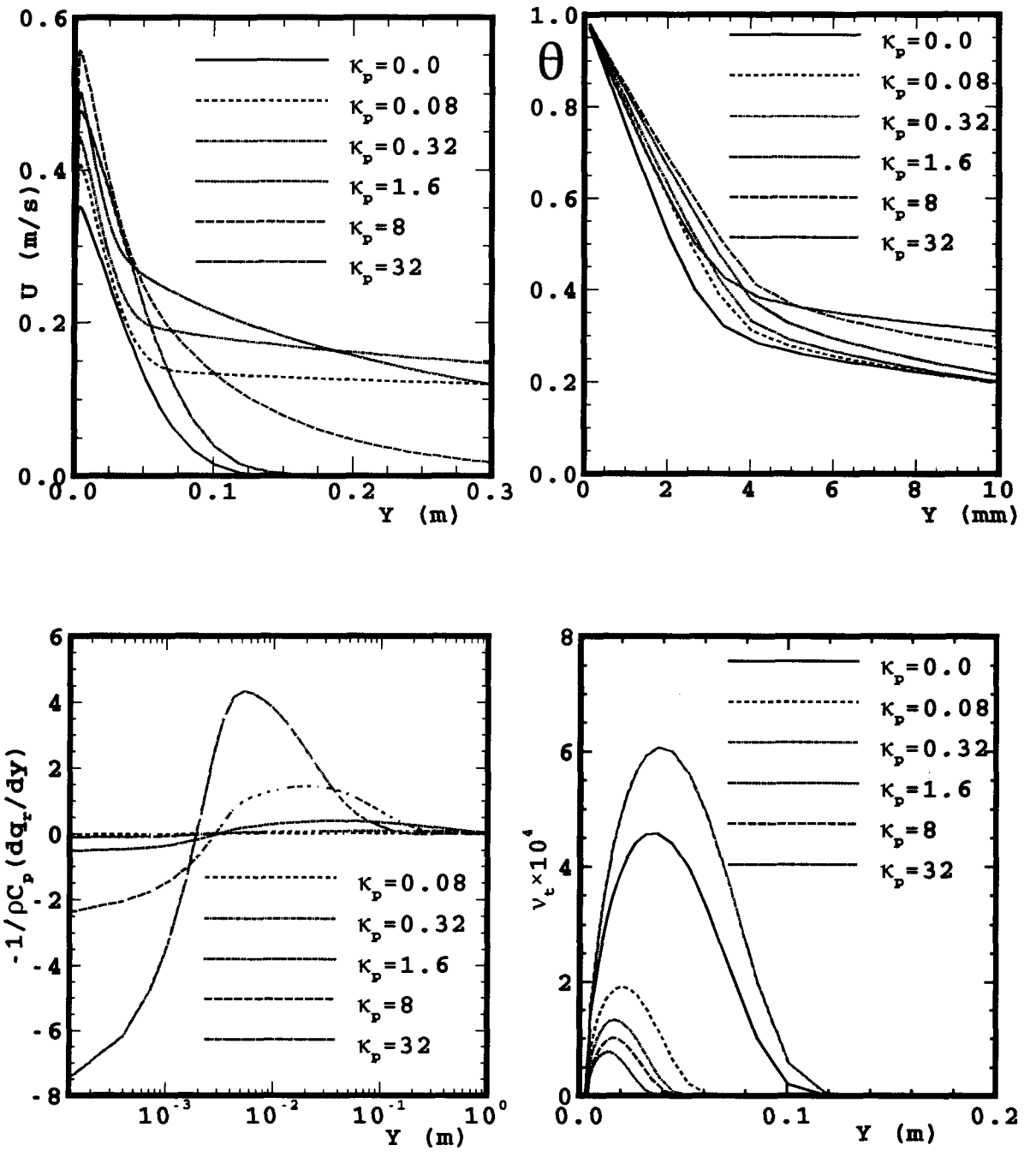


Figure 6.13: Velocity, temperature, net radiative energy to fluid and turbulent viscosity in absorbing and emitting gases with different absorption coefficients, $Gr_x = 5.72 \times 10^9$.

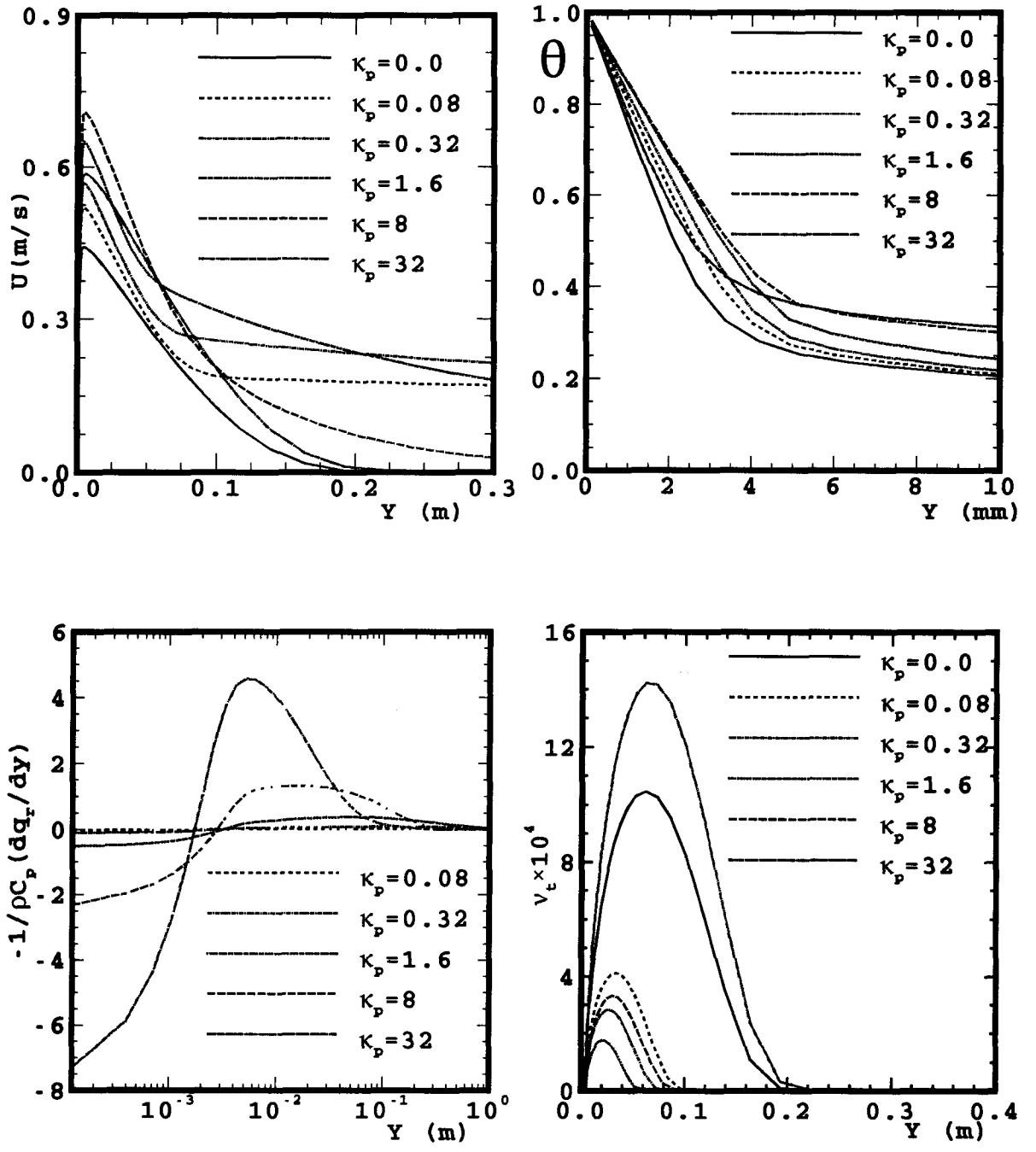


Figure 6.14: Velocity, temperature, net radiative energy to fluid and turbulent viscosity in absorbing and emitting gases with different absorption coefficients, $Gr_x = 3.33 \times 10^{10}$.

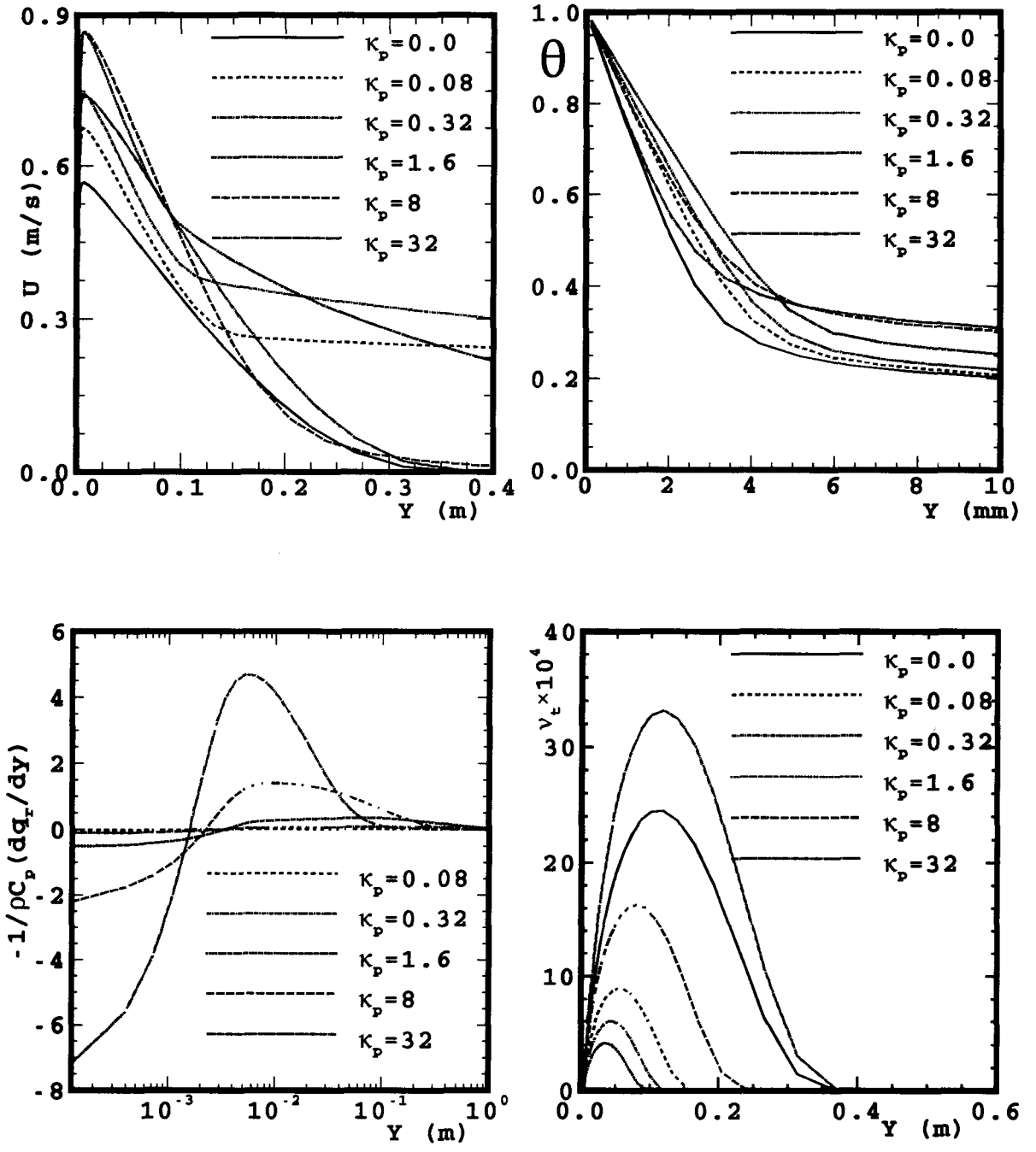


Figure 6.15: Velocity, temperature, net radiative energy to fluid and turbulent viscosity in absorbing and emitting gases with different absorption coefficients, $Gr_x = 2.25 \times 10^{11}$.

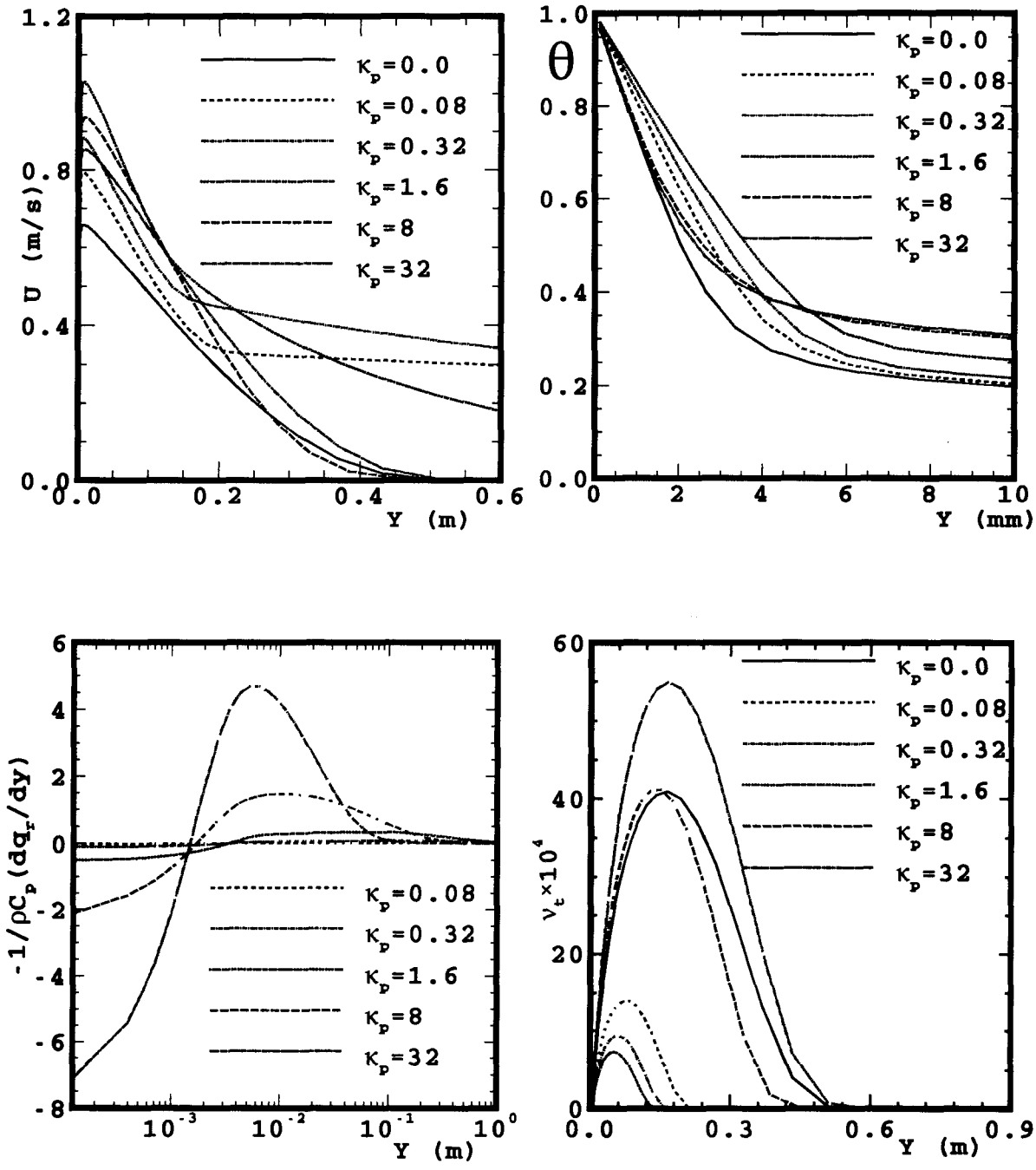


Figure 6.16: Velocity, temperature, net radiative energy to fluid and turbulent viscosity in absorbing and emitting gases with different absorption coefficients, $Gr_x = 7.15 \times 10^{11}$.

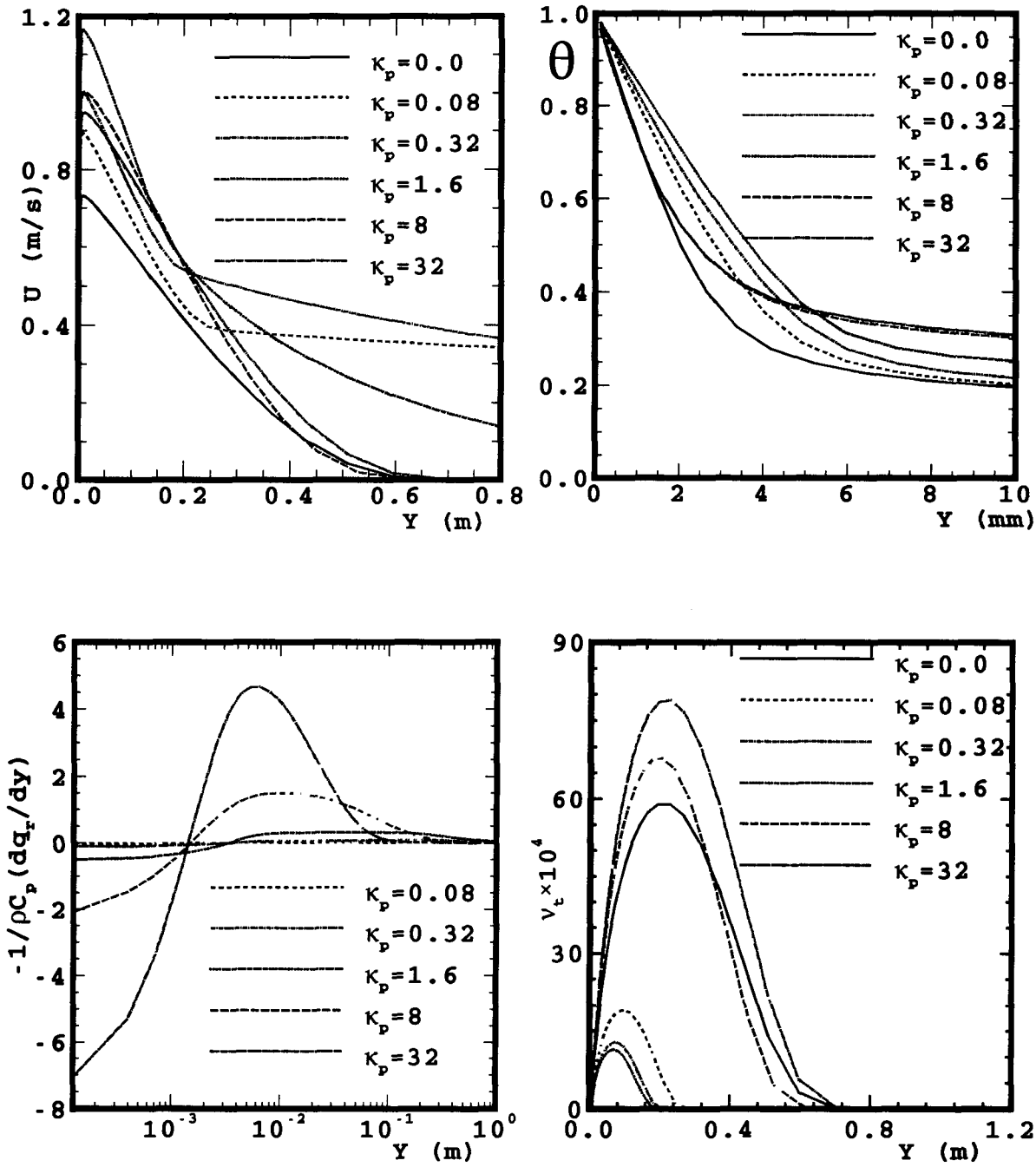


Figure 6.17: Velocity, temperature, net radiative energy to fluid and turbulent viscosity in absorbing and emitting gases with different absorption coefficients, $Gr_x = 1.64 \times 10^{12}$.

numbers. It is very interesting to look at the relative positions of the velocity profiles for $\kappa_p = 1.6m^{-1}$ and $\kappa_p = 8m^{-1}$ in each of these figures. For the lowest Grashof number, Fig. 6.13, the velocities for $\kappa_p = 8m^{-1}$ are higher than those for $\kappa_p = 1.6m^{-1}$. However, for the highest Grashof number, Fig. 6.17, the situation is reversed. The reason can be found by looking at the corresponding radiative heat flux profiles for $\kappa_p = 8m^{-1}$. For the lowest Grashof number the effect of radiation goes beyond the thickness of boundary layer, close to an optically thin layer, whereas for the highest Grashof number this effect only covers less than half of the boundary layer, close to an optically thick layer.

The convection heat transfer characteristics of the boundary layer are shown in Fig. 6.18 in terms of the variation of local Nusselt number versus local Rayleigh number. It is interesting to note that the curves corresponding to the lowest and the highest values of absorption coefficients are the closest curves to the one for a non-absorbing gas. This

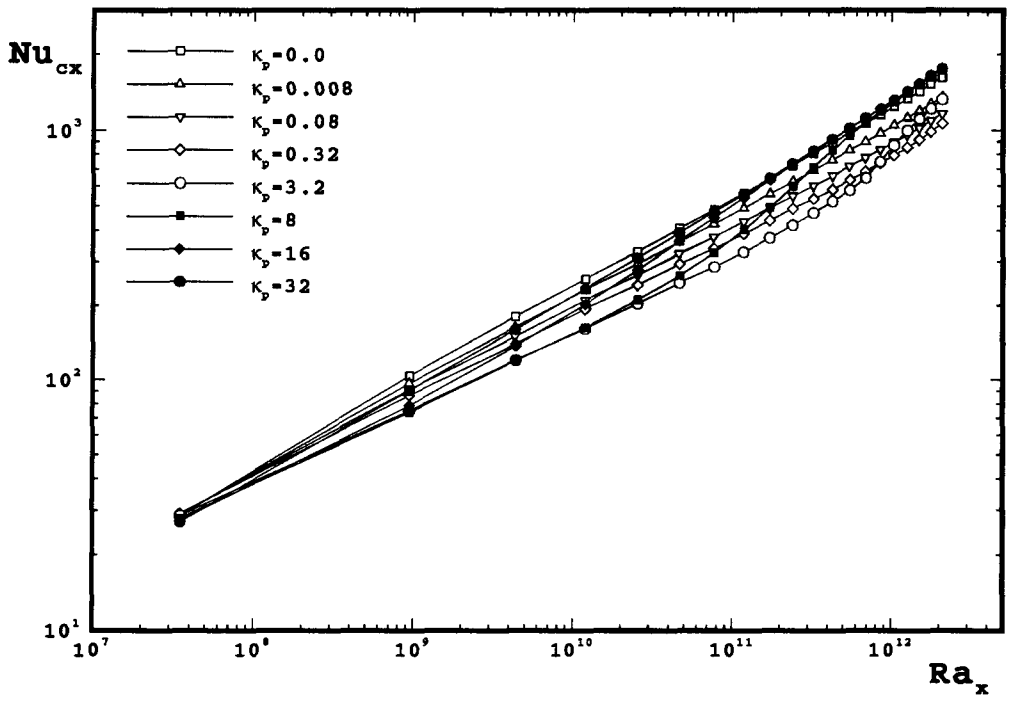


Figure 6.18: Local convective Nusselt number in a turbulent natural convection boundary layer of an absorbing and emitting gas, $T_w = 60°C$.

is in agreement to what has already been mentioned about the behavior of the boundary layer in a very strong and a very weak absorbent gases. As the absorption coefficient increases, the convective Nusselt number decreases up to some point and then, it starts increasing again. The value of absorption coefficient which gives the lowest Nusselt number is a function of Rayleigh number. For a Rayleigh number about $10^{10}$ the lowest shown Nusselt number corresponds to $\kappa_p = 3.2m^{-1}$, whereas for the Rayleigh number equal to $10^{12}$ it corresponds to $\kappa_P = 0.32m^{-1}$. For the lowest shown Rayleigh number, the Nusselt numbers for different values of the absorption coefficients are very close to each other. This is similar to what was seen before in the laminar regime. This point is actually the first computational point in the flow direction. The turbulence model predicts a laminar like behavior for this point, so the boundary layer acts as a laminar boundary layer in this point.

If the Rayleigh number is very high, and the absorption coefficient is high enough, the Nusselt number will be independent of absorption coefficient. This is shown in Fig. 6.18 for $\kappa_p = 8m^{-1}$,$16m^{-1}$ and $32m^{-1}$.

The dependence of convective Nusselt number on absorption coefficient of the gas can be better seen by looking at Fig. 6.19. The dependence is much stronger at higher values of Grashof numbers. For the lower Grashof numbers, the curves approach almost straight line which is a characteristic of the laminar boundary layer.

The effect of gas radiation on convective Nusselt number may be better understood by looking at the variation of $Nu_{cx}/Nu_{co}$, where $Nu_{cx}$ is the convective Nusselt number calculated by considering the effects of gas radiation. On the other hand, $Nu_{co}$ is the Nusselt number calculated when gas radiation is neglected. The Fig. 6.20 shows such a graph for five different Grashof numbers. The independent variable on the horizontal axis is called the radiation-conduction parameter and is a measure of the radiative heat flux to the conductive heat flux; $\zeta = (4\kappa_p x^2 \sigma T_f^3)/(kPrGr_x^{1/2})$ where $T_f = (T_w + T_\infty)/2$.

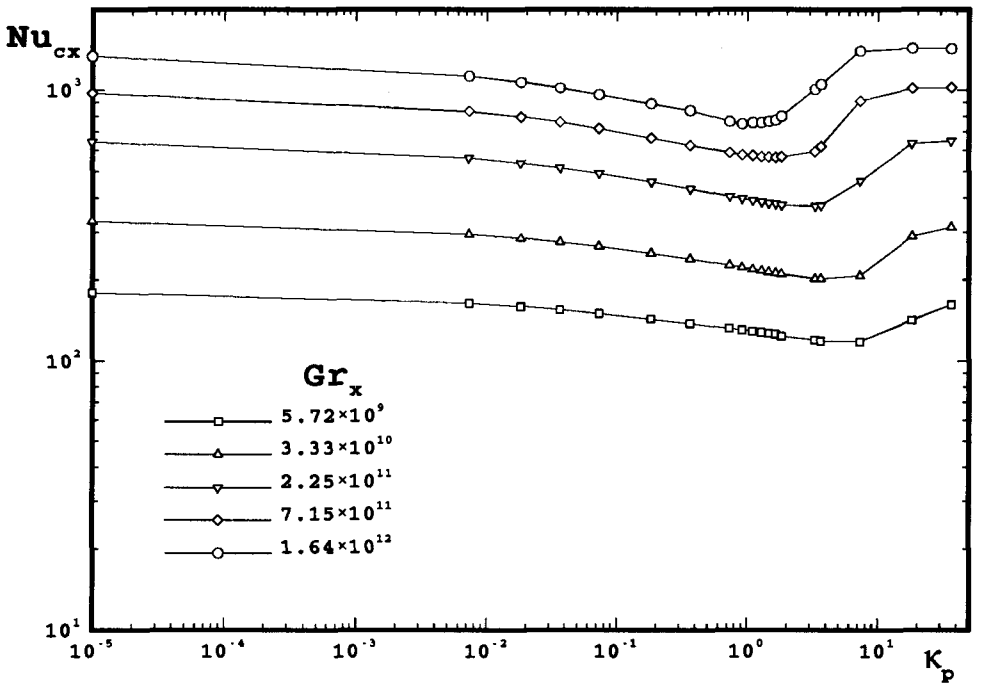


Figure 6.19: Variation of local convective Nusselt number versus absorption coefficient.

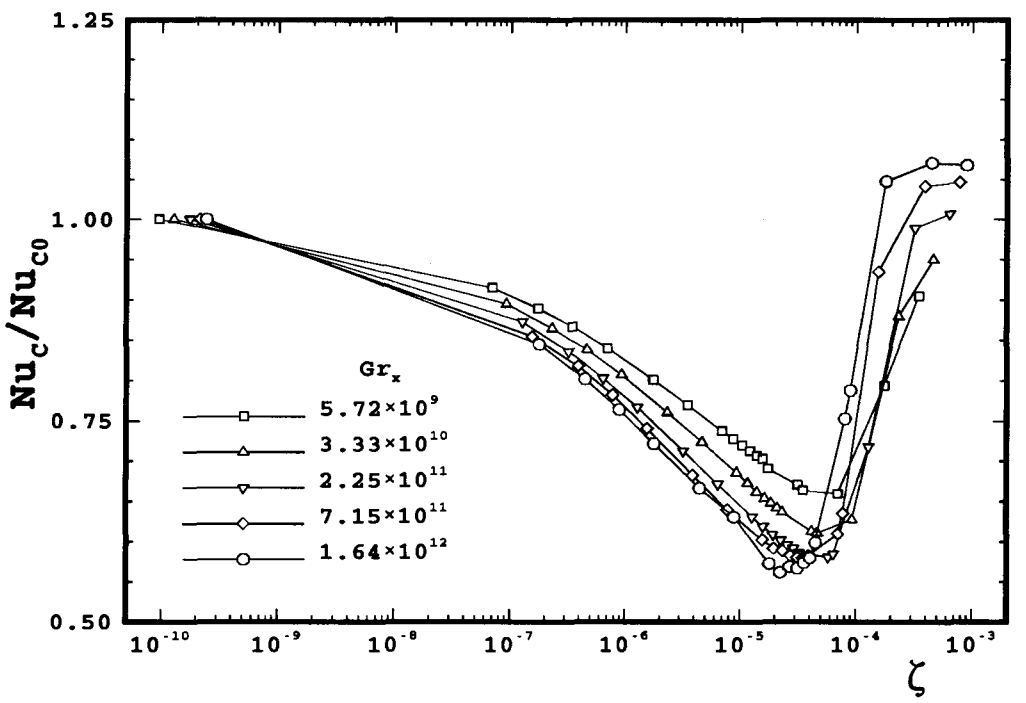


Figure 6.20: The ratio of the convective Nusselt number in an absorbing gas to the convective Nusselt number when gas radiation is neglected.

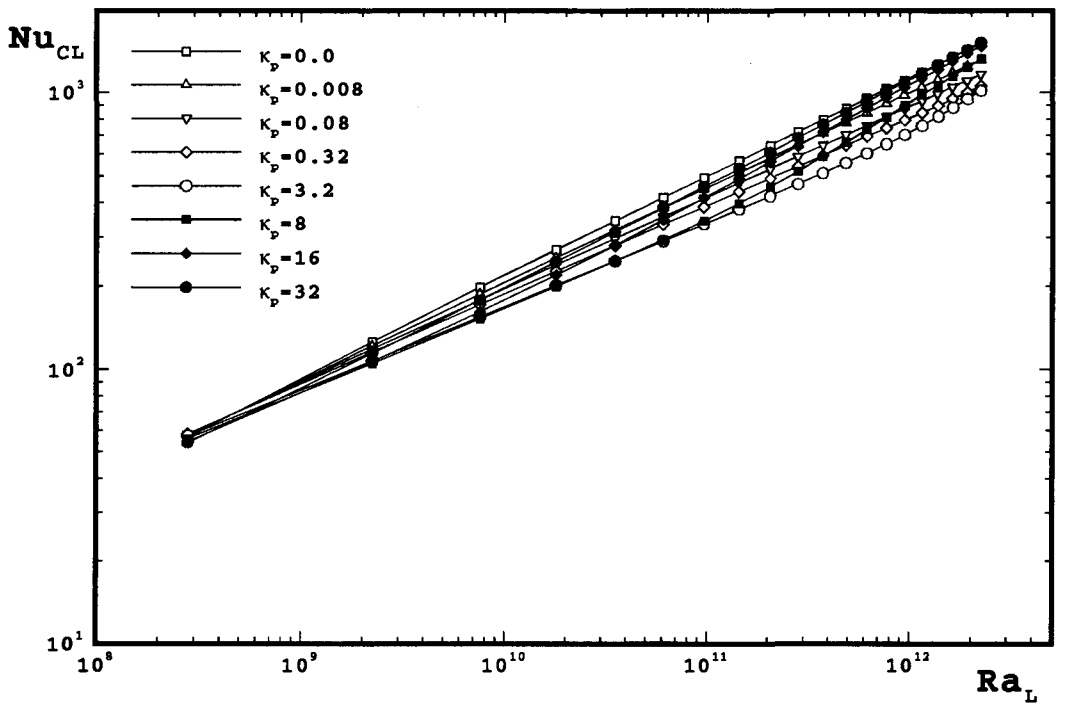


Figure 6.21: Mean convective Nusselt number in a turbulent natural convection boundary layer of an absorbing and emitting gas.

It is common to plot the variation of Nusselt number versus Rayleigh number in terms of mean values. Fig. 6.21 shows such a graph for the present problem. The mean Nusselt number was defined as $\overline{h}L/k$ and the mean heat transfer coefficient, $\overline{h}$, was found by integrating the local values over the length of the plate. Basically, the same characteristics that were observed in terms of local values can be seen in terms of mean values also.

The variation of local radiative Nusselt number is shown in Fig. 6.22. It is seen that the radiative heat transfer decreases by increasing the absorption coefficient of the gas. However unlike the laminar boundary layer, in some cases the changes in the radiative heat transfer are smaller than the changes in convective heat transfer. This means that in a turbulent natural convection boundary layer, the absorptivity of the gas affects convective heat transfer more than the radiative heat transfer.

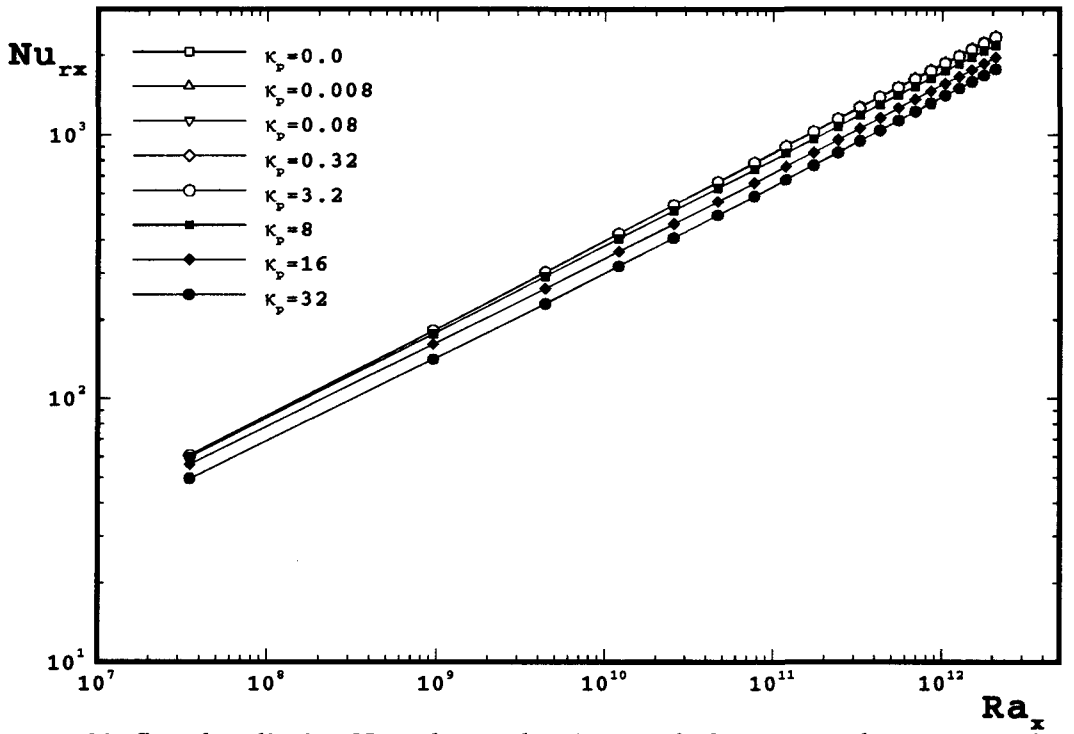


Figure 6.22: Local radiative Nusselt number in a turbulent natural convection boundary layer of an absorbing and emitting gas, $T_w = 60°C$.

### 6.4.2 High Wall Temperature

Radiative heat transfer in a boundary layer is strongly dependent on the temperature difference between the plate and the medium. This section covers the results obtained for a wall temperature of $T_w = 200°C$ and medium temperature of $T_\infty = 25°C$. A comparison can then be made between the results obtained with high and low wall temperatures.

The absorption coefficients of $CO_2$ used for the low wall temperature calculations were also used for the high wall temperature since the variation of absorption coefficient with temperature is small. Since a broad range of absorption coefficients were included in this investigation, each value of absorption coefficient could always correspond to some percent of $CO_2$ in the gas mixture.

Fig. 6.23 shows the velocity and temperature profiles for $Gr_x = 4.24 \times 10^{11}$, the same Grashof number shown in Fig. 6.10 for low wall temperature. Regardless of the velocities

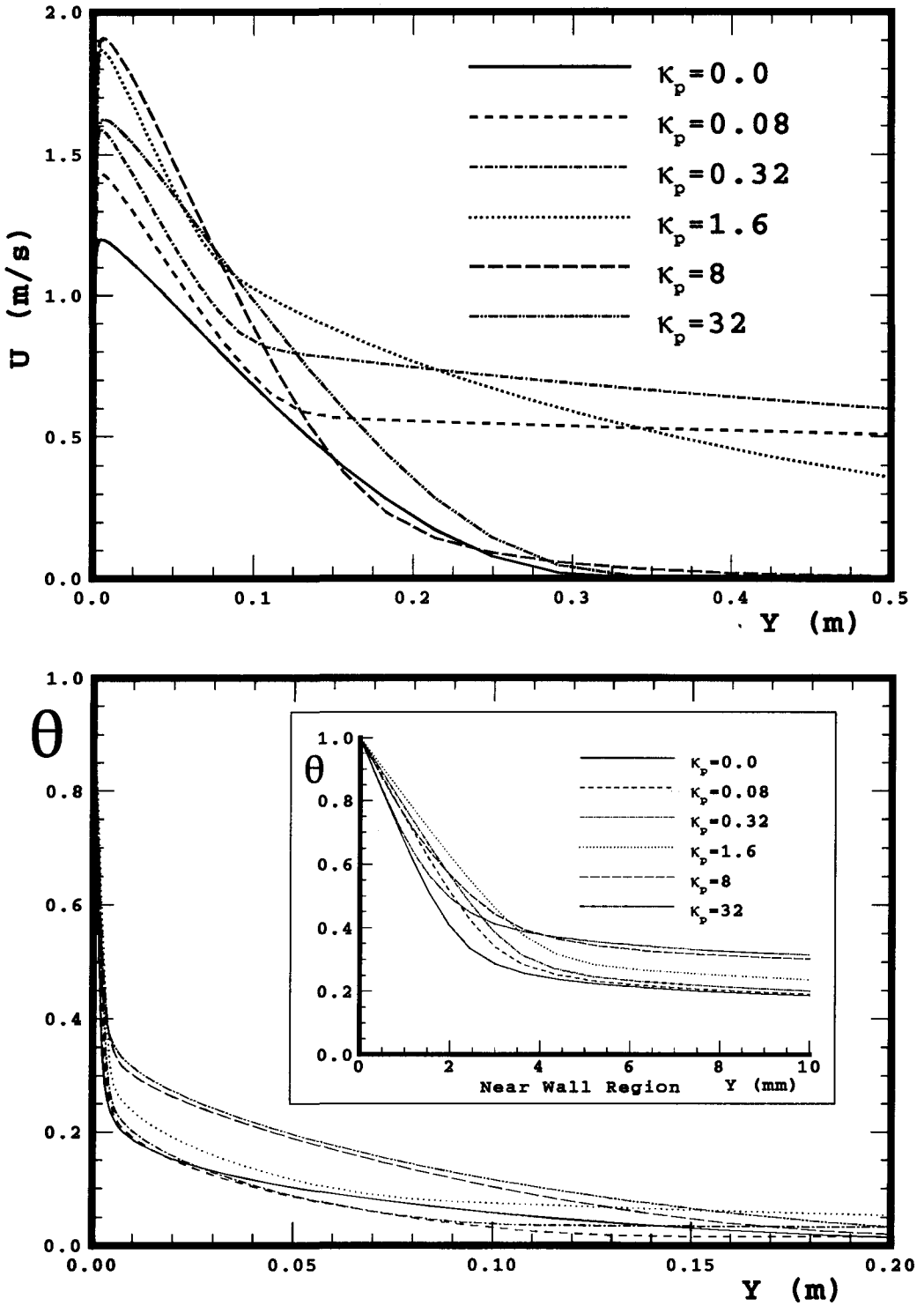


Figure 6.23: Turbulent natural convection velocity and temperature profiles in an absorbing and emitting gas, $T_w = 200°C$ and $Gr_x = 4.24 \times 10^{11}$.

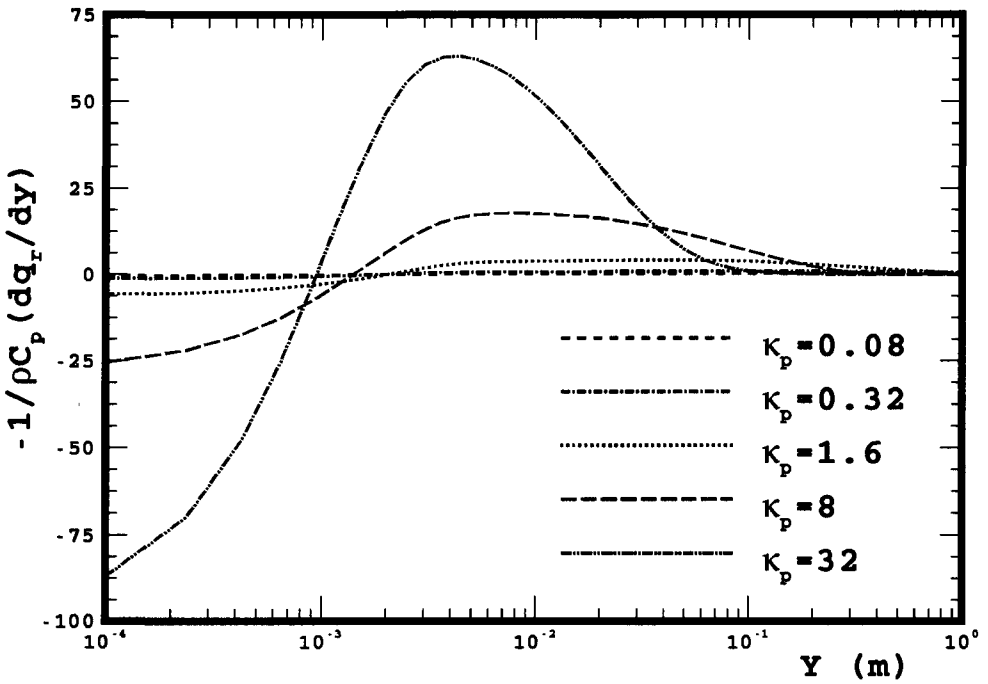


Figure 6.24: Net radiative energy to the gas in the turbulent natural convection of an absorbing and emitting gas, $T_w = 200°C$ and $Gr_x = 4.24 \times 10^{11}$.

(which are supposed to be higher) the important difference between the velocity profiles in these two cases is that for high wall temperature (Fig. 6.23) velocities keep increasing up to $\kappa_p = 8m^{-1}$ whereas, for low wall temperature (Fig. 6.10) maximum velocities were seen at $\kappa_p = 1.6m^{-1}$. However, the general behavior of velocity and temperature profiles are the same as the ones for the low wall temperature.

Fig. 6.24 shows the variation of net radiative energy to the gas in the boundary layer. Comparing this Figure with Fig. 6.11, shows that although the amount of radiative heat flux increases with temperature, the range in which the radiation affects the boundary layer remains the same. Having the same behavior in velocity and temperature profiles for high and low wall temperatures supports this idea that the effects of radiation on the boundary layer are more related to the range of penetration of radiation than the amount of radiative heat flux.

It is well known that if the velocities and temperature in a non-absorbing gas, at a specified Grashof number, are normalized with friction velocity, $u_\tau$, and friction temperature, $t_\tau$, and plotted versus dimensionless coordinate, $y^+$, a unique curve can be found whatever the value of temperature difference between the wall and the medium. This was investigated for an absorbing and emitting gas. Figs. 6.25 and 6.26 show that for low and high values of absorption coefficients the profiles are independent of wall temperature; the medium temperature was kept constant. However, for medium values of absorption coefficients, $\kappa_p = 8m^{-1}$, there is a temperature dependence behavior in the region around the point of maximum velocity. Therefore, it is believed that, except for the optically thin and thick limits, the behavior of the boundary layer depends on the temperature difference between the wall and the medium as well as the absorption coefficient of the medium.

The convective and radiative heat transfer characteristics of a boundary layer are illustrated in Figs. 6.27 and 6.28. Fig. 6.29 compares the variation of convective Nusselt number versus Rayleigh number for two different values of wall temperature. It can be seen that for low and high values of absorption coefficients, Nusselt number is only a function of Rayleigh number and absorption coefficient. On the other hand, for a moderate value of $\kappa_p$ there is a small dependence on wall temperature. It is noted that in the graph for $\kappa_p = 32m^{-1}$ the lower range of Rayleigh numbers correspond to a smaller boundary layer thickness and therefore an optically moderate layer.

### 6.4.3 Comparison with Experimental Data

The only experimental work found on the turbulent natural convection boundary layer of an absorbing and emitting gas is that was done by Hood [46]. He measured the temperature and velocity profiles at one location of a constant temperature plate, over a range of carbon dioxide and nitrogen gas mixtures. In order to change the absorption

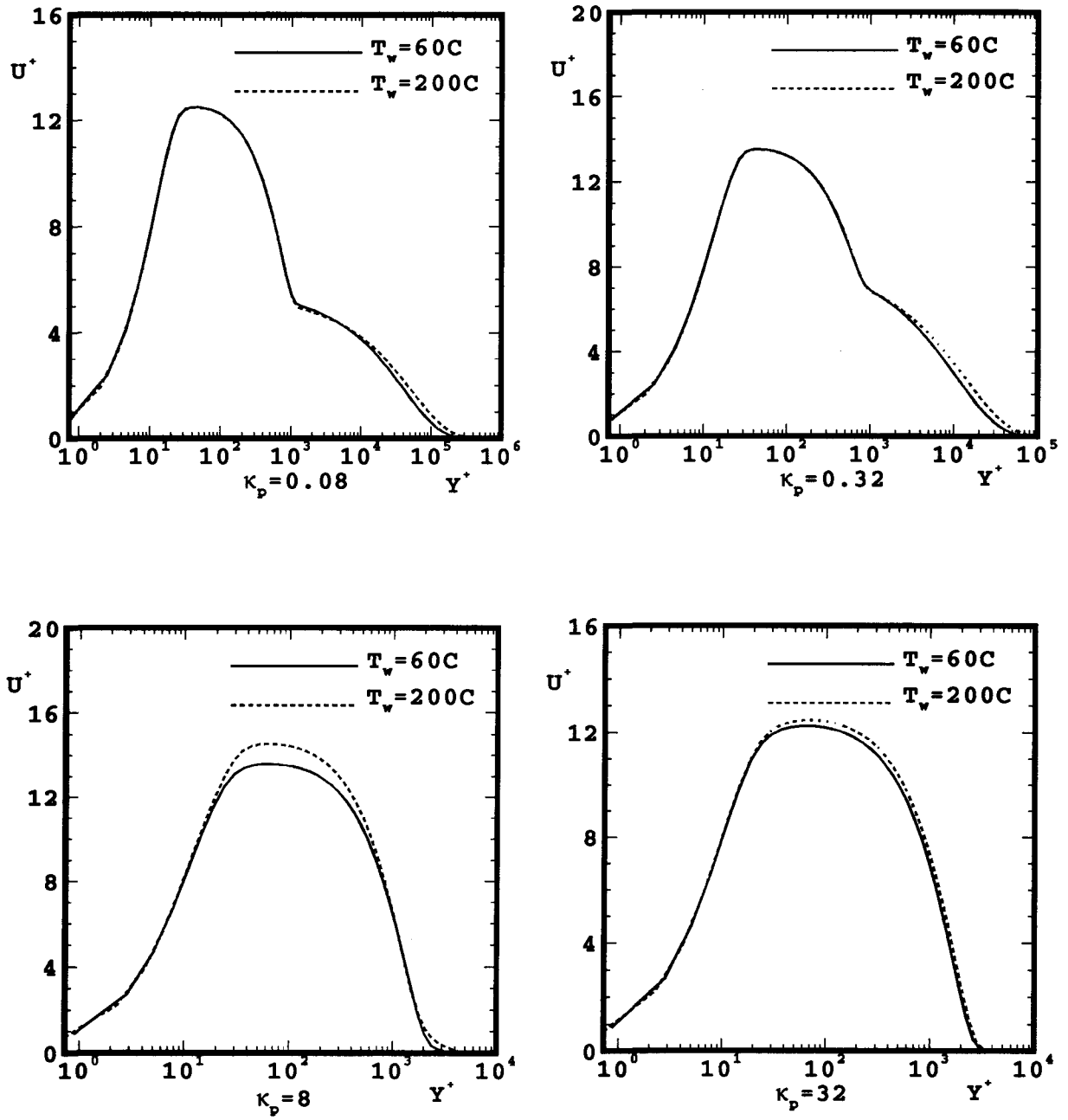


Figure 6.25: Dimensionless velocity profiles in a turbulent natural convection boundary layer of an absorbing and emitting gas.

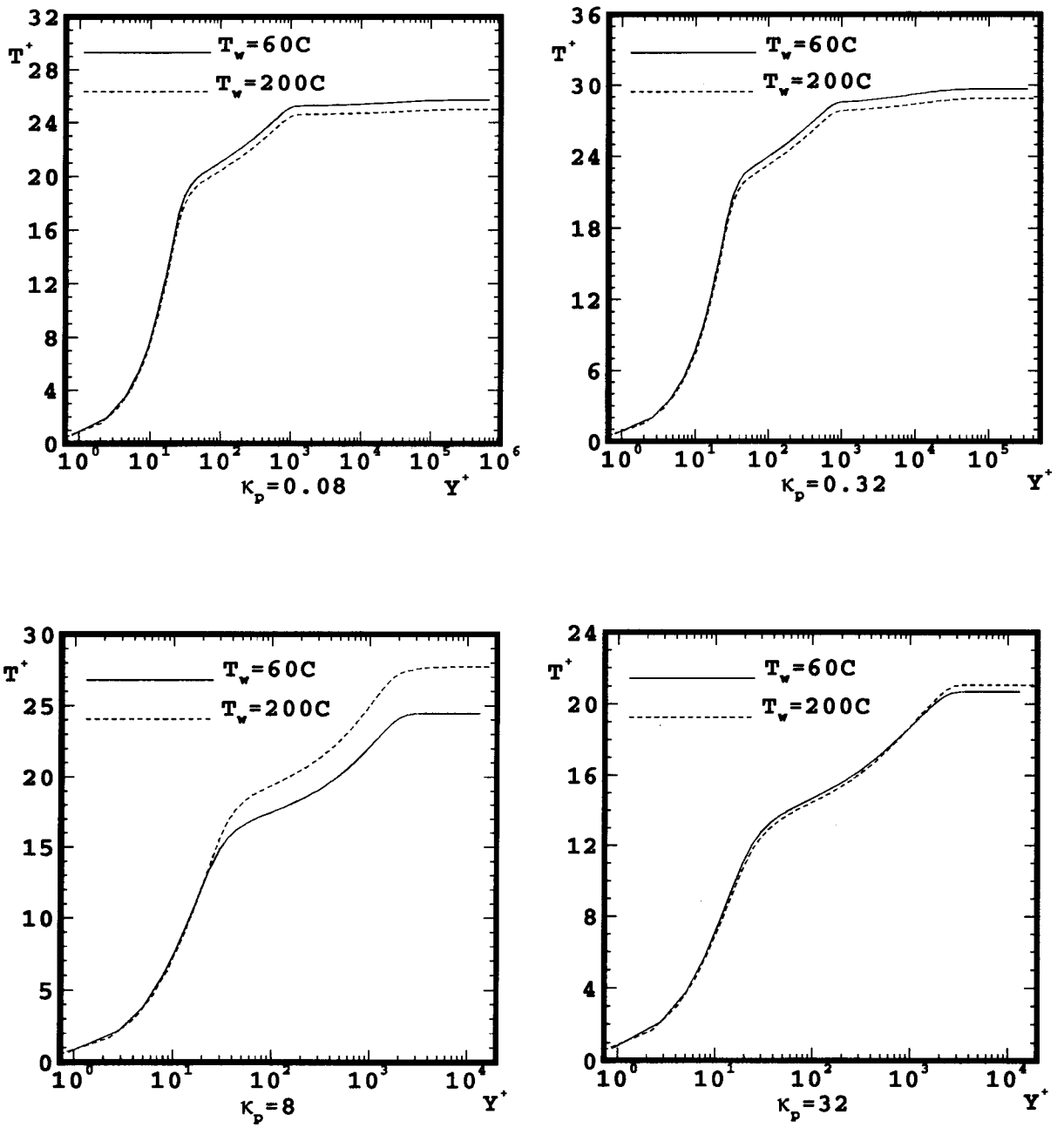


Figure 6.26: Dimensionless temperature profiles in a turbulent natural convection boundary layer of an absorbing and emitting gas.

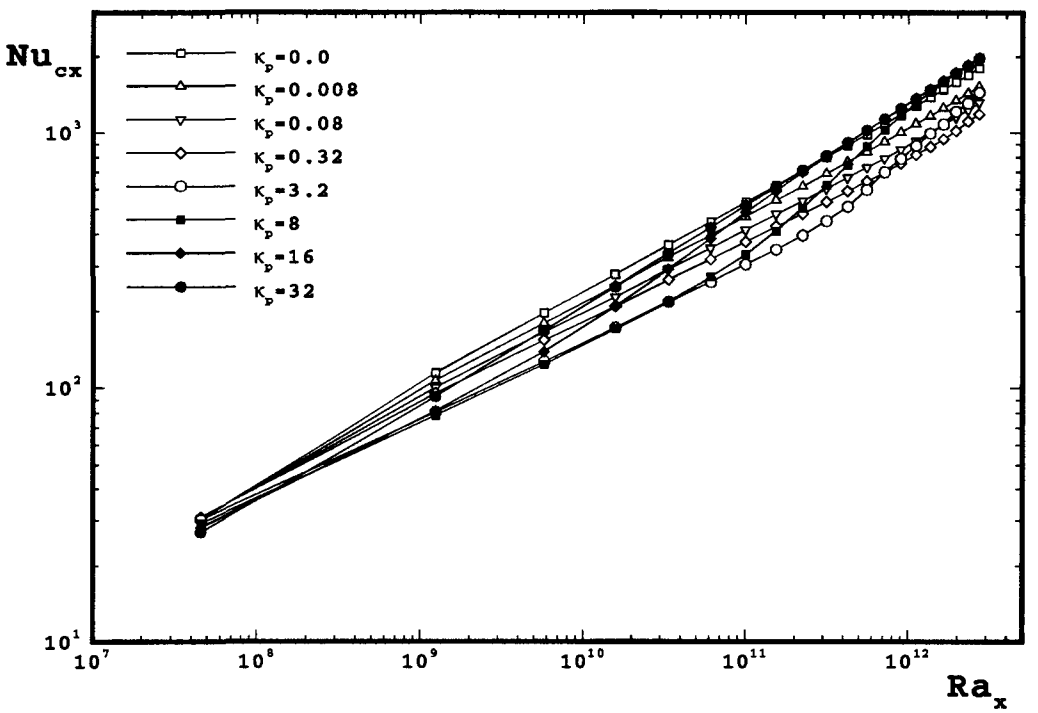


Figure 6.27: Local convective Nusselt number in a turbulent natural convection boundary layer of an absorbing and emitting gas, $T_w = 200°C$.

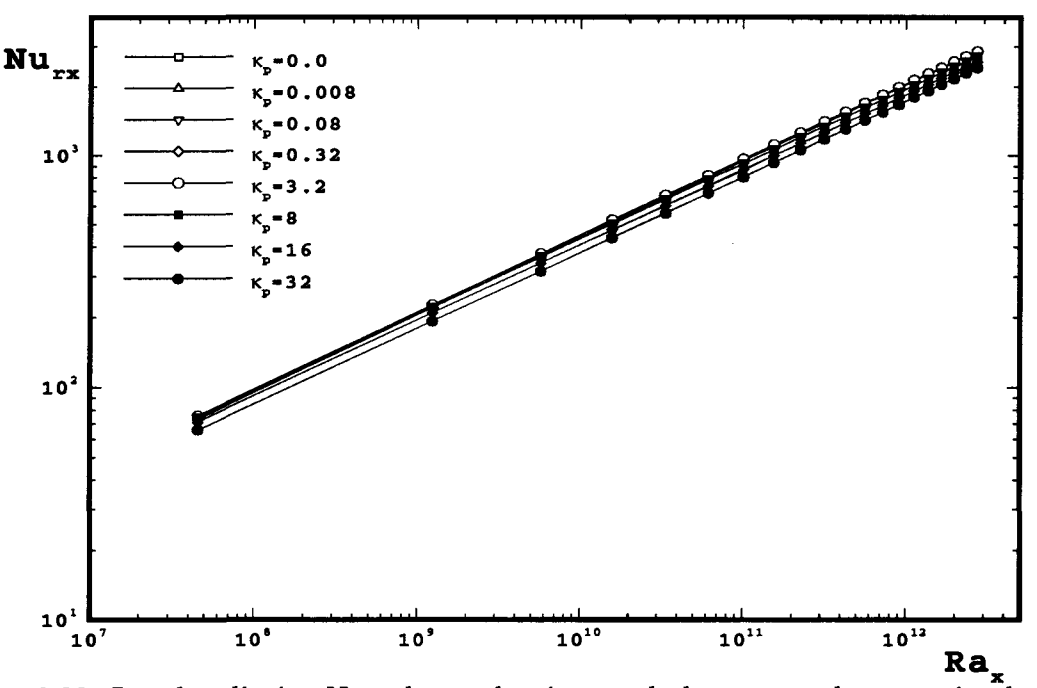


Figure 6.28: Local radiative Nusselt number in a turbulent natural convection boundary layer of an absorbing and emitting gas, $T_w = 200°C$.

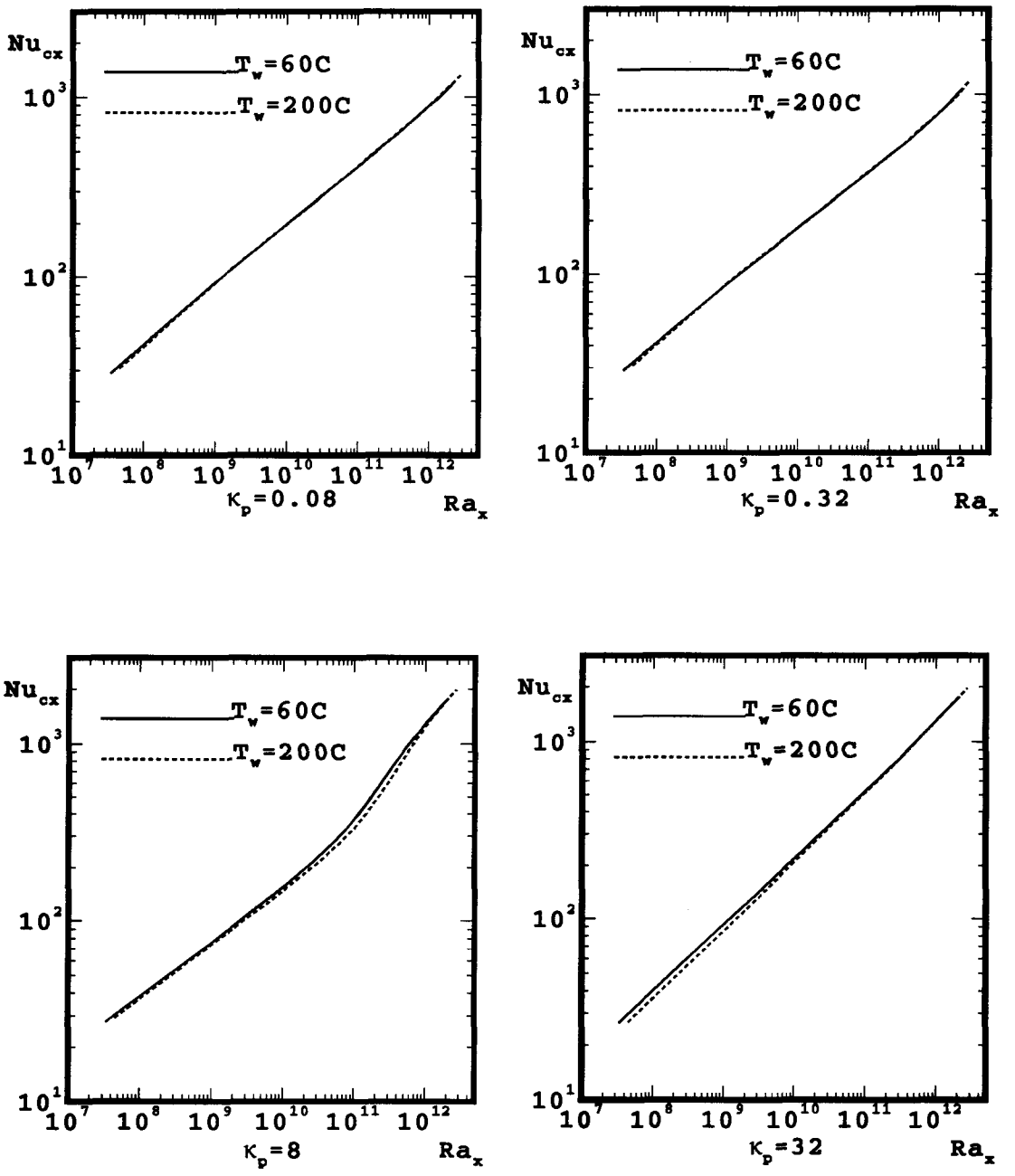


Figure 6.29: Comparison between the variation of convective Nusselt numbers along the wall in turbulent natural convection of an absorbing and emitting gas with different wall temperatures.

coefficient of the gas, the gas composition was controlled. The heated plate was constructed of stainless steel, coated with a high temperature black paint, with dimensions of $84cm \times 38cm$. The box enclosing the plate was made with an aluminum back and base and acrylic sheets sides and top. The dimensions of the enclosure were $1.6m$ high, $1.2m$ wide and $0.8m$ deep. In order to obtain a turbulent boundary layer, the plate had a sharp leading edge exposed to the flow, and a tripping wire was used. The velocity and temperature profiles were obtained with a constant temperature hot wire anemometer.

Numerical solutions were obtained for the same conditions as the experiments. The plate and the medium temperatures were chosen as $T_w = 410°C$ and $T_\infty = 55°C$. All properties including the absorption coefficient were calculated at the film temperature; $(T_w + T_\infty)/2$. The calculations were done for four mixtures of carbon dioxide and nitrogen gases; $0\%CO_2$, $10\%CO_2$, $50\%CO_2$ and $75\%CO_2$. The case of $0\%CO_2$ is actually pure nitrogen and therefore a non-absorbing gas. In Sec. 5.3 it was shown that the numerical simulation of turbulent natural convection in a non-absorbing gas could predict the flow very well. Therefore, the comparison between the experimental data and the calculated results in pure nitrogen can be used to understand the degree of accuracy of measurements.

Fig. 6.30 shows the experimental and calculated velocity and temperature profiles in nitrogen. The experimental velocity data show a lot of scatter. However, the predicted and the measured maximum velocities agree fairly with each other. On the other hand, the measured boundary layer thickness is much smaller than that predicted. There might be some concerns raised regarding the way the velocities were measured by Hood. First, the velocity in most part of the boundary layer was smaller than the smallest calibrated velocity; $0.5m/s$, and an extrapolation of the calibration curve was used in this range. Second, hot wire measurements are usually limited to flows with velocities greater than $0.1m/s$. Therefore, it may be that the outer region of the boundary layer could not

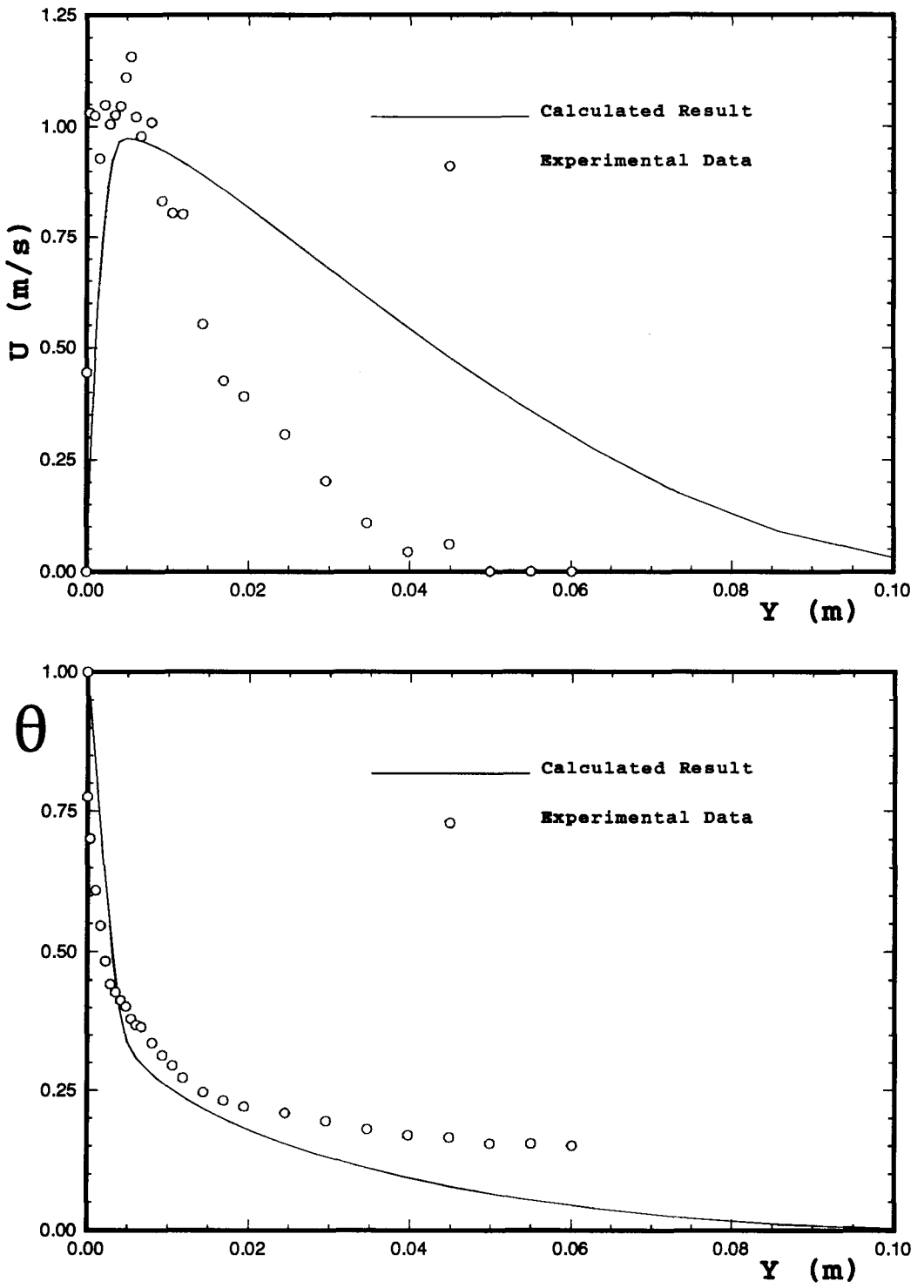


Figure 6.30: Comparison between measured [46] and calculated velocity and temperature profiles in nitrogen.

be measured very accurately. Third, the turbulence intensity can affect the velocity measurements. Fourth, the wall proximity can affect the accuracy of measurements near the wall; there were no considerations regarding this effect.

Temperature profiles in Fig. 6.30 show a fair agreement between the experimental data and the calculated results. One important concern about the temperature measurements is that the measured temperatures, at the outer layer, approach a value much higher than the measured ambient temperature which was used for the calculation. It seems that the cross-stream depth of the enclosure used by Hood was too small to simulate the "infinity" for the boundary layer. Another boundary layer might be present at the opposite wall of the enclosure, between the cold wall and the hot gas.

As a final comment on Fig. 6.30, it should be mentioned that the assumption of constant properties in the calculation can produce some errors in this high value of temperature difference. The amount of these errors is not known.

Figs. 6.31-6.33 compare the calculated and measured velocity and temperature profiles in three different mixtures of carbon dioxide and nitrogen gases. It is seen that the predicted peak velocities are about $20\% - 50\%$ higher than those measured. The calculated temperatures are higher than those measured almost everywhere. The best agreement between the measured and the calculated temperature profiles is seen in Fig. 6.31 for a mixture of $10\% CO_2$ and $90\% N_2$. The higher temperatures predicted by the calculations might be a result of the gray gas assumption. It is believed that this assumption overestimates the absorbing and emitting capability of the gas. On the other hand the Planck's mean absorption coefficient, $\kappa_p$, which is used in gray gas model may not be a suitable choice but no other model is available. Another assumption in the calculations is the assumption of a black wall, which did not match exactly with the experimental condition. The emissivity of the plate was assumed to be about 0.95. No attempt was made to verify this value. Regarding the uncertainty in the measured velocities and

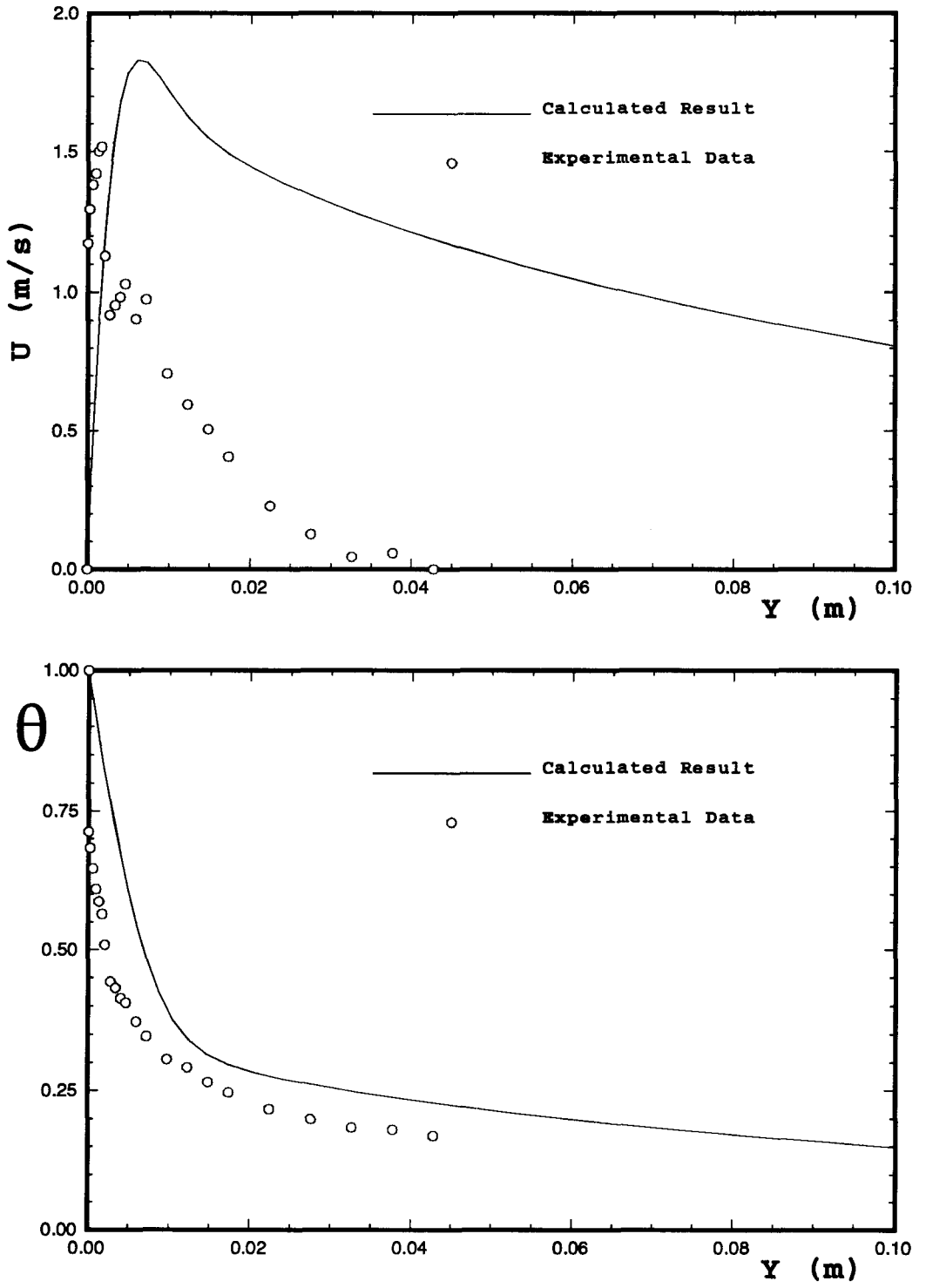


Figure 6.31: Comparison between measured [46] and calculated velocity and temperature profiles in a mixture of $10\% CO_2$ and $90\% N_2$.

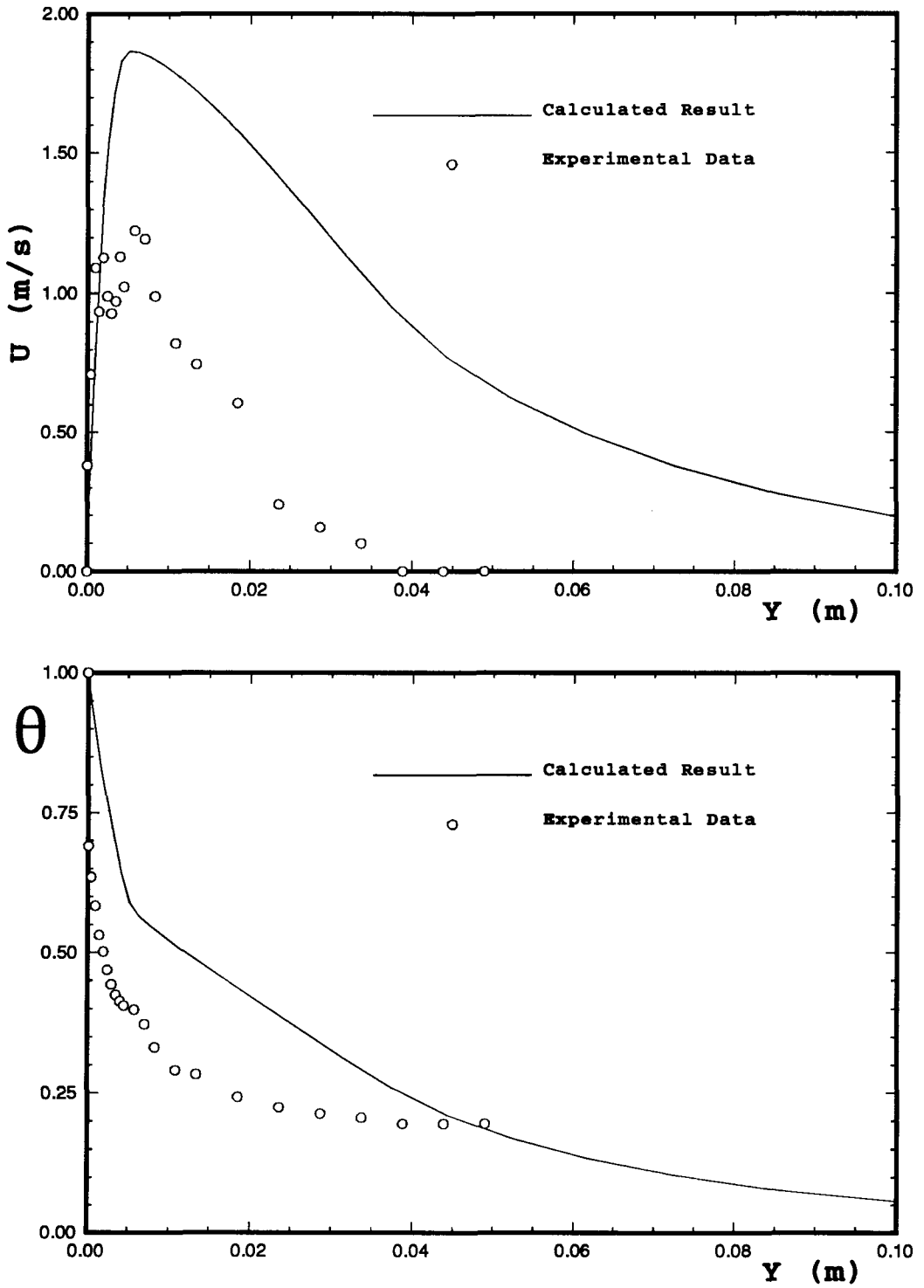


Figure 6.32: Comparison between measured [46] and calculated velocity and temperature profiles in a mixture of 50%$CO_2$ and 50%$N_2$.

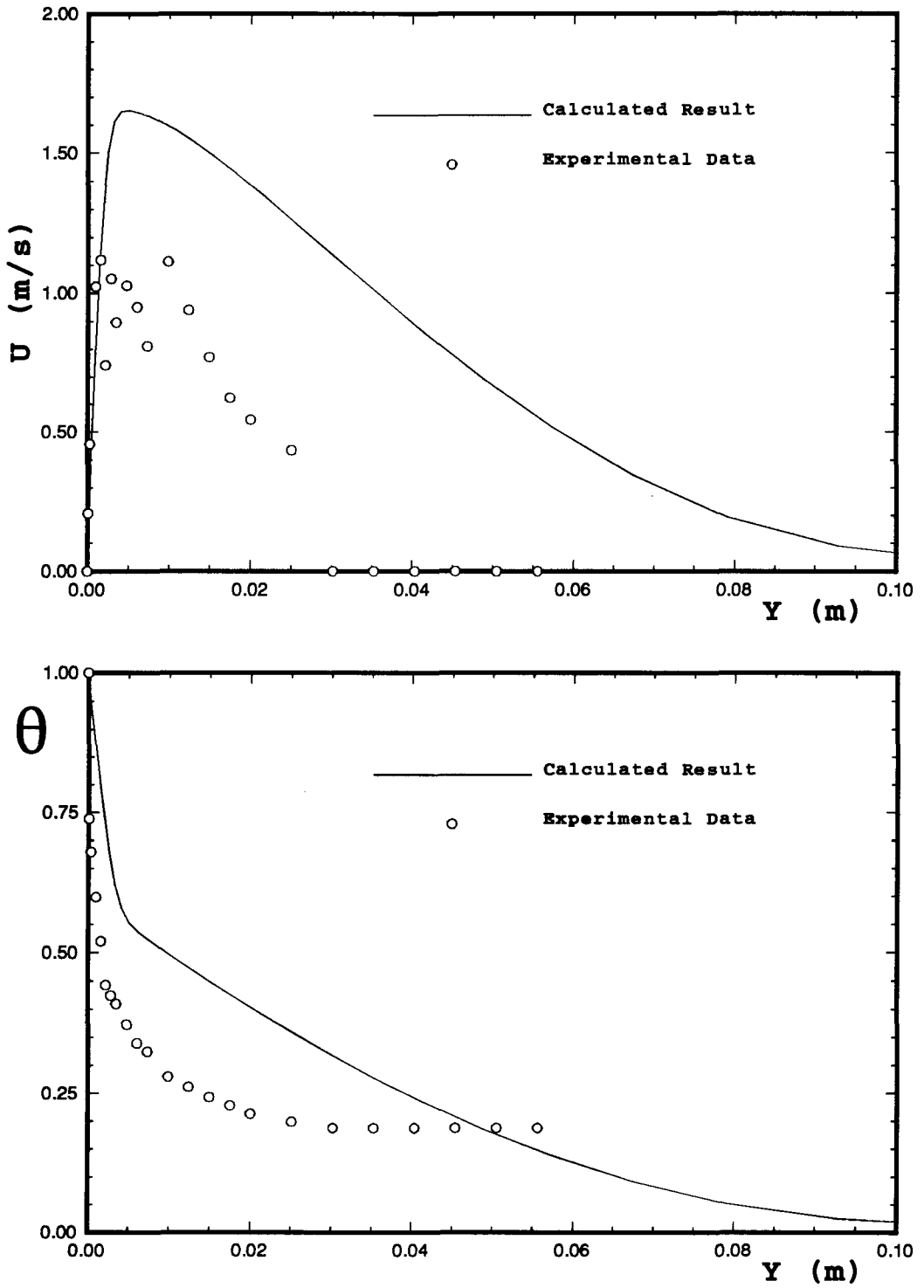


Figure 6.33: Comparison between measured [46] and calculated velocity and temperature profiles in a mixture of 75%$CO_2$ and 25%$N_2$.

temperatures, all comments following discussion about Fig. 6.30 apply here as well. In addition, it should be noted that the calibration of hot wire for velocity measurements was done in air at room temperature, whereas the measurements were performed in a $CO_2$-$N_2$ mixture over a range of temperatures.

# Chapter 7

# CONCLUSIONS AND RECOMMENDATIONS

Numerical simulation of a turbulent natural convection boundary layer in an absorbing and emitting gas was the main purpose of this investigation. First, a few turbulence models were examined for the prediction of the mean characteristics of a natural convection boundary layers in a non-absorbing gas. Then, the most suitable turbulence model was used for the calculation of turbulent natural convection boundary layers in an absorbing and emitting gas. A brief explanation of the conclusions drawn in this work, followed by some recommendations for possible future work will be given here.

## 7.1 Conclusions

1. The range of Rayleigh number in which the Jones and Launder low-Reynolds-number $k$-$\epsilon$ model can give a fully turbulent flow solution is dependent on the grids sizes in the flow direction. For grids sizes equal to $0.35m$ the Nusselt numbers predicted by this model were within 10% accuracy compared to the experimental data for $Ra_x \geq 10^{11}$.

2. If the wall functions and the extra source terms in the $k$ and $\epsilon$ equations of the Jones and Launder model are applied only before the location of maximum velocity, the model can predict a grid independent turbulent flow solution for $Ra_x \geq 10^9$. When applied in this case the model was called modified Jones and Launder model.

3. The modified Jones and Launder model predicts fairly reasonably the mean velocity and temperature profiles of turbulent natural convection boundary layer. The calculated near wall velocity and temperature profiles are within 15% and 5% accuracy respectively. The heat transfer rates predicted by this model are within 10% accuracy compared with the experimental data.

4. If the absorption coefficient of the gas is such that the radiation effects go beyond the thickness of the boundary layer (optically thin layer), the increase of absorption coefficient causes the velocities and temperatures in the boundary layer to increase and the turbulent viscosities to decrease.

5. If the absorption coefficient of the gas is such that the radiation affects only part of the boundary layer (optically thick layer), the increase of absorption coefficient causes the velocities and temperatures in the boundary layer to decrease and the turbulent viscosities to increase.

6. As a result of the effects of gas radiation on the boundary layer mentioned above the convective heat transfer rate first decreases and then increases when the absorption coefficient of the gas is increased.

7. The behavior of the boundary layer depends more on the range of penetration of radiative energy than the amount of radiative heat flux itself. The results obtained for high wall temperature, and therefore higher radiative heat flux, showed almost the same behavior as those obtained for low wall temperature.

8. In optically thin and thick limits, corresponding to $\kappa_p \leq 0.32m^{-1}$ and $\kappa_p \geq 32m^{-1}$ in this study, the profiles of the dimensionless velocity, $u_\tau$, and temperature, $t_\tau$, are only functions of dimensionless coordinate, $y^+$, and absorption coefficient of the gas. Also, the Nusselt number is only a function of Rayleigh number and

absorption coefficient of the gas. However, for an optically intermediate layer, $\kappa_p = 8m^{-1}$, there is a dependence on the temperature difference between the wall and the medium.

## 7.2 Recommendations

1. Natural convection turbulent flows still lack a satisfactory $k$-$\epsilon$ turbulence model. A fundamental study in this area is highly recommended. This study can be done by following the procedure of the development for $k$-$\epsilon$ models for forced convection flows. The validity of model constants and wall functions originally developed for forced convection flows should be investigated for natural convection flows.

2. A detailed experimental study of natural convection boundary layers in an absorbing and emitting gas is necessary to support the numerical simulation. Since the effect of radiation goes far from the wall when the gas is a weak absorber, the experimental investigations in these cases may be difficult. Therefore, the experiments should be limited to strongly absorptive gases. The validity of experimental data must be checked against the available data for the case of non-absorbing gases.

3. It was observed that the less absorptive the gas, the thicker the boundary layer. Therefore, a fully two-dimensional numerical simulation of this problem is recommended to justify or reject the validity of boundary layer approximations when the gas is a weak absorber.

4. In this study, the gas was assumed to be gray in order to simplify the problem. The next logical improvement of the solutions might be the inclusion of the nongrayness behavior of the gas.

## Bibliography


[1] Cheesewright, R.,"Turbulent Natural Convection From a Vertical Plane Surface", J. of Heat Transfer, Vol. 90, pp. 1-8(1968)

[2] Warner, C. Y. and Arpaci, V. S.,"An Experimental Investigation of Turbulent Natural Convection in Air at Low Pressure Along a Vertical Heated Flat Plate", Int. J. Heat Mass Transfer, Vol. 11, pp. 397-406(1968)

[3] Eckert, E. R. G. and Jackson, T. W.,"Analysis of Turbulent Free-Convection Boundary Layer on Flat Plate", NACA TN 2207 (1950)

[4] Lock, G. S. H. and Trotter, F. J. B.,"Observations on the Structure of a Turbulent Free Convection Boundary Layer", Int. J. Heat Mass Transfer, Vol. 11, pp. 1225-1232(1968)

[5] Vliet, G. C. and Liu, C. K.,"An Experimental Study of Turbulent Natural Convection Boundary Layers", J. of Heat Transfer, Vol. 91, pp. 517-531(1969)

[6] Kutateladze, S. S., Kirdyashkin, A. G. and Ivakin, V. P.,"Turbulent Natural Convection on a Vertical Plate and in a Vertical Layer", Int. J. Heat Mass Transfer, Vol. 15, pp. 193-202(1972)

[7] Papailiou, D. D. and Lykoudis, P. S.,"Turbulent Free Convection Flow", Int. J. Heat Mass Transfer, Vol. 17, pp. 161-172(1974)

[8] Cheesewright, R. and Doan, K. S.,"Space-Time Correlation Measurements in a Turbulent Natural Convection Boundary Layer", Int. J. Heat Mass Transfer, Vol. 21, pp. 911-921(1978)

[9] Bill, R. G. and Gebhart, B.,"The Development of Turbulent Transport in a Vertical Natural Convection Boundary Layer", Int. J. Heat Mass Transfer, Vol. 22, pp. 267-277(1979)

[10] Cheesewright, R. and Ierokiopitis, E.,"Velocity Measurements in a Turbulent Natural Convection Boundary Layer", Proc. of the 7th Int. Heat Transfer Conference, pp. 305-309(1982)

[11] Miyamoto, M., Kajino, H., Kurima, J. and Takanami, I.,"Development of Turbulence Characteristics in a Vertical Free Convection Boundary Layer", Proc. of the 7th Int. Heat Transfer Conference, pp. 323-328(1982)

[12] Tsuji, T. and Nagano, Y.,"Characteristics of a Turbulent Natural Convection Boundary Layer Along a Vertical Flat Plate", Int. J. Heat Mass Transfer, Vol. 31, pp. 1723-1734(1988)

[13] Mason, H. B. and Seban, R. A.,"Numerical Predictions for Turbulent Free Convection from Vertical Surfaces", Int. J. Heat Mass Transfer, Vol. 17, pp. 1329-1336(1974)

[14] Cebeci, T. and Khattab, A.,"Prediction of Turbulent-Free-Convection-Heat Transfer from a Vertical Flat Plate", J. of Heat Transfer, Vol. 97, pp. 469-471(1975)

[15] Cebeci, T. and Smith, A. M. O.,"Analysis of Turbulent Boundary Layers", Academic Press, New York(1974)

[16] Plumb, O. A. and Kennedy, L. A.,"Application of a $k$-$\epsilon$ Turbulence Model to Natural Convection from a Vertical Isothermal Surface", J. of Heat Transfer, Vol. 99, pp. 79-85(1977)

[17] Jones, W. P. and Launder, B. E.,"The Prediction of Laminarization with a Two-Equation Model of Turbulence", Int. J. Heat Mass Transfer, Vol. 15, pp. 301-314(1972)

[18] Lin, S. J. and Churchill, S. W.,"Turbulent Free Convection from a Vertical, Isothermal Plate", Numerical Heat Transfer, Vol. 1, pp. 129-145(1978)

[19] George, W. K. and Capp, S. P. ,"A Theory for Natural Convection Turbulent Boundary Layers Next to Heated Vertical Surfaces", Int. J. Heat Mass Transfer, Vol. 22, pp. 813-826(1979)

[20] To, W. M. and Humphrey, J. A. C. ,"Numerical Simulation of Buoyant, Turbulent Flow-I, Free Convection Along a Heated, Vertical, Flat Plate", Int. J. Heat Mass Transfer, Vol. 29, pp. 573-591(1986)

[21] Fedotov, A. V. and Chumakov, Y. S. ,"Modeling Turbulent Processes in Freely Convective Boundary Layer", High Temperature, Vol. 26, No. 3, pp. 374-377(1988)

[22] Henkes, R. A. W. M. and Hoogendoorn, C. J. ,"Comparison of Turbulence Models for the Natural Convection Boundary Layer Along a Heated Vertical Plate", Int. J. Heat Mass Transfer, Vol. 32, pp. 157-169(1989)

[23] Lam, C. K. G. and Bremhorst, K. ,"A Modified Form of the $k$-$\epsilon$ Model for Predicting Wall Turbulence", J. of Fluids Engineering, Vol. 103, pp. 456-460(1981)

[24] Chien, K. Y. ,"Prediction of Channel and Boundary-Layer Flows with a Low-Reynolds-Number Turbulence Model", AIAA Journal, Vol. 20, No. 1, pp. 33-38(1982)

[25] Henkes, R. A. W. M. and Hoogendoorn, C. J. ,"Numerical Determination of Wall Functions for the Turbulent Natural Convection Boundary Layer", Int. J. Heat Mass Transfer, Vol. 33, pp. 1087-1097(1990)

[26] Cess, R. D. ,"The Interaction of Thermal Radiation with Conduction and Convection Heat Transfer", Advances in Heat Transfer, Vol. 1, pp. 1-50(1964)

[27] Cess, R. D. ,"The Interaction of Thermal Radiation with Free Convection Heat Transfer", Int. J. Heat Mass Transfer, Vol. 9, pp. 1269-1277(1966)

[28] Novotny, J. L. and Kelleher, M. D. ,"Free-Convection Stagnation Flow of an Absorbing-Emitting Gas", Int. J. Heat Mass Transfer, Vol. 10, pp. 1171-1178(1967)

[29] Novotny, J. L. ,"Radiation Interaction in Nongray Boundary Layers", Int. J. Heat Mass Transfer, Vol. 11, pp. 1823-1826(1968)

[30] Edwards, D. K. and Menard, W. A. ,"Comparison of Models for Correlation of Total Band Absorptance", Applied Optics, Vol. 3, pp. 621-625(1964)

[31] Tien, C. L. and Lowder, J. E. ,"A Correlation for Total Band Absorptance of Radiating Gases", Int. J. Heat Mass Transfer, Vol. 9, pp. 698-701(1966)

[32] Arpaci, V. S. ,"Effect of Thermal Radiation on the Laminar Free Convection from a Heated Vertical Plate". Int. J. Heat Mass Transfer, Vol. 11, pp. 871-881(1968)

[33] England, W. G. and Emery, A. F. ,"Thermal Radiation Effects on the Laminar Free Convection Boundary Layer of an Absorbing Gas", J. of Heat Transfer, Vol. 91, pp. 37-44(1969)

[34] Audunson, T. and Gebhart, B. ,"An Experimental and Analytical Study of Natural Convection with Appreciable Thermal Radiation Effects", J. of Fluid Mechanics, Vol. 52, Part 1, pp. 57-97(1972)

[35] Cheng, E. H. and Ozisik, M. N. ,"Radiation with Free Convection in an Absorbing, Emitting and Scattering Medium", Int. J. Heat Mass Transfer, Vol. 15, pp. 1243-1252(1972)

[36] Bratis, J. C. and Novotny, J. L. ,"Radiation-Convection Interaction in the Boundary Layer regime of an Enclosure", Int. J. Heat Mass Transfer, Vol. 17, pp. 23-36(1974)

[37] Lauriat, G. ,"Combined Radiation-Convection in Gray Fluids Enclosed in Vertical Cavities", J. of Heat Transfer, Vol 104, pp. 609-615(1982)

[38] Lauriat, G. ,"Numerical Study of the Interaction of Natural Convection with Radiation in Nongray Gases in a Narrow Vertical Cavity", Proc. 7th Int. Heat Transfer Conference, Vol. 2, pp. 153-158(1982)

[39] Kurosaki, Y., Mishina, H. and Kashiwagi, T. ,"Heat Transfer Combined with Radiation and Natural Convection in a Rectangular Enclosure", Proc. 7th Int. Heat Transfer Conference, paper NC16, pp. 215-220(1982)

[40] Chang, L. C., Yang, K. T. and Lloyd, J. R. ,"Radiation-Natural Convection Interactions in Two-Dimensional Complex Enclosures", J. of Heat Transfer, Vol. 105, pp. 89-95(1983)

[41] Ratzel, A. C. and Howell, J. R. ,"Two-Dimensional Radiation in Absorbing-Emitting Media Using the P-N Approximation", J. of Heat Transfer, Vol. 105, pp. 333-340(1983)

[42] Desrayaud, G. and Lauriat, G. ,"Natural Convection of a Radiating Fluid in a Vertical Layer", J. of Heat Transfer, Vol. 107, pp. 710-712(1985)

[43] Webb, B. W. and Viskanta, R. ,"Radiation-Induced Buoyancy-Driven Flow in Rectangular Enclosures: Experiment and Analysis", J. of Heat Transfer, Vol. 109, pp. 427-433(1987)

[44] Fusegi, T. and Farouk, B. ,"Laminar and Turbulent Natural Convection-Radiation Interactions in a Square Enclosure Filled with a Nongray Gas", Numerical Heat Transfer, Part A, Vol. 15, pp. 303-322(1989)

[45] Fusegi, T. and Farouk, B. ,"A Computational and Experimental Study of Natural Convection and Surface/Gas Radiation Interaction in a Square Cavity", J. of Heat Transfer, Vol. 112, pp. 802-804(1990)

[46] Hood, I. W. ,"Turbulent Natural Convection Coupled with Thermal Radiation in a Boundary Layer", M. A. Sc. Thesis, The University of British Columbia(1989)

[47] Schlichting, H. "Boundary-Layer Theory", McGraw-Hill Publishing Company(1979)

[48] Gebhart, B. ,"Natural Convection Flows and Stability", Advances in Heat Transfer, Vol. 9, pp. 273-348(1973)

[49] Sparrow, E. M. and Cess, R. D. ,"Radiation Heat Transfer", Hemisphere Publication, Washington(1978)

[50] Arpaci, V. S. and Larsen, P. S. ,"Convection Heat Transfer", Prentice-Hall Inc., New Jersey(1984)

[51] Launder, B. E. and Spalding, D. E. ,"The Numerical Computation of Turbulent Flows", Computer Methods in Applied Mechanics and Engineering, Vol. 3, pp. 269-289(1974).

[52] Modest, M. F. ,"Radiative Heat Transfer", McGraw-Hill Inc.(1993)

[53] Patankar, S. V. ,"Numerical Heat Transfer and Fluid Flow", Hemisphere Publishing Corp.(1980)

## Appendix A

### The Modified Jones and Launder $k$-$\epsilon$ Model

The complete form of the Jones and Launder low-Reynolds-number $k$-$\epsilon$ model, proposed originally for the forced convection flows, is

$$\frac{\partial k}{\partial t} + \frac{\partial Uk}{\partial x} + \frac{\partial Vk}{\partial y} = \frac{\partial}{\partial y}[(\nu + \frac{\nu_t}{\sigma_k})\frac{\partial k}{\partial y}] + \nu_t(\frac{\partial U}{\partial y})^2 - \epsilon + D, \tag{A.1}$$

$$\frac{\partial \epsilon}{\partial t} + \frac{\partial U\epsilon}{\partial x} + \frac{\partial V\epsilon}{\partial y} = \frac{\partial}{\partial y}[(\nu + \frac{\nu_t}{\sigma_\epsilon})\frac{\partial \epsilon}{\partial y}] + [C_{1\epsilon}f_1\nu_t(\frac{\partial U}{\partial y})^2 - C_{2\epsilon}f_2\epsilon]\frac{\epsilon}{k} + E, \tag{A.2}$$

$$\nu_t = C_\mu f_\mu \frac{k^2}{\epsilon}. \tag{A.3}$$

where $D = -2\nu(\frac{\partial\sqrt{k}}{\partial y})^2$ and $E = 2\nu\nu_t(\frac{\partial^2 U}{\partial y^2})^2$ are extra terms compared to the high-Reynolds-number $k$-$\epsilon$ model. These terms and the $f$'s functions make the turbulent energy and turbulent viscosity to be damped in the viscous sublayer. However, in natural convection flows, these terms will also act in the outer region of the boundary layer. Therefore, a modified form of this model was used in this study. In the modified Jones and Launder model the wall terms, $D$ and $E$, and the $f$'s functions are applied only in the region before the location of the maximum velocity. To justify the use of the modified Jones and Launder model, it must be shown that the variation of all turbulent quantities in the vicinity of the point of maximum velocity is smooth and without discontinuity.

The Figs. A.1-A.3 show the variation of turbulent kinetic energy, turbulent dissipation, and turbulent viscosity across the boundary layer and at different locations along the plate. The logarithmic scale was used for the horizontal axis to make the near wall region more visible. The points corresponding to the maximum velocity were marked

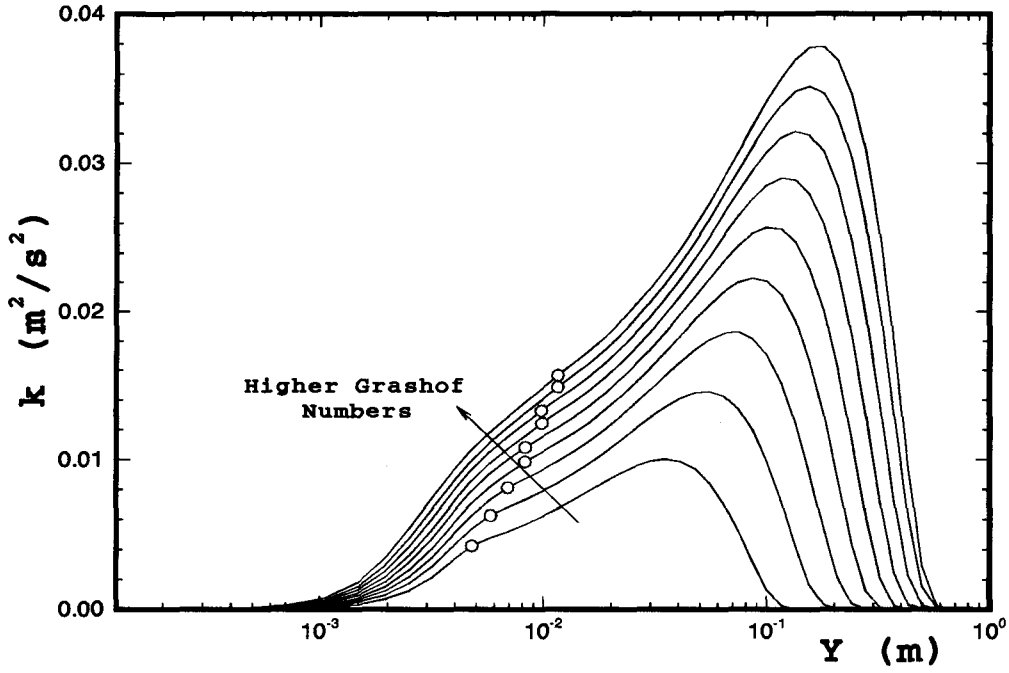


Figure A.1: The variation of turbulent kinetic energy across the boundary layer ($Gr_x = 3.49 \times 10^9 - 6.03 \times 10^{11}$).

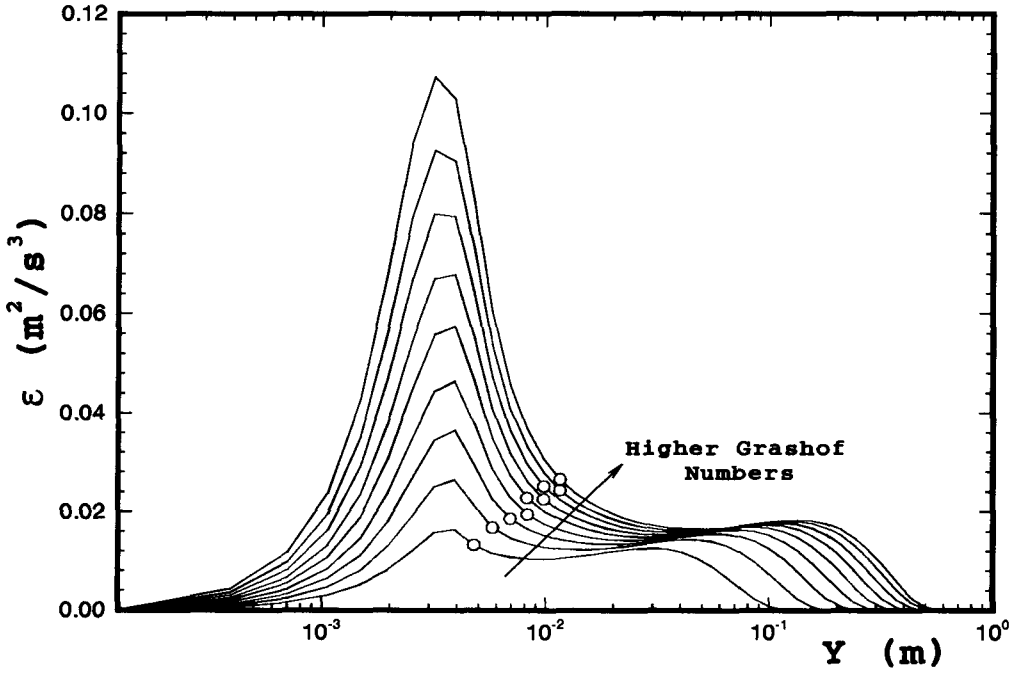


Figure A.2: The variation of turbulent dissipation across the boundary layer ($Gr_x = 3.49 \times 10^9 - 6.03 \times 10^{11}$).

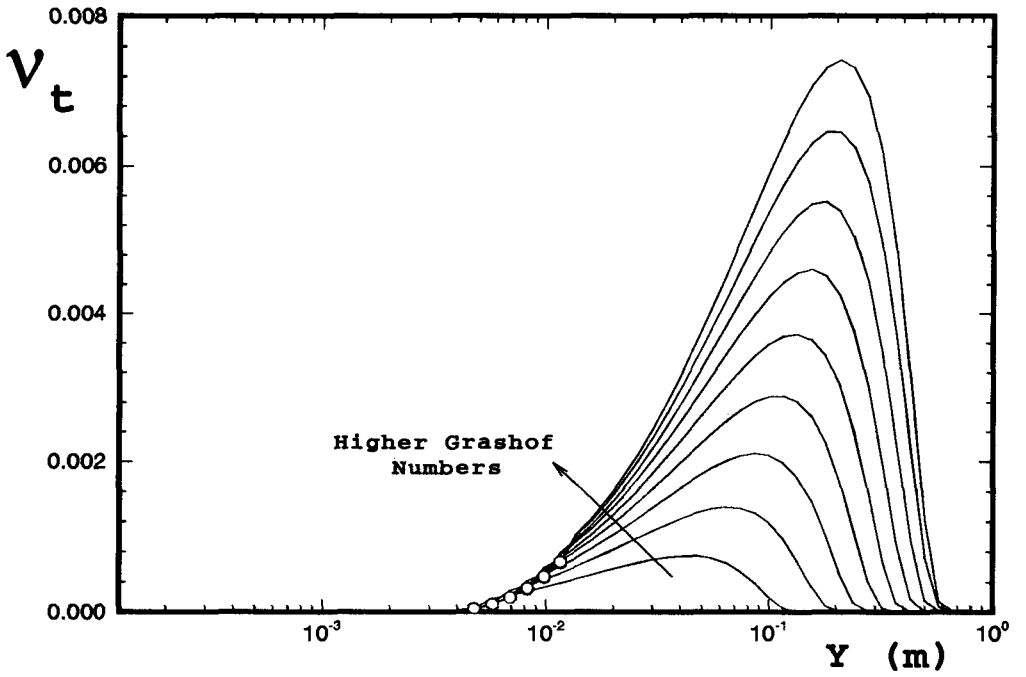


Figure A.3: The variation of turbulent viscosity across the boundary layer ($Gr_x = 3.49 \times 10^9 - 6.03 \times 10^{11}$).

with small circles. It is seen that the profiles of $k$ and $\epsilon$ are smooth and without any discontinuity at the points marked with the circles. On the other hand, the profiles of turbulent viscosity show that in the region before the maximum velocity the values of $\nu_t$ are very small compared to those in the outer layer. Therefore, even if there are small jumps in the profiles at the point of maximum velocity, the effect of those jumps can be negligible.

The variations of extra terms $D$ and $E$ across the boundary layer are shown in Figs. A.4 and A.5. It is seen that these terms are important only in the near wall region and approach to zero as the points of maximum velocity are reached.

The sum of the terms of the Eq. A.2 that contain $f_1$ and $f_2$ is shown in Fig. A.6. It is again seen that, at the points corresponding to the maximum velocities, the variation of this sum is smooth.

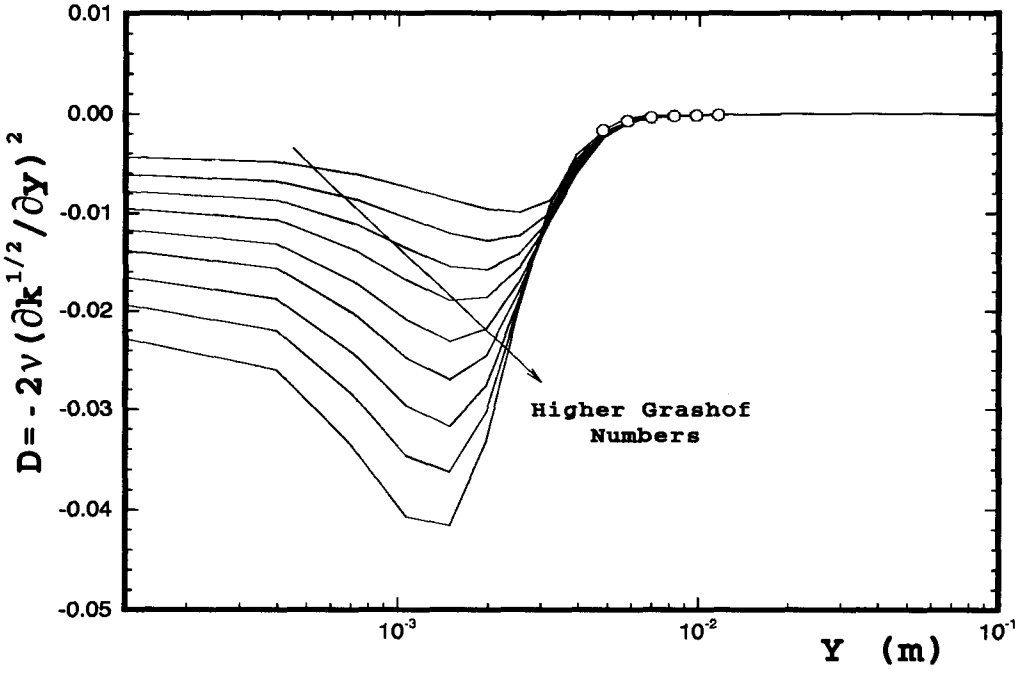


Figure A.4: The variation of $D$ across the boundary layer ($Gr_x = 3.49 \times 10^9 - 6.03 \times 10^{11}$).

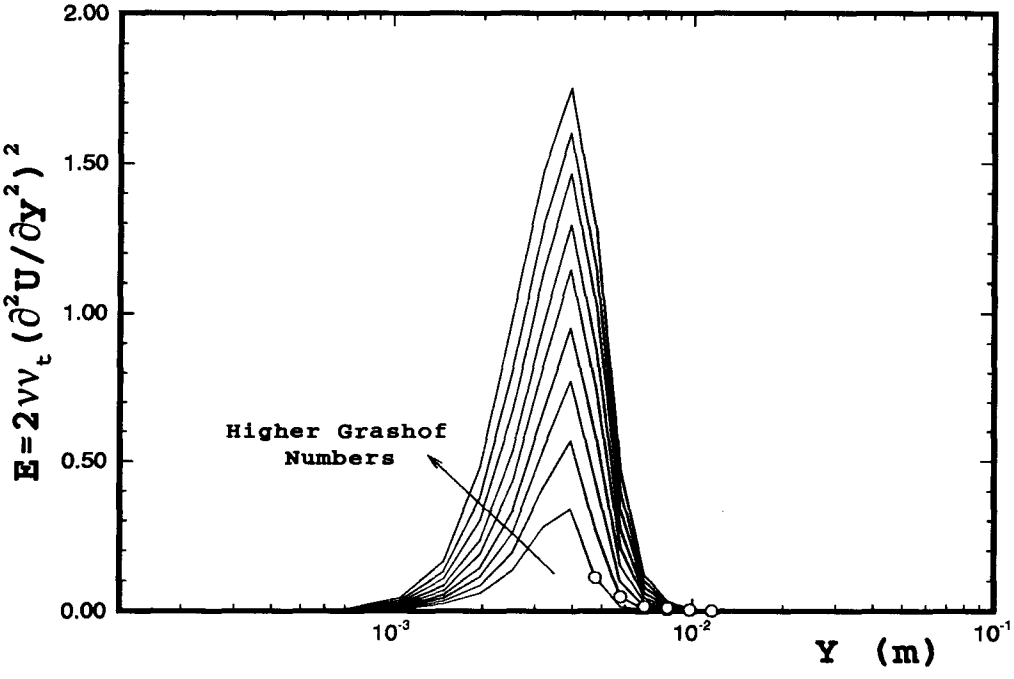


Figure A.5: The variation of $E$ across the boundary layer ($Gr_x = 3.49 \times 10^9 - 6.03 \times 10^{11}$).

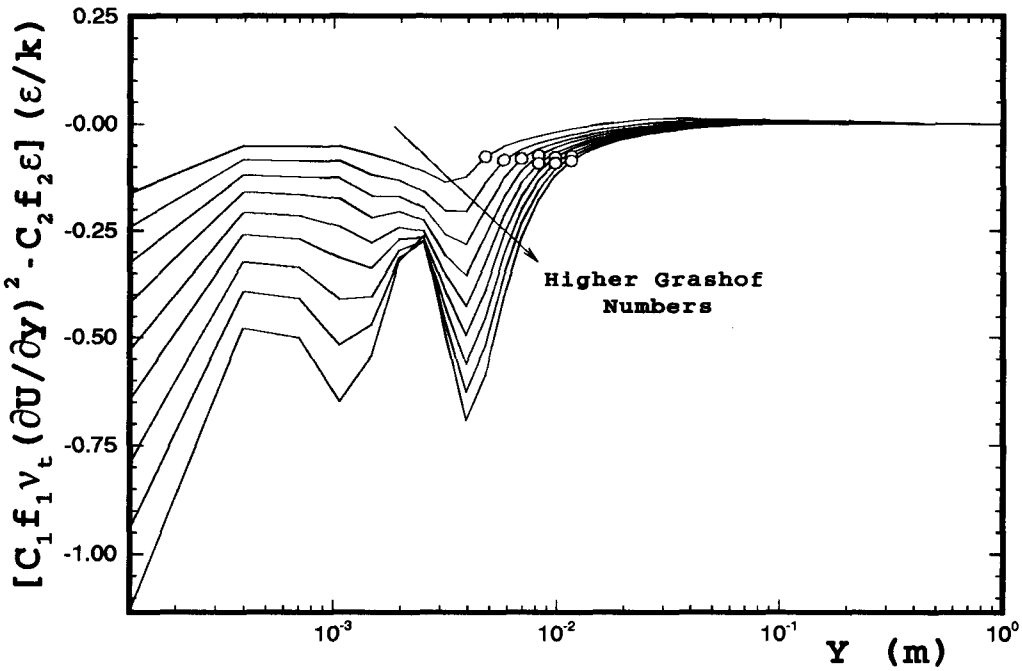


Figure A.6: The sum of the terms of the disspation equation that contain $f_1$ and $f_2$ ($Gr_x = 3.49 \times 10^9 - 6.03 \times 10^{11}$).